# NOT ALL CLIENTS ARE EQUAL: COLLABORATIVE MODEL PERSONALIZATION ON HETEROGENEOUS MULTI-MODAL CLIENTS

**Anonymous authors**
Paper under double-blind review

## ABSTRACT

As AI becomes more personal, *e.g.*, Agentic AI, there is an increasing need for personalizing models for various use cases. Personalized federated learning (PFL) enables each client to *collaboratively* leverage other clients' knowledge for better adaptation to the task of interest, without privacy risks. Despite its potential, existing PFL methods remain confined to rather simplified scenarios where data and models are the same across clients. To move towards realistic scenarios, we propose FedMosaic, a method that jointly addresses data and model heterogeneity with a task-relevance-aware model aggregation strategy to reduce parameter interference, and a dimension-invariant module that enables knowledge sharing across heterogeneous architectures without huge computational cost. To mimic the real-world task diversity, we propose a multi-modal PFL benchmark spanning 40 distinct tasks with distribution shifts over time. The empirical study shows that FedMosaic outperforms the state-of-the-art PFL methods, excelling in both personalization and generalization capabilities under challenging, realistic scenarios.

## 1 INTRODUCTION

Multimodal Large Language Models (MLLMs) with billions of parameters often employ centralized training on massive, heterogeneous datasets using high-performance computing resources (Hurst et al., 2024; Yang et al., 2024a; Team et al., 2024). Such centralized training raises significant concerns about data privacy and high transmission costs (Alvi et al., 2022; Yang et al., 2023). Moreover, as the demand for personalization grows, further fine-tuning is essential to adapt these centrally trained general-purpose models to individual user preferences (Lau et al., 2024; Zhang, 2024).

To address both privacy and personalization, personalized federated learning (PFL) (Smith et al., 2017) has emerged as a decentralized alternative. Recent PFL methods demonstrate that collaboratively leveraging knowledge from other clients significantly improves personalization to the task of interest (Scott et al., 2024; Xie et al., 2024). Unfortunately, despite its potential, most PFL studies overlook the heterogeneity inherent in real-world clients (Zhang et al., 2024b; Bujotzek et al., 2025), where clients typically have distinct models depending on their computational resources (*i.e.*, *model heterogeneity*) and deal with highly personalized data (*i.e.*, *data heterogeneity*), as in agentic AI.

Although some recent work addresses client heterogeneity, it mostly considers either model heterogeneity (Fang et al., 2023; Wu et al., 2024a; Yi et al., 2023) or data heterogeneity (Chen et al., 2024; Xie et al., 2024; Tamirisa et al., 2024). Some tackle both, but in less realistic, simplified setups, *e.g.*, assigning each client a model with different LoRA (Hu et al., 2022) adapter ranks while keeping the base architecture identical (Cho et al., 2024; Bai et al., 2024), or lacking data heterogeneity by simply splitting a single dataset into non-i.i.d. partitions (Li & Wang, 2019; Alam et al., 2022).

As a realistic setup tackling both challenges, illustrated in Fig. 1, we consider (i) *data heterogeneity*, where clients tackle highly personalized tasks, and (ii) *model heterogeneity*, where clients employ models of different families (*e.g.*, Llama-based (Grattafiori et al., 2024)- vs. Qwen-based (Yang et al., 2024a) MLLMs) and scales (*e.g.*, 1B vs. 3B). To mimic the real-world data heterogeneity, we first introduce DRAKE, a comprehensive benchmark for multi-modal PFL with 40 diverse tasks. Unlike prior works that simulate heterogeneity via non-i.i.d. splits of a single dataset (Xie et al., 2024; Long et al., 2024; Morafah et al., 2024), our benchmark assigns each client a distinct multi-modal task (*e.g.*, visual question answering or visual reasoning), while also incorporating temporal distribution shifts

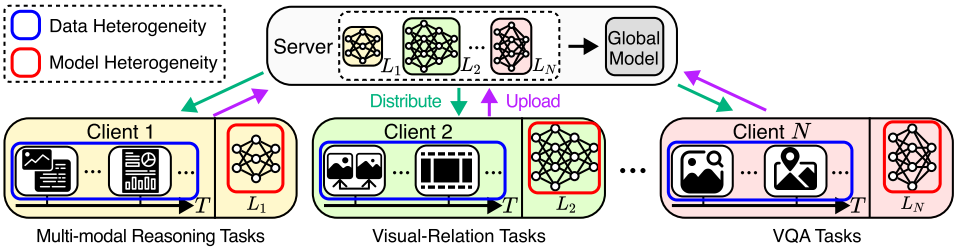


Figure 1: **Overview of the heterogeneous personalized federated learning scenarios.** $L_i$ refers to the local model for the $i_{th}$ client. Clients focus on different tasks (*i.e.*, data heterogeneity) where new data are encountered continuously. In addition to data heterogeneity, model architectures may differ across clients (*i.e.*, model heterogeneity) due to differences in hardware constraints.

inherent in the real world. To the best of our knowledge, this is the first benchmark for multi-modal FL that considers data heterogeneity, as well as distribution shifts.

To address the real-world challenge, we propose **FedMosaic** that jointly addresses both data and model heterogeneity in the realistic scenario. Under data heterogeneity, naive model averaging (McMahan et al., 2017) often degrades performance (Wu et al., 2024c; Yadav et al., 2023) due to interference between models trained on unrelated tasks. To mitigate the interference, inspired by the fact that models trained on similar tasks have less conflict (Gurulingan et al., 2022), we propose **REL**evance-guided **A**ggregation (**RELA**), which constructs a customized global model for each client based on task-relatedness. This enables related clients to share knowledge more effectively.

Under model heterogeneity, aggregating model weights is infeasible since it requires identical architectures across clients (Fan et al., 2024). Although federated distillation (FD) has been proposed to aggregate heterogeneous models' knowledge using logits from public data (Xie et al., 2024; Li et al., 2024e), domain discrepancies between public and client data hinder effective knowledge transfer (Wang et al., 2023), and logit extraction is computationally expensive (Malladi et al., 2023), especially for large models. Instead, we propose **PQ-LoRA**, which incorporates dimension-invariant modules $P \in \mathbb{R}^{r \times r}$ and $Q \in \mathbb{R}^{r}$, whose dimensions depend only on low-rank size $r$, while *independent* of hidden dimension, making them shareable among heterogeneous models.

We summarize our contributions as follows:

- Proposing DRAKE, a comprehensive multi-modal federated learning benchmark.
- Proposing RELA, a model aggregation strategy that promotes selective knowledge sharing among models learning relevant tasks only, addressing data heterogeneity.
- Proposing PQ-LoRA, shareable across heterogeneous models, addressing model heterogeneity.

## 2 Related Work

**Personalized Federated Learning.** Federated learning aims to train a strong global model in a distributed manner while preserving privacy by sharing model weights instead of raw data (Yurdem et al., 2024; Hu et al., 2024). With the growing importance of model personalization, which allows large foundation models to adapt to individual user preferences, contexts, and needs (Zhang et al., 2024c), personalized federated learning (PFL) (Smith et al., 2017) has emerged. PFL aims to train a personalized model on each client's local data by leveraging shared knowledge from other clients to enhance both personalization and generalization while preserving privacy (Xie et al., 2024).

**Data Heterogeneity.** Prior work simulates data heterogeneity by partitioning a single image classification dataset (*e.g.*, MNIST (Deng, 2012)) into non-i.i.d. subsets per client. However, such label-skew fails to capture real-world data heterogeneity (Borazjani et al., 2025), where clients tackle different tasks across vision and language domains (Madni et al., 2024). Recent work (Chen et al., 2024) moves beyond label skew by assigning different VQA datasets to clients, but remains confined to a single task type and single-image inputs. In contrast, our proposed benchmark, DRAKE, spans a broader range of multi-modal tasks, including VQA, visual reasoning, and visual relation, covering single- and multi-image inputs, while also modeling temporal distribution shifts within each client, reflecting the evolving and non-stationary nature of real-world data (Garg et al., 2024).

**Model Heterogeneity.** Federated distillation (FD) transfers knowledge across heterogeneous models by sharing logits on public data. FedMD (Li & Wang, 2019) and PerAda (Xie et al., 2024) average

logits from local models, while FedMKT (Fan et al., 2025) uses those with the lowest loss. However, public-client domain gaps limit transferability (Wang et al., 2023), and logit sharing introduces both privacy risks (Lyu et al., 2022) and high computational cost for large models (Malladi et al., 2023).

Recent works address the limitations of FD through direct model aggregation for heterogeneous models under LoRA-based fine-tuning. HETLoRA (Cho et al., 2024) and FLEXLoRA (Bai et al., 2024) handle varying LoRA ranks through zero-padding/truncation and SVD-based redistribution, respectively. Although they address the varying rank sizes, both assume (i) identical hidden dimensions and (ii) uniform depths across clients, limiting their applicability to heterogeneous architectures that differ in both dimensions and depths (Yao, 2024). In contrast, our proposed PQ-LoRA accommodates both dimensional and depth heterogeneity, enabling more general heterogeneous setups.

## 3 PRELIMINARIES

**Low-Rank Adaptation (LoRA).** LoRA (Hu et al., 2022) assumes that fine-tuning updates lie in a low-rank space. Building on this assumption, LoRA constrains the weight update $\Delta W$ for a pre-trained weight matrix $W_p \in \mathbb{R}^{d_O \times d_I}$ through low rank decomposition using matrices $A \in \mathbb{R}^{r \times d_I}$ and $B \in \mathbb{R}^{d_O \times r}$, where the rank $r \ll \min(d_O, d_I)$. During training, only $A$ and $B$ are updated, while $W_p$ remains frozen. With LoRA, the original output $h_O = W_p h_I \in \mathbb{R}^{d_O}$ for an input hidden state $h_I \in \mathbb{R}^{d_I}$ is modified by incorporating the low-rank update as $h_O = (W_p + \Delta W)h_I = (W_p + BA)h_I$.

**Problem Statement of Personalized Federated Learning.** We consider a PFL setup with $N$ clients, where each client $i \in [N]$ has a local dataset $\mathcal{D}_i$. Reflecting real-world scenarios where data arrives incrementally (Seo et al., 2024; 2025), we assume that each client receives a continuous stream of samples $(x_1^{(i)}, y_1^{(i)}), (x_2^{(i)}, y_2^{(i)}), \cdots$. Given a set of model architectures $W = \{W_1, \ldots, W_K\}$, each client $i$ selects its local pre-trained model $W_{(p,i)} = V(i)$, based on its hardware constraints, where $V$ is a mapping function $V : \{1, \ldots, N\} \to W$. For efficiency, each client trains and shares only its local LoRA adapter $L_i$, while freezing $W_{(p,i)}$. Let $f(W_{(p,i)}, L_i, x)$ denote the forward pass that outputs logits for input $x$, and let the loss function be $\ell(f(W_{(p,i)}, L_i, x), y)$. The empirical loss for client $i$ over its local dataset $\mathcal{D}_i$ can be defined as $\mathcal{J}_i(L_i) = \frac{1}{|\mathcal{D}_i|} \sum_{(x,y)\in\mathcal{D}_i} \ell(f(W_{(p,i)}, L_i, x), y)$. The objective of PFL is then formulated as $\min_{\{L_1,\ldots,L_N\}} \frac{1}{N} \sum_{i=1}^{N} \mathcal{J}_i(L_i)$.

## 4 PROPOSED METHOD

To address the real-world heterogeneities, *i.e.*, *data heterogeneity* and *model heterogeneity*, that hinder client collaborations in personalized federated learning, we propose **FedMosaic**, illustrated in Fig. 2, comprising of: **RELA** (**REL**evance-guided **A**ggregation) and **PQ-LoRA**. RELA mitigates data heterogeneity by restricting knowledge sharing to local models trained on *related* tasks, thus reducing interference during aggregation (*i.e.*, merging by parameter averaging). Under model heterogeneity, model aggregation becomes infeasible. To aggregate different models, we introduce PQ-LoRA, which incorporates shareable modules $P \in \mathbb{R}^{r \times r}, Q \in \mathbb{R}^{r}$ in LoRA, whose dimensions depend only on low-rank size $r$, not on the hidden dimension size. We provide a pseudocode in Sec. A.28.

### 4.1 RELEVANCE-GUIDED AGGREGATION

Model aggregation builds a single model that excels in multiple tasks without accessing raw data (Wei et al., 2025). It is thus widely used to construct a shared global model in federated learning. However, naively averaging models trained on different tasks often causes parameter interference (Yadav et al., 2023; Yang et al., 2024b). Recent work shows that models solving similar tasks share more transferable knowledge with fewer conflicts (Gurulingan et al., 2022). Motivated by this, we replace the uniform averaging with a relevance-guided strategy that assigns a higher aggregation weight to clients with closer task relations, providing each client with a customized global model.

**Client-Wise Gradient $g_i$.** To measure task relevance between clients, we calculate the similarity of client-wise gradients. Formally, we calculate $g_i$, the gradient for $i_{\text{th}}$ client as follows:

$$g_i = \mathbb{E}_{z\subset\mathcal{D}_i} \left[\nabla_{W_s} \ell(z)\right], \tag{1}$$

where $\mathcal{D}_i$ is $i_{\text{th}}$ client's data stream, $\ell$ refers to the loss function, $z \subset \mathcal{D}_i$ is a mini-batch, and $W_s$ is a small-scale frozen pre-trained model $W_s$. For efficiency, we (i) use gradients from a small-scale frozen

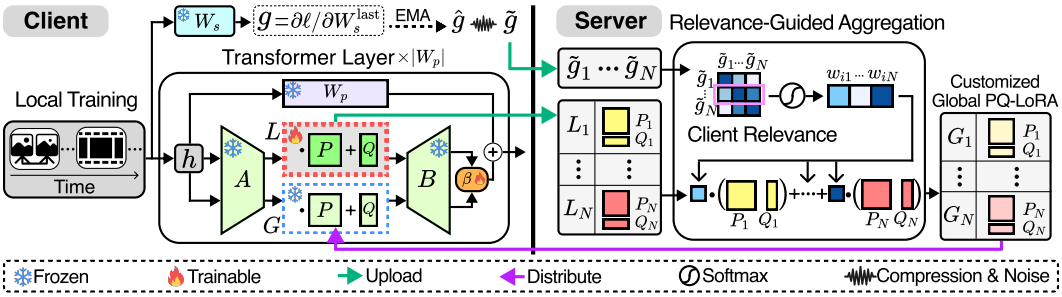


Figure 2: **Overview of proposed FedMosaic.** On every round, the local PQ-LoRA $L_i$ fine-tuned during local training and the sanitized last layer gradient $\tilde{g}_i$ are uploaded from the $i_{\text{th}}$ client to server. The last layer gradient $g$ is extracted from the small pre-trained model $W_s$, which is then EMA updated to $\hat{g}$ and then compressed to $\tilde{g}$, sequentially. Note that the gradient computation is performed every $m$ iterations. In server, the sanitized gradients $\tilde{g}_i$ are used to measure client task relevance and to build customized global PQ-LoRA $G_i$, which is distributed and kept frozen. $h$ and $W_p$ denote the hidden state input and the pre-trained weight, respectively. $\beta$ is a learnable gating parameter that balances the output from the global and local models, and $|W_p|$ is the number of layers in the model.

pre-trained model $W_s$ that provides sufficient representativeness with reduced overhead (Lee et al., 2024), and (ii) compute only the last-layer gradient, as preceding layers' gradients are proportional to it based on the chain rule (Seo et al., 2025). Moreover, we compute the gradient $g_i$ every $m$ batch iterations rather than every batch, thus incurring negligible additional cost, as shown in Sec. A.8. Note that we measure gradients from a frozen pre-trained model, not the actual training model. This is because in heterogeneous PFL, clients train on diverse tasks, and gradient similarities from models trained on heterogeneous data may not capture task similarity (Tang et al., 2020; Evans et al., 2024).

**Decayed Client-Wise Gradient $\hat{g}_i$.** However, $g_i$ may not reflect learned task relevance under shifting data distributions, as it is an expectation over the entire data stream $D_i$ (Eq. 1), *i.e.*, unweighted average of gradients across all time points, ignoring forgetting of the model over time. Consequently, client 1 learning $A \rightarrow B$ and client 2 learning $B \rightarrow A$ yield the same $g_i$, despite retaining different knowledge due to catastrophic forgetting (McCloskey & Cohen, 1989; Ratcliff, 1990). To reflect the model knowledge shifts under distribution shifts, we introduce decayed gradient $\hat{g}_i$, computed using the exponential moving average (EMA) of past gradients, inspired by the exponential decay of knowledge in forgetting (Mahto et al., 2021; Chien et al., 2021; Seo et al., 2025). Formally, for the $i_{\text{th}}$ client, $\hat{g}_i(t)$ with EMA ratio $\alpha$ at timestep $t$ is defined recursively as:

$$\hat{g}_i(t) = (1-\alpha) \cdot \hat{g}_i(t-1) + \alpha \cdot g_i(t), \tag{2}$$

where $g_i(t) = \nabla_{W_s} \ell(z_t)$ is the gradient vector for the given batch $z_t \subset \mathcal{D}_i$ at timestep $t$.

**Sanitized Client-Wise Gradient $\tilde{g}_i$.** Transmitting EMA-aggregated gradients (*i.e.*, $\hat{g}_i$) rather than per-sample gradients mitigates gradient-based privacy attacks, as gradient mixing (*i.e.*, aggregating) increases resistance to gradient inversion (Mo et al., 2021). We further prevent privacy risks by transmitting sanitized gradient $\tilde{g}_i$ through: (i) adding Gaussian noise $\epsilon$ to $\hat{g}_i$ and (ii) applying gradient compression (*i.e.*, randomly selecting only $N_s\%$ of the gradient vector dimensions from $\hat{g}_i \in \mathbb{R}^d$), as randomly sampled dimensions can approximate full-gradient distributions (Li et al., 2023b) while making gradient inversion substantially more difficult than using full gradients (Zhu et al., 2019) and simultaneously reducing transmission costs (detailed in Sec. A.9). Formally, $\tilde{g}_i$ is defined as:

$$\tilde{g}_i(t) = \mathbf{M} \odot (\hat{g}_i(t) + \mu\epsilon), \quad \epsilon \sim \mathcal{N}(0, \boldsymbol{I}_d) \tag{3}$$

where $\mathbf{M} \in \{0,1\}^d$ is the binary mask for random subsampling and $\mu$ denotes the noise scale.

Using the sanitized client-wise gradients $\{\tilde{g}_1, \ldots, \tilde{g}_N\}$ from $N$ clients, we construct a client-relevence matrix $S \in \mathbb{R}^{N \times N}$, where $S_{ij} = \cos(\tilde{g}_i, \tilde{g}_j)$. The customized global module for the $i_{\text{th}}$ client, $G_i$, is then constructed by weighted aggregation of local modules $\mathcal{L} = \{L_1, \ldots, L_N\}$ as follows:

$$G_i = \sum_{j=1}^{N} w_{ij}\, L_j, \quad w_{ij} = \frac{e^{\cos(\tilde{g}_i, \tilde{g}_j)/\tau}}{\sum_{n=1}^{N} e^{\cos(\tilde{g}_i, \tilde{g}_n)/\tau}}, \tag{4}$$

where $\tau$ denotes the softmax temperature and $\cos(\cdot,\cdot)$ denotes cosine similarity.

### 4.2 PQ-LoRA

LoRA matrices $A \in \mathbb{R}^{r \times d_I}$ and $B \in \mathbb{R}^{d_O \times r}$ depend on model-specific hidden dimensions $d_I$ and $d_O$, preventing direct aggregation across different models. To enable knowledge sharing among heterogeneous architectures, we introduce PQ-LoRA, which inserts dimension-invariant modules $P \in \mathbb{R}^{r \times r}$ and $Q \in \mathbb{R}^r$ between $A$ and $B$. Their dimensions depend only on the low-rank $r$, making them shareable across heterogeneous models. We illustrate a comparison of PQ-LoRA with conventional LoRA in Fig. 3. Formally, PQ-LoRA outputs $h_O$ as:

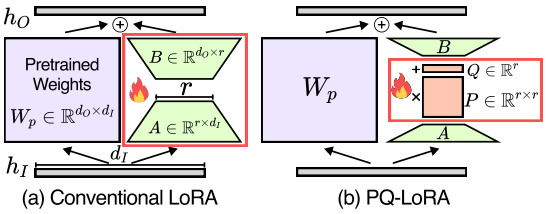


Figure 3: **Illustration of (a) Conventional LoRA and (b) PQ-LoRA.** While $A$ and $B$ are trainable in conventional LoRA, PQ-LoRA freezes both, updating only the dimension-invariant modules $P \in \mathbb{R}^{r \times r}$ and $Q \in \mathbb{R}^r$ during training.

$$h_O = W_p h_I + B(PAh_I + Q), \tag{5}$$

for input hidden states $h_I$ and pre-trained weight $W_p$. After local training on each client, the $P$ and $Q$ modules are aggregated and shared between heterogeneous clients for knowledge sharing.

Although $P$ and $Q$ are shareable across heterogeneous architectures having different dimensions, two main challenges hinder their aggregation: (i) depth heterogeneity - heterogeneous architectures often differ in depth, making it non-trivial to determine which layers across models should be aggregated; and (ii) weight misalignment - interpolating weights with different optimization trajectories can degrade performance (Jordan et al., 2023; Stoica et al., 2025). We address these challenges with two strategies: (i) block-wise aggregation, which aligns layers at the same relative depth, and (ii) weight alignment, ensuring heterogeneous models share the same initialization. For simplicity, we consider aggregating two heterogeneous models, though it naturally extends to multiple heterogeneous models.

#### 4.2.1 Block-Wise Aggregation

To decide which layers of heterogeneous models should share knowledge, we measure layer-wise representation alignment between two MLLMs, $W_i$ and $W_j$, of different depths using CKA (Kornblith et al., 2019). We observe high similarity between layers at similar relative depths, *i.e.*, approximately linear alignment (Fig. 4). Accordingly, we divide each model into $N_B$ blocks linearly and attach a PQ-LoRA to each block's final layer, enabling cross-model sharing at relevant depths. The attachment layer index $I_k$ of the $k$-th PQ-LoRA in a $|W|$-layer model is defined as:

$$I_k = \begin{cases} k \cdot \left\lfloor \frac{|W|}{N_B} \right\rfloor & \text{for} \quad k = 1, 2, \ldots, N_B - 1 \\ |W| & \text{for} \quad k = N_B. \end{cases} \tag{6}$$

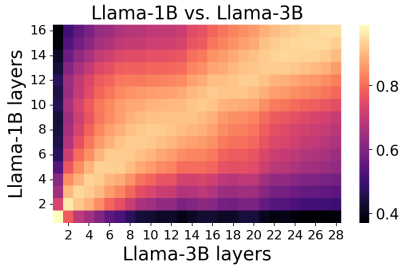


Figure 4: **Layer-wise similarity between Llama-1B and Llama-3B measured with CKA.** The diagonal brightest band shows the strongest alignment between layers at similar relative depths (*e.g.*, Llama-1B layer 8 - Llama-3B layer 14).

#### 4.2.2 Weight Alignment in PQ-LoRA

We then align the $N_B$ number of PQ-LoRA modules at layer indices $\mathcal{I}_i = \{I_1^i, \ldots, I_{N_B}^i\}$ in model $M_i$ and $\mathcal{I}_j = \{I_1^j, \ldots, I_{N_B}^j\}$ in model $M_j$. For simplicity, we describe the alignment for a single pair $X = (\{P_i, Q_i, A_i, B_i\}, \{P_j, Q_j, A_j, B_j\})$, which is generalized across all $N_B$ pairs.

Motivated by findings that models fine-tuned from the same initialization share optimization paths and can be merged without interference (Wortsman et al., 2022a;b; Yadav et al., 2023), we set the pair $X$ to share a common initialization. Dimension-invariant modules, $P_i, P_j \in \mathbb{R}^{r \times r}$ and $Q_i, Q_j \in \mathbb{R}^r$, can share the same weight directly, but dimension-dependent modules, $A_i \in \mathbb{R}^{r \times d_I^{(i)}}$, $A_j \in \mathbb{R}^{r \times d_I^{(j)}}$ and $B_i \in \mathbb{R}^{d_O^{(i)} \times r}$, $B_j \in \mathbb{R}^{d_O^{(j)} \times r}$, cannot due to dimension mismatches. Although only $P$ and $Q$ are shared between heterogeneous models $M_i$ and $M_j$, $A$ and $B$ should also be aligned, as they affect the output $h_O$ (Eq. 5) and optimization trajectories. Therefore, we align $A_i, A_j$ and $B_i, B_j$, ensuring aligned representations for the same input, even in parameter spaces with different dimensions.

**Aligning $A$ Matrices.** We first align $A_i \in \mathbb{R}^{r \times d_I^{(i)}}$ and $A_j \in \mathbb{R}^{r \times d_I^{(j)}}$ using L2 loss in the shared $r$-dimensional space with publicly available data $\mathcal{D}_p$. For $\mathcal{D}_p$, we use a subset of the MLLMs' pre-training data, as detailed in Sec. A.17. In particular, we use the smaller model $A_i$ (where $d_I^{(i)} < d_I^{(j)}$) as the pivot model by freezing it and updating the larger model $A_j$ to minimize the L2 loss on $r$-dimensional representations obtained from $\mathcal{D}_p$, as $\min_{A_j} \frac{1}{|\mathcal{D}_p|} \sum_{(x,y)\in\mathcal{D}_p} \|(A_i(x) - A_j(x)\|_2^2$, where $A(x)$ denotes $r$-dimensional feature extracted by $A$ for input $x$.

**Aligning $B$ Matrices.** We then align $B_i$ and $B_j$. Since their output dimensions differ ($d_O^{(i)} \neq d_O^{(j)}$), L2 loss is inapplicable. Instead, we employ canonical correlation analysis (CCA) (De Bie et al., 2005), which finds projection matrices maximizing the correlation between two feature sets. Using $m$ public data $\{(x_k, y_k)\}_{k=1}^m \subset D_p$, we extract output features $H_i \in \mathbb{R}^{m \times d_O^{(i)}}$ and $H_j \in \mathbb{R}^{m \times d_O^{(j)}}$ from $B_i$ and $B_j$, then find projection matrices $\Pi_i \in \mathbb{R}^{d_O^{(i)} \times r}$ and $\Pi_j \in \mathbb{R}^{d_O^{(j)} \times r}$, which project them to the maximally correlated space of dimension $r$ (*i.e.*, $H_i\Pi_i \approx H_j\Pi_j$). We project $B_i$ to the shared maximally correlated space, *i.e.*, $(\Pi_i)^T \cdot B_i$, and subsequently bring it to $B_j$ space by inverse projection, as $B_j = (\Pi_j{}^\dagger)^T \cdot (\Pi_i)^T \cdot B_i$, where $\Pi_j{}^\dagger$ denotes the pseudo-inverse of $\Pi_j$.

During the alignment of $A$ and $B$, we enforce orthogonality in $A$ and $B$ to maximize the expressive capacity (*i.e.*, span) of PQ-LoRA weight updates, following Theorem 1. We provide details of enforcing orthogonality in Sec. A.5 and the proof of Theorem 1 in Sec. A.2.

**Theorem 1.** *If the column vectors of matrix $B \in \mathbb{R}^{d_O \times r}$ are orthogonal and the row vectors of matrix $A \in \mathbb{R}^{r \times d_I}$ are orthogonal, then the span of the weight update space of PQ-LoRA, span$\{\Delta W\}$, has $r^2$ dimension, which is the maximum possible dimension under frozen $B$ and $A$.*

In addition, our method does not incur much computational cost since (i) PQ-LoRA aligning is performed *once before federated training* to establish a shared initialization, (ii) it is required only for *heterogeneous model-type pairs* (since some clients may share the same architecture). After aligning $A$ and $B$, we update shareable modules $P$ and $Q$, while freezing $A$ and $B$ during local training to preserve alignment. We provide theoretical justification for this freezing approach in Sec. A.1. This freezing design also reduces the communication cost of PQ-LoRA relative to conventional LoRA, as it requires communication of only $P, Q$ modules. See Sec. A.9 for details of communication costs.

After receiving the aggregated PQ-LoRA (*i.e.*, global PQ-LoRA) by RELA at each communication round, clients freeze it during training to preserve global knowledge and update only the local model for personalization. Specifically, at the $l_{\text{th}}$ layer, given an input hidden state $h_I$, we combine the output of the local LoRA (*i.e.*, $h_L$), the frozen global LoRA (*i.e.*, $h_G$), and the pre-trained weights (*i.e.*, $W_p h_I$), by adaptively balancing them using a learnable gating parameter $\beta$. With sigmoid-normalized balancing parameter $\tilde{\beta} = \sigma(\beta)$, the output hidden state $h_O$ is computed as follows:

$$h_O = W_p h_I + (1 - \tilde{\beta})h_L + \tilde{\beta} h_G. \tag{7}$$

# 5 DRAKE BENCHMARK

We propose a novel multi-modal FL benchmark, called DRAKE, with three key merits: (i) **Task heterogeneity**: Each client handles distinct multi-modal tasks (*e.g.*, visual reasoning, VQA), while existing benchmarks merely assign non-i.i.d. subsets from a single dataset. (ii) **Dynamic distribution**: Client datasets contain progressive tasks (*e.g.*, encountering new visual concepts), simulating real-world temporal distribution shifts. To the best of our knowledge, DRAKE is the first benchmark supporting multi-modal federated learning under distribution shifts. (iii) **Generalizability Evaluation**: DRAKE incorporates unseen task data to evaluate the generalizability of FL models. We summarize the comparison with existing FL benchmarks in Tab. 1. DRAKE consists of three training task subgroups, *i.e.*, VQA, visual relation, and multi-modal reasoning, and two unseen task subgroups, comprising 40 heterogeneous tasks sourced from 19 different multi-modal datasets, totaling 375k images and 274k questions, illustrated in Fig. 5. Please refer to Sec. A.24 for more details.

# 6 EXPERIMENTS

## 6.1 SETUPS

**Models.** To simulate model heterogeneity in federated MLLM training, we employ LLaVA-1.5 (Liu et al., 2023b) variants. For LLM of LLaVA, we employ various sizes of Llama-3 (Grattafiori et al.,

| Dataset | Multi-Data Sources | Distribution Shifts | Multi-Image Support | Multi-Modalities | Unseen Evaluation |
|---|---|---|---|---|---|
| Split-CIFAR (ICML 2021) | ✗ | ✓ | ✗ | ✗ | ✗ |
| NonIID-50 (ICML 2021) | ✓ | ✓ | ✗ | ✗ | ✗ |
| LEAF-FCL (ICLR 2023) | ✓ | ✓ | ✗ | ✗ | ✗ |
| MNIST-Shuffle (ICLR 2024) | ✗ | ✓ | ✗ | ✗ | ✗ |
| HC-FMTL (CVPR 2024) | ✓ | ✗ | ✗ | ✗ | ✗ |
| Fed-SNI (NeurIPSW 2023) | ✓ | ✗ | - | ✗ | ✗ |
| FEDLEGAL (ACL 2023) | ✓ | ✗ | - | ✗ | ✗ |
| Fed-Aya (NeurIPS 2024) | ✗ | ✗ | - | ✗ | ✗ |
| Fed-FLAN (NeurIPS 2024) | ✓ | ✗ | - | ✗ | ✗ |
| HFLB (AAAI 2024) | ✓ | ✗ | ✗ | ✓ | ✗ |
| DRAKE (**Ours**) | ✓ | ✓ | ✓ | ✓ | ✓ |

Table 1: **Comparison of FL benchmarks across key dimensions:** Multi-Data Sources (using diverse datasets vs. non-i.i.d. splits of a single dataset), Distribution Shifts (evolving client data distributions), Multi-Image Support (handling multiple images per input), and Unseen Evaluation (testing on tasks unseen during training). See Sec. A.25 for the detailed comparisons.

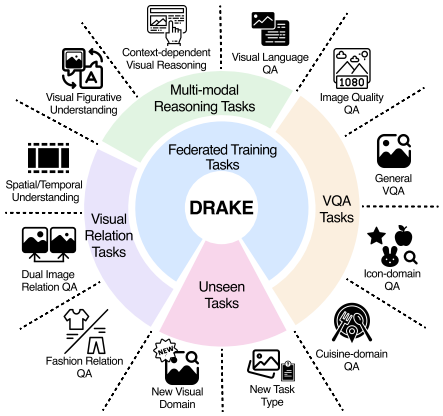


Figure 5: Overview of DRAKE.

2024) (Llama-3.2-1B, Llama-3.2-3B, Llama-3.1-8B) and Qwen-2.5 (Yang et al., 2024a) (Qwen2.5-0.5B, Qwen2.5-1.5B, Qwen2.5-3B). We use the Llama-3 series for text-only benchmarks.

**Metrics.** We report $A_{last}$, the accuracy at the end of training, and $A_{\text{AUC}}$ (Koh et al., 2022), which computes the area under the accuracy curve by measuring accuracy at each evaluation period to capture intermediate performance. All experiments use five rounds of evaluation intervals and are averaged over three different random seeds, with standard deviations reported.

**Benchmarks.** We evaluate FedMosaic on multi-modal PFL benchmarks: HFLB (Chen et al., 2024) and our proposed DRAKE. Our evaluation covers PFL-Static (*i.e.*, i.i.d. client data distributions) and the more realistic PFL-Dynamic setup (*i.e.*, intra-client distribution shifts with four incremental tasks). For PFL-Dynamic on HFLB, we partition client data by question types (*e.g.*, color, shape, count, and size). We also evaluate on text-only PFL benchmarks, *i.e.*, Fed-Scope (Kuang et al., 2024), Fed-Aya (Singh et al., 2024), and Fed-LLM-Large that we combined Fed-LLM (Ye et al., 2024) and Fed-FLAN (Long et al., 2024). See Sec. A.6 for the details of experiment setup.

**Baselines.** We compare FedMosaic with SOTA PFL methods: DITTO (Li et al., 2021), FedSim (Pillutla et al., 2022), FedIT (Zhang et al., 2024a), TAKFL (Morafah et al., 2024), FedDPA (Long et al., 2024), FedDAT (Chen et al., 2024), PerAda (Xie et al., 2024), and FedMKT (Fan et al., 2025). We also compare with supervised fine-tuning (SFT), where clients train independently without knowledge sharing and often outperforming FL methods under data heterogeneity (Ghari & Shen, 2024).

### 6.2 Quantitative Analysis

In all experiments, we evaluate each client's model on its own task (*i.e.*, 'Self') and on other clinets' tasks (*i.e.*, 'Others'), reporting average performance across clients. 'Self' performance shows personalization, while 'Others' indicates generalizability. Although personalization is PFL's main goal, generalization ability is also crucial for continual personalization, as it enables rapid adaptation to new tasks in the future during training (Finn et al., 2017; Rao et al., 2023).

**Heterogeneous Multi-Modal Clients.** We evaluate FedMosaic in multi-modal heterogeneous PFL-Dynamic and -Static setups, where clients employ different architectures (LLaVA-Llama3-1B or 3B). As shown in Tab. 2 and Tab. 3, FedMosaic consistently outperforms baselines on both clients' own tasks ('Self') and others' tasks ('Others') under static and dynamic distributions. HFLB's single VQA task with single-image inputs converges faster than DRAKE, yielding smaller gaps among baselines.

Note that Tab. 2 reports the average performance across all clients. Local client training (SFT) can suffice for simpler tasks (Mosbach et al., 2021; Woźniak et al., 2024), *e.g.*, single-image VQA (clients 2, 3 in Tab. 5), making average improvements appear small. In contrast, FedMosaic significantly enhances personalization for complex multi-image tasks (clients 5, 7, 9 in Tab. 5) through effective knowledge sharing. See Sec.A.16 for additional per-client results and Sec. A.24 for task descriptions.

As shown in Tab.5, not only do clients using smaller models (*i.e.*, LLaVA-Llama3.2-1B) benefit from knowledge sharing through PFL, but larger models (*i.e.*, LLaVA-Llama3.2-3B) also see significant gains. We attribute this to (i) RELA accurately measuring task relevance under distribution shifts,

| Method | DRAKE-Dynamic | | | | HFLB-Dynamic | | | |
|---|---|---|---|---|---|---|---|---|
| | Self | | Others | | Self | | Others | |
| | $A_{last}$ ↑ | $A_{\text{AUC}}$ ↑ | $A_{last}$ ↑ | $A_{\text{AUC}}$ ↑ | $A_{last}$ ↑ | $A_{\text{AUC}}$ ↑ | $A_{last}$ ↑ | $A_{\text{AUC}}$ ↑ |
| SFT | 65.79±0.20 | 57.62±0.26 | 47.66±0.13 | 46.67±0.11 | 79.99±0.66 | 77.14±0.35 | 61.66±0.56 | 61.43±0.14 |
| DITTO (ICML 2021) | 59.91±0.18 | 54.16±0.06 | 47.45±0.36 | 46.70±0.10 | 79.10±0.11 | 76.05±0.08 | 61.86±0.82 | 61.43±0.08 |
| FedSim (ICML 2022) | 63.98±1.19 | 56.42±0.70 | 47.04±0.16 | 46.15±0.17 | 79.90±0.09 | 76.47±0.01 | 59.92±0.54 | 59.56±0.13 |
| FedIT (ICASSP 2024) | 66.11±0.27 | 57.86±0.27 | 47.63±0.16 | 46.62±0.04 | 79.87±0.50 | 77.04±0.38 | 61.73±0.54 | 61.45±0.18 |
| TAKFL (NeurIPS 2024) | 64.54±0.85 | 56.19±0.98 | 47.38±0.06 | 46.47±0.14 | 79.76±0.06 | 76.86±0.04 | 61.42±0.44 | 61.22±0.10 |
| FedDPA (NeurIPS 2024) | 63.34±0.23 | 55.74±0.38 | 47.61±0.21 | 46.64±0.20 | 70.06±0.24 | 77.10±0.36 | 61.58±0.27 | 61.19±0.09 |
| FedDAT (AAAI 2024) | 58.47±1.10 | 54.38±0.28 | 48.91±0.42 | 47.78±0.18 | 79.61±0.42 | 77.43±1.02 | 64.15±0.08 | 64.51±0.13 |
| PerAda (CVPR 2024) | 59.75±1.06 | 54.48±0.13 | 47.30±0.45 | 46.72±0.03 | 79.03±0.01 | 75.92±0.01 | 61.76±0.80 | 61.39±0.06 |
| FedMKT (COLING 2025) | 61.38±0.18 | 55.45±0.31 | 47.50±0.07 | 46.68±0.08 | 79.48±0.01 | 76.57±0.06 | 61.54±0.61 | 61.41±0.19 |
| FedMosaic (**Ours**) | **67.86±0.51** | **59.83±0.16** | **51.16±0.04** | **49.36±0.08** | **80.80±0.26** | **78.43±0.14** | **67.07±0.25** | **66.02±0.16** |

Table 2: **Quantitative comparison in heterogeneous PFL.** 'Self' denotes evaluation on a client's own data, while 'Others' denotes evaluation on data from other clients. In DRAKE, 4 clients use LLaVA-Llama3.2-1B and 6 clients use LLaVA-Llama3.2-3B, while in HFLB, 3 clients use LLaVA-Llama3.2-1B and 6 clients use LLaVA-Llama3.2-3B. SFT refers to supervised fine-tuning on each client's data without cross-client knowledge sharing.

| Method | Self | | Others | |
|---|---|---|---|---|
| | $A_{last}$ ↑ | $A_{\text{AUC}}$ ↑ | $A_{last}$ ↑ | $A_{\text{AUC}}$ ↑ |
| SFT | 68.50±0.42 | 63.84±0.27 | 47.91±0.39 | 47.56±0.23 |
| DITTO | 63.67±1.50 | 59.17±1.25 | 48.22±0.09 | 47.65±0.03 |
| FedSim | 66.75±0.56 | 61.70±0.60 | 46.93±0.25 | 46.76±0.02 |
| FedIT | 68.71±0.04 | 63.89±0.55 | 47.91±0.22 | 47.60±0.17 |
| TAKFL | 67.28±0.01 | 62.42±0.36 | 47.55±0.23 | 47.51±0.07 |
| FedDPA | 66.09±1.51 | 61.36±0.14 | 47.93±0.30 | 47.69±0.11 |
| FedDAT | 61.28±0.07 | 57.92±0.02 | 49.37±0.02 | 48.78±0.04 |
| PerAda | 63.67±1.01 | 59.03±1.19 | 48.13±0.03 | 47.60±0.05 |
| FedMKT | 65.81±1.09 | 60.37±1.16 | 47.19±0.86 | 46.44±1.49 |
| FedMosaic | **70.10±0.53** | **64.64±0.40** | **51.57±0.24** | **50.42±0.12** |

Table 3: **Quantitative comparison in PFL on DRAKE-static.** 4 clients use LLaVA-Llama3.2-1B, 6 clients use LLaVA-Llama3.2-3B.

| Method | Self | | Others | |
|---|---|---|---|---|
| | $A_{last}$ ↑ | $A_{\text{AUC}}$ ↑ | $A_{last}$ ↑ | $A_{\text{AUC}}$ ↑ |
| SFT | 68.60±0.57 | 61.33±1.03 | 48.34±0.18 | 47.53±0.22 |
| DITTO | 66.77±0.96 | 60.67±0.77 | 49.04±0.63 | 48.33±0.53 |
| FedSim | 66.65±0.26 | 59.49±0.17 | 46.77±0.29 | 46.42±0.10 |
| FedIT | 68.72±0.97 | 60.88±0.81 | 48.22±0.17 | 47.25±0.22 |
| TAKFL | 67.77±0.46 | 60.13±0.32 | 48.18±0.07 | 47.51±0.14 |
| FedDPA | 67.38±0.58 | 60.20±0.40 | 48.40±0.22 | 47.32±0.33 |
| FedDAT | 66.08±0.95 | 60.00±0.22 | 50.05±0.02 | 49.10±0.11 |
| PerAda | 64.86±0.51 | 58.73±0.48 | 47.89±0.70 | 47.45±0.45 |
| FedMKT | 65.44±0.91 | 59.18±0.62 | 48.09±0.41 | 47.51±0.18 |
| FedMosaic | **70.67±0.61** | **63.51±0.40** | **52.31±0.15** | **50.60±0.26** |

Table 4: **Quantitative comparison in cross-family PFL on DRAKE-dynamic.** 3 clients use LLaVA-Llama3.2-3B, 4 use LLaVA-Qwen2.5-1.5B, 3 use LLaVA-Qwen2.5-3B.

| Method | Self $A_{last}$ / $A_{\text{AUC}}$ | | | | | | | | | |
|---|---|---|---|---|---|---|---|---|---|---|
| | LLaVA-Llama3.2-**1B** | | | | LLaVA-Llama3.2-**3B** | | | | | |
| | Client 1 | Client 2 | Client 3 | Client 4 | Client 5 | Client 6 | Client 7 | Client 8 | Client 9 | Client 10 |
| SFT | 76.45 / 59.87 | 58.10 / 54.35 | 66.63 / 59.57 | 62.85 / 53.16 | 62.00 / 61.51 | 76.56 / 66.88 | 62.59 / 54.63 | 68.54 / 59.65 | 65.92 / 51.93 | 58.30 / 54.61 |
| FedMosaic | **77.42 / 60.45** | **58.50 / 55.26** | **66.71 / 59.60** | **63.13 / 55.84** | **68.87 / 63.60** | **77.61 / 69.80** | **69.19 / 56.66** | **70.54 / 58.93** | **70.68 / 54.09** | **59.21 / 55.32** |
| *Gain* | +0.97 / +0.57 | +0.40 / +0.91 | +0.08 / +0.04 | +0.27 / +2.67 | +6.86 / +2.09 | +1.05 / +2.93 | +6.61 / +2.03 | +2.00 / -0.72 | +4.76 / +2.16 | +0.91 / +0.71 |

Table 5: **Per-client 'Self' performance of FedMosaic vs. SFT in a heterogeneous PFL-Dynamic setup on DRAKE.** The *Gain* row shows positive gain of FedMosaic in blue, negative in red against SFT. Clients 1-4 use LLaVA-Llama3.2-1B, while Clients 5-10 use LLaVA-Llama3.2-3B.

reducing interference during aggregation, and (ii) PQ-LoRA enabling effective knowledge transfer between heterogeneous architectures, allowing smaller and larger models to mutually benefit.

We also emphasize that FedMosaic significantly outperforms baselines in generalization ('Others'), which is crucial under distribution shifts where new, unseen tasks continuously emerge. This enhanced generalizability enables faster adaptation and accelerates future personalization, as shown in Fig. 6.

**Cross-family Heterogeneity.** Beyond varying model sizes within the same family (*e.g.*, LLaVA-Llama-1B/3B), we further simulate cross-family heterogeneity (*e.g.*, Qwen- *vs.* Llama-based MLLMs). Tab. 4 shows FedMosaic consistently outperforms baselines under cross-family heterogeneity, highlighting its generality. See Sec. A.14 for additional cross-family experiments.

**Fast Adaptation Evaluation.** In real-world scenarios, unseen tasks continuously emerge, making rapid adaptation crucial for future personalization. We evaluate adaptation speed by initializing models with each PFL method's aggregated model and fine-tuning on unseen tasks for 200 iterations. Fig. 6 shows that while sufficient training eventually yields similarly high performance regardless of initialization, models initialized with FedMosaic achieve high performance within few steps, highlighting enhanced generalizability through effective knowledge sharing in heterogeneous PFL.

**Large-Scale Evaluation of Heterogeneous PFL in LLMs**. Beyond multi-modal PFL, we evaluate FedMosaic in heterogeneous PFL for LLM training (*i.e.*, text-only NLP domain). Tab. 6 shows FedMosaic significantly outperforms baselines in both 'Self' and 'Others', consistent with our

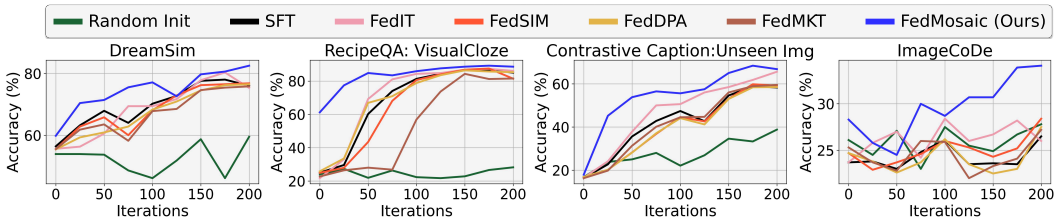


Figure 6: **Comparison of adaptation speed.** We use DRAKE's unseen tasks as downstream tasks. Random init starts from randomly initialized models, while other baselines are initialized from aggregated local models trained on DRAKE using each respective FL baseline.

| Method | Self | | Others | |
|---|---|---|---|---|
| | $A_{last}$ ↑ | $A_{\text{AUC}}$ ↑ | $A_{last}$ ↑ | $A_{\text{AUC}}$ ↑ |
| SFT | 18.03±0.52 | 17.11±0.56 | 14.18±0.69 | 13.70±0.35 |
| FedSim (ICML 2022) | 16.29±0.46 | 16.57±0.26 | 12.62±0.08 | 12.60±0.10 |
| FedIT (ICASSP 2024) | 17.10±0.20 | 16.83±0.37 | 14.03±0.49 | 13.68±0.32 |
| TAKFL (NeurIPS 2024) | 14.04±0.21 | 16.37±0.82 | 11.36±0.13 | 12.57±0.06 |
| FedDPA (NeurIPS 2024) | 17.60±0.25 | 16.66±0.42 | 13.98±0.05 | 13.66±0.07 |
| FedDAT (AAAI 2024) | 17.06±0.13 | 15.83±0.03 | 13.72±0.04 | 13.02±0.01 |
| PerAda (CVPR 2024) | 18.83±0.80 | 17.32±0.85 | 14.66±0.05 | 13.79±0.05 |
| FedMKT (COLING 2025) | 17.34±0.14 | 17.03±0.08 | 14.38±0.01 | 13.89±0.02 |
| FedMosaic (**Ours**) | **20.87±0.13** | **19.07±0.30** | **15.71±0.14** | **14.77±0.11** |

Table 6: **Large-Scale Experiments with 52 heterogeneous LLMs (Llama-1B/3B) on Fed-LLM-Large.**

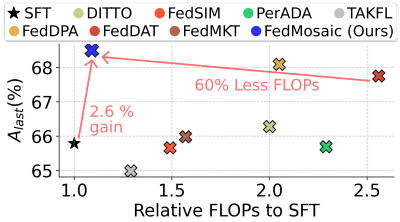


Figure 7: **Accuracy and relative FLOPs in DRAKE-Dynamic.**

| Method | DRAKE | | | | Fed-Scope | | | |
|---|---|---|---|---|---|---|---|---|
| | Self | | Others | | Self | | Others | |
| | $A_{last}$ ↑ | $A_{\text{AUC}}$ ↑ | $A_{last}$ ↑ | $A_{\text{AUC}}$ ↑ | $A_{last}$ ↑ | $A_{\text{AUC}}$ ↑ | $A_{last}$ ↑ | $A_{\text{AUC}}$ ↑ |
| Vanilla | 66.10±0.27 | 57.87±0.27 | 47.63±0.16 | 46.62±0.04 | 25.06±1.36 | 28.89±0.66 | 25.86±0.94 | 27.94±0.44 |
| (+) PQ-LoRA | 66.99±0.77 | 58.39±0.38 | **51.33±0.06** | 48.78±0.03 | 28.47±0.52 | 31.64±0.21 | 30.85±1.37 | 32.27±0.82 |
| (+) PQ-LoRA &RELA (**Ours**) | **67.86±0.51** | **59.83±0.16** | 51.16±0.04 | **49.36±0.08** | **30.58±0.84** | **32.68±0.64** | **31.01±1.46** | **32.50±0.62** |

Table 7: **Ablations for proposed components of FedMosaic in heterogeneous PFL.** 'Vanilla' aggregates homogeneous local models within each model type by averaging them with equal weights.

MLLM-FL benchmark results. This experiment involves 52 clients, highlighting the scalability of FedMosaic to large client populations and its applicability in real-world deployments.

**Computation and Communication Cost Analysis.** We compare accuracy and relative FLOPs in Fig. 7. FedMosaic demonstrates higher personalization performance with computation comparable to SFT. See Sec. A.8 and Sec. A.9 for detailed analyses of computation and communication costs.

**Additional Experiments.** Additional results include: heterogeneous PFL with LLaVA-Llama3.2-1B/3B/8B (Sec.A.11), LLaVA-Qwen2.5 variants (Sec.A.13), text-only benchmarks (Sec. A.15), homogeneous PFL setup (Sec. A.12), extended fast adaptation evaluations (Sec. A.23), comparison of RELA with similarity-aware aggregation methods (Sec. A.22), and client model selection details (Sec. A.3) and configurations (Sec. A.7). We further provide hyperparameter analysis Sec. A.18), effect of weight alignment in PQ-LoRA (Sec. A.21), effect of client model assignment (Sec. A.4), effect of decayed client-wise gradient $\hat{g}$ in RELA (Sec. A.19), and limitations (Sec. A.26).

**Ablation Study.** We ablate FedMosaic to investigate each proposed component's benefit, and summarize the results in Tab. 7. Our observations indicate that each component significantly enhances both the personalization ('Self') and the generalization ('Others') performance. Specifically, PQ-LoRA enhances generalization by transferring knowledge across heterogeneous architectures, while RELA improves personalization by promoting knowledge sharing among relevant-task models only.

## 7 Conclusion

We address both data heterogeneity and model heterogeneity in PFL while prior works tackle only one challenge or both under simplified assumptions. For that, we propose FedMosaic, which handles both forms of heterogeneity through two components: RELA and PQ-LoRA. Moreover, to better reflect real-world data heterogeneity in PFL scenarios, we introduce DRAKE, a comprehensive multi-modal FL benchmark capturing task heterogeneity and distribution shifts. Extensive evaluation shows FedMosaic achieves superior personalization compared to local training, while improving generalizability and few-shot adaptation capabilities essential for future personalization.

## REPRODUCIBILITY STATEMENT

We take reproducibility in deep learning very seriously and highlight some of the contents of the manuscript that might help to reproduce our work. We will definitely release our implementation of the proposed method in Sec. 4, benchmark in Sec. 5, and the data splits and the baselines used in our experiments in Sec. 6 in a public repository.

## THE USE OF LARGE LANGUAGE MODELS

We use large language models (LLMs) to support labor-intensive and mistake-prone work. Specifically, we use LLMs (*e.g.*, GPT-4) to categorize samples from a single dataset into multiple tasks based on keywords or topics, to assess generation quality in specific benchmarks using LLMs, and to detect grammatical errors during writing.

## REFERENCES

Samiul Alam, Luyang Liu, Ming Yan, and Mi Zhang. Fedrolex: Model-heterogeneous federated learning with rolling sub-model extraction. *NeurIPS*, 2022.

Mohammed Aljahdali, Ahmed M Abdelmoniem, Marco Canini, and Samuel Horváth. Flashback: Understanding and mitigating forgetting in federated learning. *arXiv preprint arXiv:2402.05558*, 2024.

Sheeraz A Alvi, Yi Hong, and Salman Durrani. Federated learning cost disparity for iot devices. In *ICC Workshops*, pp. 818–823. IEEE, 2022.

Stanislaw Antol, Aishwarya Agrawal, Jiasen Lu, Margaret Mitchell, Dhruv Batra, C Lawrence Zitnick, and Devi Parikh. Vqa: Visual question answering. In *ICCV*, pp. 2425–2433, 2015.

Haoping Bai, Shancong Mou, Tatiana Likhomanenko, Ramazan Gokberk Cinbis, Oncel Tuzel, Ping Huang, Jiulong Shan, Jianjun Shi, and Meng Cao. Vision datasets: A benchmark for vision-based industrial inspection. *arXiv preprint arXiv:2306.07890*, 2023.

Jiamu Bai, Daoyuan Chen, Bingchen Qian, Liuyi Yao, and Yaliang Li. Federated fine-tuning of large language models under heterogeneous tasks and client resources. In *NeurIPS*, 2024.

Kasra Borazjani, Payam Abdisarabshali, Naji Khosravan, and Seyyedali Hosseinalipour. Redefining non-iid data in federated learning for computer vision tasks: Migrating from labels to embeddings for task-specific data distributions. *arXiv preprint arXiv:2503.14553*, 2025.

Markus Ralf Bujotzek, Ünal Akünal, Stefan Denner, Peter Neher, Maximilian Zenk, Eric Frodl, Astha Jaiswal, Moon Kim, Nicolai R Krekiehn, Manuel Nickel, et al. Real-world federated learning in radiology: hurdles to overcome and benefits to gain. *Journal of the American Medical Informatics Association*, 2025.

Haokun Chen, Yao Zhang, Denis Krompass, Jindong Gu, and Volker Tresp. Feddat: An approach for foundation model finetuning in multi-modal heterogeneous federated learning. In *AAAI*, volume 38, pp. 11285–11293, 2024.

Mark Chen, Jerry Tworek, Heewoo Jun, Qiming Yuan, Henrique Ponde De Oliveira Pinto, Jared Kaplan, Harri Edwards, Yuri Burda, Nicholas Joseph, Greg Brockman, et al. Evaluating large language models trained on code. *arXiv preprint arXiv:2107.03374*, 2021.

Hsiang-Yun Sherry Chien, Javier S Turek, Nicole Beckage, Vy A Vo, Christopher J Honey, and Ted L Willke. Slower is better: revisiting the forgetting mechanism in lstm for slower information decay. *arXiv preprint arXiv:2105.05944*, 2021.

Yae Jee Cho, Andre Manoel, Gauri Joshi, Robert Sim, and Dimitrios Dimitriadis. Heterogeneous ensemble knowledge transfer for training large models in federated learning. In *IJCAI*, 2022.

Yae Jee Cho, Luyang Liu, Zheng Xu, Aldi Fahrezi, and Gauri Joshi. Heterogeneous lora for federated fine-tuning of on-device foundation models. In *EMNLP*, pp. 12903–12913, 2024.

Karl Cobbe, Vineet Kosaraju, Mohammad Bavarian, Mark Chen, Heewoo Jun, Lukasz Kaiser, Matthias Plappert, Jerry Tworek, Jacob Hilton, Reiichiro Nakano, et al. Training verifiers to solve math word problems. *arXiv preprint arXiv:2110.14168*, 2021.

Liam Collins, Shanshan Wu, Sewoong Oh, and Khe Chai Sim. Profit: Benchmarking personalization and robustness trade-off in federated prompt tuning. In *NeurIPSW*, 2023.

Tijl De Bie, Nello Cristianini, and Roman Rosipal. *Eigenproblems in Pattern Recognition*, pp. 129–167. Springer Berlin Heidelberg, Berlin, Heidelberg, 2005. ISBN 978-3-540-28247-1. doi: 10.1007/3-540-28247-5_5. URL https://doi.org/10.1007/3-540-28247-5_5.

Li Deng. The mnist database of handwritten digit images for machine learning research. *IEEE Signal Processing Magazine*, pp. 141–142, 2012.

Chuntao Ding, Xu Cao, Jianhang Xie, Linlin Fan, Shangguang Wang, and Zhichao Lu. Lora-c: Parameter-efficient fine-tuning of robust cnn for iot devices. *arXiv preprint arXiv:2410.16954*, 2024.

Nathaniel J Evans, Gordon B Mills, Guanming Wu, Xubo Song, and Shannon McWeeney. Data valuation with gradient similarity. *ArXiv*, pp. arXiv–2405, 2024.

Boyu Fan, Chenrui Wu, Xiang Su, and Pan Hui. Fedtsa: A cluster-based two-stage aggregation method for model-heterogeneous federated learning. In *ECCV*. Springer, 2024.

Tao Fan, Guoqiang Ma, Yan Kang, Hanlin Gu, Yuanfeng Song, Lixin Fan, Kai Chen, and Qiang Yang. Fedmkt: Federated mutual knowledge transfer for large and small language models. In *COLING*, 2025.

Xiuwen Fang, Mang Ye, and Xiyuan Yang. Robust heterogeneous federated learning under data corruption. In *ICCV*, 2023.

Tiantian Feng, Digbalay Bose, Tuo Zhang, Rajat Hebbar, Anil Ramakrishna, Rahul Gupta, Mi Zhang, Salman Avestimehr, and Shrikanth Narayanan. Fedmultimodal: A benchmark for multimodal federated learning. In *Proceedings of the 29th ACM SIGKDD conference on knowledge discovery and data mining*, pp. 4035–4045, 2023.

Chelsea Finn, Pieter Abbeel, and Sergey Levine. Model-agnostic meta-learning for fast adaptation of deep networks. In *ICML*, pp. 1126–1135. PMLR, 2017.

Chaoyou Fu, Peixian Chen, Yunhang Shen, Yulei Qin, Mengdan Zhang, Xu Lin, Jinrui Yang, Xiawu Zheng, Ke Li, Xing Sun, Yunsheng Wu, and Rongrong Ji. Mme: A comprehensive evaluation benchmark for multimodal large language models. *arXiv preprint arXiv:2306.13394*, 2023a.

Stephanie Fu, Netanel Tamir, Shobhita Sundaram, Lucy Chai, Richard Zhang, Tali Dekel, and Phillip Isola. Dreamsim: Learning new dimensions of human visual similarity using synthetic data. *arXiv preprint arXiv:2306.09344*, 2023b.

Noa Garcia, Chentao Ye, Zihua Liu, Qingtao Hu, Mayu Otani, Chenhui Chu, Yuta Nakashima, and Teruko Mitamura. A dataset and baselines for visual question answering on art. In *ECCV Workshops*, pp. 92–108. Springer, 2020.

Saurabh Garg, Mehrdad Farajtabar, Hadi Pouransari, Raviteja Vemulapalli, Sachin Mehta, Oncel Tuzel, Vaishaal Shankar, and Fartash Faghri. Tic-clip: Continual training of clip models. In *ICLR*, 2024.

Pouya M. Ghari and Yanning Shen. Personalized federated learning with mixture of models for adaptive prediction and model fine-tuning. In *NeurIPS*, 2024.

Yash Goyal, Tejas Khot, Douglas Summers-Stay, Dhruv Batra, and Devi Parikh. Making the v in vqa matter: Elevating the role of image understanding in visual question answering. In *CVPR*, pp. 6904–6913, 2017.

Aaron Grattafiori, Abhimanyu Dubey, Abhinav Jauhri, Abhinav Pandey, Abhishek Kadian, Ahmad Al-Dahle, Aiesha Letman, Akhil Mathur, Alan Schelten, Alex Vaughan, et al. The llama 3 herd of models. *arXiv preprint arXiv:2407.21783*, 2024.

Pengxin Guo, Shuang Zeng, Yanran Wang, Huijie Fan, Feifei Wang, and Liangqiong Qu. Selective aggregation for low-rank adaptation in federated learning. In *ICLR*, 2025.

Danna Gurari, Qing Li, Abigale J Stangl, Anhong Guo, Chi Lin, Kristen Grauman, Jiebo Luo, and Jeffrey P Bigham. Vizwiz grand challenge: Answering visual questions from blind people. In *CVPR*, pp. 3608–3617, 2018.

Naresh Kumar Gurulingan, Elahe Arani, and Bahram Zonooz. Curbing task interference using representation similarity-guided multi-task feature sharing. In *CoLLAs*, pp. 937–951. PMLR, 2022.

Xintong Han, Zuxuan Wu, Phoenix X Huang, Xiao Zhang, Menglong Zhu, Yuan Li, Yang Zhao, and Larry S Davis. Automatic spatially-aware fashion concept discovery. In *ICCV*, pp. 1463–1471, 2017.

Junxian He, Chunting Zhou, Xuezhe Ma, Taylor Berg-Kirkpatrick, and Graham Neubig. Towards a unified view of parameter-efficient transfer learning. In *ICLR*, 2022.

Dan Hendrycks, Collin Burns, Steven Basart, Andy Zou, Mantas Mazeika, Dawn Song, and Jacob Steinhardt. Measuring massive multitask language understanding. *arXiv preprint arXiv:2009.03300*, 2020.

Edward J Hu, Phillip Wallis, Zeyuan Allen-Zhu, Yuanzhi Li, Shean Wang, Lu Wang, Weizhu Chen, et al. Lora: Low-rank adaptation of large language models. In *ICLR*, 2022.

Kai Hu, Sheng Gong, Qi Zhang, Chaowen Seng, Min Xia, and Shanshan Jiang. An overview of implementing security and privacy in federated learning. *Artificial Intelligence Review*, 57(8):204, 2024.

Wei Hu, Lechao Xiao, and Jeffrey Pennington. Provable benefit of orthogonal initialization in optimizing deep linear networks. In *ICLR*, 2020.

Drew A Hudson and Christopher D Manning. Gqa: A new dataset for real-world visual reasoning and compositional question answering. In *CVPR*, pp. 6700–6709, 2019.

Mude Hui, Siwei Yang, Bingchen Zhao, Yichun Shi, Heng Wang, Peng Wang, Cihang Xie, and Yuyin Zhou. HQ-edit: A high-quality dataset for instruction-based image editing. In *ICLR*, 2025. URL https://openreview.net/forum?id=mZptYYttFj.

Aaron Hurst, Adam Lerer, Adam P Goucher, Adam Perelman, Aditya Ramesh, Aidan Clark, AJ Ostrow, Akila Welihinda, Alan Hayes, Alec Radford, et al. Gpt-4o system card. *arXiv preprint arXiv:2410.21276*, 2024.

Phillip Isola, Joseph J Lim, and Edward H Adelson. Discovering states and transformations in image collections. In *CVPR*, pp. 1383–1391, 2015.

Mohit Iyyer, Varun Manjunatha, Anupam Guha, Yogarshi Vyas, Jordan Boyd-Graber, Hal Daume, and Larry S Davis. The amazing mysteries of the gutter: Drawing inferences between panels in comic book narratives. In *CVPR*, pp. 7186–7195, 2017.

Adrián Javaloy and Isabel Valera. Rotograd: Gradient homogenization in multitask learning. In *ICLR*, 2022. URL https://openreview.net/forum?id=T8wHz4rnuGL.

Dongfu Jiang, Xuan He, Huaye Zeng, Cong Wei, Max Ku, Qian Liu, and Wenhu Chen. Mantis: Interleaved multi-image instruction tuning. *TMLR*, 2024. ISSN 2835-8856. URL https://openreview.net/forum?id=skLtdUVaJa.

Huaizu Jiang, Xiaojian Ma, Weili Nie, Zhiding Yu, Yuke Zhu, and Anima Anandkumar. Bongard-hoi: Benchmarking few-shot visual reasoning for human-object interactions. In *CVPR*, pp. 19056–19065, 2022.

Keller Jordan, Hanie Sedghi, Olga Saukh, Rahim Entezari, and Behnam Neyshabur. Repair: Renormalizing permuted activations for interpolation repair. In *ICLR*, 2023.

Kushal Kafle, Brian Price, Scott Cohen, and Christopher Kanan. Dvqa: Understanding data visualizations via question answering. In *CVPR*, pp. 5648–5656, 2018.

Aniruddha Kembhavi, Minjoon Seo, Dustin Schwenk, Jonghyun Choi, Ali Farhadi, and Hannaneh Hajishirzi. Are you smarter than a sixth grader? textbook question answering for multimodal machine comprehension. In *CVPR*, pp. 4999–5007, 2017.

Hyunseo Koh, Dahyun Kim, Jung-Woo Ha, and Jonghyun Choi. Online continual learning on class incremental blurry task configuration with anytime inference. In *ICLR*, 2022.

Hyunseo Koh, Minhyuk Seo, Jihwan Bang, Hwanjun Song, Deokki Hong, Seulki Park, Jung-Woo Ha, and Jonghyun Choi. Online boundary-free continual learning by scheduled data prior. In *ICLR*, 2023.

Simon Kornblith, Mohammad Norouzi, Honglak Lee, and Geoffrey Hinton. Similarity of neural network representations revisited. In *ICML*, pp. 3519–3529. PMLR, 2019.

Benno Krojer, Vaibhav Adlakha, Vibhav Vineet, Yash Goyal, Edoardo Ponti, and Siva Reddy. Image retrieval from contextual descriptions. In Smaranda Muresan, Preslav Nakov, and Aline Villavicencio (eds.), *ACL*, Dublin, Ireland, May 2022. Association for Computational Linguistics.

Weirui Kuang, Bingchen Qian, Zitao Li, Daoyuan Chen, Dawei Gao, Xuchen Pan, Yuexiang Xie, Yaliang Li, Bolin Ding, and Jingren Zhou. Federatedscope-llm: A comprehensive package for fine-tuning large language models in federated learning. In *Proceedings of the 30th ACM SIGKDD Conference on Knowledge Discovery and Data Mining*, pp. 5260–5271, 2024.

Allison Lau, Younwoo Choi, Vahid Balazadeh, Keertana Chidambaram, Vasilis Syrgkanis, and Rahul Krishnan. Personalized adaptation via in-context preference learning. In *Adaptive Foundation Models: Evolving AI for Personalized and Efficient Learning*, 2024.

Jaewoo Lee, Boyang Li, and Sung Ju Hwang. Concept-skill transferability-based data selection for large vision-language models. In *EMNLP*, 2024.

Bohao Li, Rui Wang, Guangzhi Wang, Yuying Ge, Yixiao Ge, and Ying Shan. Seed-bench: Benchmarking multimodal llms with generative comprehension. *arXiv preprint arXiv:2307.16125*, 2023a.

Bohao Li, Yuying Ge, Yixiao Ge, Guangzhi Wang, Rui Wang, Ruimao Zhang, and Ying Shan. Seed-bench: Benchmarking multimodal large language models. In *CVPR*, pp. 13299–13308, 2024a.

Daliang Li and Junpu Wang. Fedmd: Heterogenous federated learning via model distillation. *arXiv preprint arXiv:1910.03581*, 2019.

Hongyang Li, Caesar Wu, Mohammed Chadli, Said Mammar, and Pascal Bouvry. Trustworthiness of stochastic gradient descent in distributed learning. *arXiv preprint arXiv:2410.21491*, 2024b.

Juncheng Li, Kaihang Pan, Zhiqi Ge, Minghe Gao, Wei Ji, Wenqiao Zhang, Tat-Seng Chua, Siliang Tang, Hanwang Zhang, and Yueting Zhuang. Fine-tuning multimodal LLMs to follow zero-shot demonstrative instructions. In *ICLR*, 2024c. URL https://openreview.net/forum?id=BXY6fe7q31.

Juncheng Li, Kaihang Pan, Zhiqi Ge, Minghe Gao, Wei Ji, Wenqiao Zhang, Tat-Seng Chua, Siliang Tang, Hanwang Zhang, and Yueting Zhuang. Fine-tuning multimodal LLMs to follow zero-shot demonstrative instructions. In *ICLR*, 2024d.

Lin Li, Jianping Gou, Baosheng Yu, Lan Du, and Zhang Yiand Dacheng Tao. Federated distillation: A survey. *arXiv preprint arXiv:2404.08564*, 2024e.

Sheng Li, Geng Yuan, Yue Dai, Youtao Zhang, Yanzhi Wang, and Xulong Tang. SmartFRZ: An efficient training framework using attention-based layer freezing. In *ICLR*, 2023b. URL https://openreview.net/forum?id=i9UlAr1T_xl.

Tian Li, Shengyuan Hu, Ahmad Beirami, and Virginia Smith. Ditto: Fair and robust federated learning through personalization. In *ICML*, pp. 6357–6368. PMLR, 2021.

Yifan Li, Yifan Du, Kun Zhou, Jinpeng Wang, Wayne Xin Zhao, and Ji-Rong Wen. Evaluating object hallucination in large vision-language models. *arXiv preprint arXiv:2305.10355*, 2023c.

Zexi Li, Tao Lin, Xinyi Shang, and Chao Wu. Revisiting weighted aggregation in federated learning with neural networks. In *ICML*, pp. 19767–19788. PMLR, 2023d.

Chin-Yew Lin. Rouge: A package for automatic evaluation of summaries. In *Text summarization branches out*, pp. 74–81, 2004.

Yang Lin, Xinyu Ma, Xu Chu, Yujie Jin, Zhibang Yang, Yasha Wang, and Hong Mei. Lora dropout as a sparsity regularizer for overfitting control. *CoRR*, 2024.

Fangyu Liu, Guy Emerson, and Nigel Collier. Visual spatial reasoning. *Transactions of the Association for Computational Linguistics*, 11:635–651, 2023a.

Haotian Liu, Chunyuan Li, Qingyang Wu, and Yong Jae Lee. Visual instruction tuning. *Advances in neural information processing systems*, 36:34892–34916, 2023b.

Yuan Liu, Haodong Duan, Yuanhan Zhang, Bo Li, Songyang Zhang, Wangbo Zhao, Yike Yuan, Jiaqi Wang, Conghui He, Ziwei Liu, et al. Mmbench: Is your multi-modal model an all-around player? In *ECCV*, pp. 216–233. Springer, 2024.

Zheyuan Liu, Cristian Rodriguez-Opazo, Damien Teney, and Stephen Gould. Image retrieval on real-life images with pre-trained vision-and-language models. In *ICCV*, pp. 2125–2134, 2021.

Guodong Long, Tao Shen, Jing Jiang, Michael Blumenstein, et al. Dual-personalizing adapter for federated foundation models. *Advances in Neural Information Processing Systems*, 37:39409–39433, 2024.

Ilya Loshchilov and Frank Hutter. Decoupled weight decay regularization. In *ICLR*, 2019.

Pan Lu, Liang Qiu, Jiaqi Chen, Tony Xia, Yizhou Zhao, Wei Zhang, Zhou Yu, Xiaodan Liang, and Song-Chun Zhu. Iconqa: A new benchmark for abstract diagram understanding and visual language reasoning. In *NeurIPS 2021*, 2021.

Pan Lu, Swaroop Mishra, Tanglin Xia, Liang Qiu, Kai-Wei Chang, Song-Chun Zhu, Oyvind Tafjord, Peter Clark, and Ashwin Kalyan. Learn to explain: Multimodal reasoning via thought chains for science question answering. *NeurIPS*, 35:2507–2521, 2022.

Yuxiang Lu, Suizhi Huang, Yuwen Yang, Shalayiding Sirejiding, Yue Ding, and Hongtao Lu. Fedhca2: Towards hetero-client federated multi-task learning. In *Proceedings of the IEEE/CVF Conference on Computer Vision and Pattern Recognition*, pp. 5599–5609, 2024.

Lingjuan Lyu, Han Yu, Xingjun Ma, Chen Chen, Lichao Sun, Jun Zhao, Qiang Yang, and Philip S Yu. Privacy and robustness in federated learning: Attacks and defenses. *IEEE transactions on neural networks and learning systems*, 2022.

Hussain Ahmad Madni, Rao Muhammad Umer, and Gian Luca Foresti. Exploiting data diversity in multi-domain federated learning. *Machine Learning: Science and Technology*, 5(2):025041, 2024.

Shivangi Mahto, Vy Ai Vo, Javier S Turek, and Alexander Huth. Multi-timescale representation learning in lstm language models. In *ICLR*, 2021.

Sadhika Malladi, Tianyu Gao, Eshaan Nichani, Alex Damian, Jason D Lee, Danqi Chen, and Sanjeev Arora. Fine-tuning language models with just forward passes. *NeurIPS*, 2023.

Michael McCloskey and Neal J. Cohen. Catastrophic interference in connectionist networks: The sequential learning problem. volume 24 of *Psychology of Learning and Motivation*, pp. 109–165. Academic Press, 1989.

Brendan McMahan, Eider Moore, Daniel Ramage, Seth Hampson, and Blaise Aguera y Arcas. Communication-efficient learning of deep networks from decentralized data. In *AISTATS*. PMLR, 2017.

Fan Mo, Anastasia Borovykh, Mohammad Malekzadeh, Soteris Demetriou, Deniz Gündüz, and Hamed Haddadi. Quantifying and localizing usable information leakage from neural network gradients. *arXiv preprint arXiv:2105.13929*, 2021.

Mahdi Morafah, Vyacheslav Kungurtsev, Hojin Matthew Chang, Chen Chen, and Bill Lin. Towards diverse device heterogeneous federated learning via task arithmetic knowledge integration. In *NeurIPS*, 2024.

Marius Mosbach, Maksym Andriushchenko, and Dietrich Klakow. On the stability of fine-tuning {bert}: Misconceptions, explanations, and strong baselines. In *ICLR*, 2021.

Aviv Navon, Aviv Shamsian, Idan Achituve, Haggai Maron, Kenji Kawaguchi, Gal Chechik, and Ethan Fetaya. Multi-task learning as a bargaining game. In *ICML*, pp. 16428–16446. PMLR, 2022.

Behnam Neyshabur, Hanie Sedghi, and Chiyuan Zhang. What is being transferred in transfer learning? *Advances in neural information processing systems*, 2020.

Aleksandra Nowak, Łukasz Gniecki, Filip Szatkowski, and Jacek Tabor. Sparser, better, deeper, stronger: Improving static sparse training with exact orthogonal initialization. In *ICML*. PMLR, 2024.

Krishna Pillutla, Kshitiz Malik, Abdel-Rahman Mohamed, Mike Rabbat, Maziar Sanjabi, and Lin Xiao. Federated learning with partial model personalization. In *ICML*, pp. 17716–17758. PMLR, 2022.

Ameya Prabhu, Zhipeng Cai, Puneet Dokania, Philip Torr, Vladlen Koltun, and Ozan Sener. Online continual learning without the storage constraint. *arXiv preprint arXiv:2305.09253*, 2023.

Daiqing Qi, Handong Zhao, and Sheng Li. Better generative replay for continual federated learning. In *ICLR*, 2023.

Jiaxing Qi, Zhongzhi Luan, Shaohan Huang, Carol Fung, Hailong Yang, and Depei Qian. Fdlora: personalized federated learning of large language model via dual lora tuning. *arXiv preprint arXiv:2406.07925*, 2024.

Shuzhen Rao, Jun Huang, and Zengming Tang. Adaptive regularized warped gradient descent enhances model generalization and meta-learning for few-shot learning. *Neurocomputing*, 537: 271–281, 2023. ISSN 0925-2312.

Roger Ratcliff. Connectionist models of recognition memory: constraints imposed by learning and forgetting functions. *Psychological review*, 97(2):285, 1990.

Mengye Ren, Ryan Kiros, and Richard Zemel. Exploring models and data for image question answering. *NeurIPS*, 28, 2015.

Jonathan Scott, Hossein Zakerinia, and Christoph H Lampert. Pefll: Personalized federated learning by learning to learn. In *ICLR*, 2024.

Minhyuk Seo, Hyunseo Koh, Wonje Jeung, Minjae Lee, San Kim, Hankook Lee, Sungjun Cho, Sungik Choi, Hyunwoo Kim, and Jonghyun Choi. Learning equi-angular representations for online continual learning. In *CVPR*, pp. 23933–23942, 2024.

Minhyuk Seo, Hyunseo Koh, and Jonghyun Choi. Budgeted online continual learning by adaptive layer freezing and frequency-based sampling. In *ICLR*, 2025.

Amanpreet Singh, Vivek Natarajan, Meet Shah, Yu Jiang, Xinlei Chen, Dhruv Batra, Devi Parikh, and Marcus Rohrbach. Towards vqa models that can read. In *CVPR*, pp. 8317–8326, 2019.

Shivalika Singh, Freddie Vargus, Daniel D'souza, Börje Karlsson, Abinaya Mahendiran, Wei-Yin Ko, Herumb Shandilya, Jay Patel, Deividas Mataciunas, Laura O'Mahony, et al. Aya dataset: An open-access collection for multilingual instruction tuning. In *ACL*, 2024.

Virginia Smith, Chao-Kai Chiang, Maziar Sanjabi, and Ameet S Talwalkar. Federated multi-task learning. *NeurIPS*, 30, 2017.

George Stoica, Pratik Ramesh, Boglarka Ecsedi, Leshem Choshen, and Judy Hoffman. Model merging with SVD to tie the knots. In *ICLR*, 2025.

Alane Suhr, Stephanie Zhou, Ally Zhang, Iris Zhang, Huajun Bai, and Yoav Artzi. A corpus for reasoning about natural language grounded in photographs. In Anna Korhonen, David Traum, and Lluís Màrquez (eds.), *ACL*, pp. 6418–6428, Florence, Italy, July 2019. Association for Computational Linguistics. doi: 10.18653/v1/P19-1644. URL https://aclanthology.org/P19-1644/.

Youbang Sun, Zitao Li, Yaliang Li, and Bolin Ding. Improving lora in privacy-preserving federated learning. In *ICLR*, 2024.

Rishub Tamirisa, Chulin Xie, Wenxuan Bao, Andy Zhou, Ron Arel, and Aviv Shamsian. Fedselect: Personalized federated learning with customized selection of parameters for fine-tuning. In *CVPR*, 2024.

Jiahao Tan, Yipeng Zhou, Gang Liu, Jessie Hui Wang, and Shui Yu. pfedsim: Similarity-aware model aggregation towards personalized federated learning. *arXiv preprint arXiv:2305.15706*, 2023.

Shuai Tang, Wesley J Maddox, Charlie Dickens, Tom Diethe, and Andreas Damianou. Similarity of neural networks with gradients. *arXiv preprint arXiv:2003.11498*, 2020.

Gemini Team, Petko Georgiev, Ving Ian Lei, Ryan Burnell, Libin Bai, Anmol Gulati, Garrett Tanzer, Damien Vincent, Zhufeng Pan, Shibo Wang, et al. Gemini 1.5: Unlocking multimodal understanding across millions of tokens of context. *arXiv preprint arXiv:2403.05530*, 2024.

Jiaqi Wang, Xingyi Yang, Suhan Cui, Liwei Che, Lingjuan Lyu, Dongkuan DK Xu, and Fenglong Ma. Towards personalized federated learning via heterogeneous model reassembly. *Advances in Neural Information Processing Systems*, 36:29515–29531, 2023.

Penghao Wang, Qian Chen, Teng Zhang, Yingwei Zhang, Wang Lu, and Yiqiang Chen. Fhbench: Towards efficient and personalized federated learning for multimodal healthcare. *arXiv preprint arXiv:2504.10817*, 2025.

Yongxian Wei, Anke Tang, Li Shen, Chun Yuan, and Xiaochun Cao. Modeling multi-task model merging as adaptive projective gradient descent. *arXiv preprint arXiv:2501.01230*, 2025.

Genta Indra Winata, Frederikus Hudi, Patrick Amadeus Irawan, David Anugraha, Rifki Afina Putri, Yutong Wang, Adam Nohejl, Ubaidillah Ariq Prathama, Nedjma Ousidhoum, Afifa Amriani, et al. Worldcuisines: A massive-scale benchmark for multilingual and multicultural visual question answering on global cuisines. *arXiv preprint arXiv:2410.12705*, 2024.

Mitchell Wortsman, Gabriel Ilharco, Samir Ya Gadre, Rebecca Roelofs, Raphael Gontijo-Lopes, Ari S Morcos, Hongseok Namkoong, Ali Farhadi, Yair Carmon, Simon Kornblith, et al. Model soups: averaging weights of multiple fine-tuned models improves accuracy without increasing inference time. In *ICML*, pp. 23965–23998. PMLR, 2022a.

Mitchell Wortsman, Gabriel Ilharco, Jong Wook Kim, Mike Li, Simon Kornblith, Rebecca Roelofs, Raphael Gontijo Lopes, Hannaneh Hajishirzi, Ali Farhadi, Hongseok Namkoong, et al. Robust fine-tuning of zero-shot models. In *CVPR*, 2022b.

Stanisław Woźniak, Bartłomiej Koptyra, Arkadiusz Janz, Przemysław Kazienko, and Jan Kocoń. Personalized large language models. *arXiv preprint arXiv:2402.09269*, 2024.

Feijie Wu, Xingchen Wang, Yaqing Wang, Tianci Liu, Lu Su, and Jing Gao. Fiarse: Model-heterogeneous federated learning via importance-aware submodel extraction. In *NeurIPS*, 2024a.

Haoning Wu, Hanwei Zhu, Zicheng Zhang, Erli Zhang, Chaofeng Chen, Liang Liao, Chunyi Li, Annan Wang, Wenxiu Sun, Qiong Yan, et al. Towards open-ended visual quality comparison. In *ECCV*, pp. 360–377. Springer, 2024b.

Hui Wu, Yupeng Gao, Xiaoxiao Guo, Ziad Al-Halah, Steven Rennie, Kristen Grauman, and Rogerio Feris. Fashion iq: A new dataset towards retrieving images by natural language feedback. In *CVPR*, pp. 11307–11317, 2021.

Junda Wu, Hanjia Lyu, Yu Xia, Zhehao Zhang, Joe Barrow, Ishita Kumar, Mehrnoosh Mirtaheri, Hongjie Chen, Ryan A Rossi, Franck Dernoncourt, et al. Personalized multimodal large language models: A survey. *arXiv preprint arXiv:2412.02142*, 2024c.

Rujie Wu, Xiaojian Ma, Zhenliang Zhang, Wei Wang, Qing Li, Song-Chun Zhu, and Yizhou Wang. Bongard-openworld: Few-shot reasoning for free-form visual concepts in the real world. In *ICLR*, 2024d. URL https://openreview.net/forum?id=hWS4MueyzC.

Abudukelimu Wuerkaixi, Sen Cui, Jingfeng Zhang, Kunda Yan, Bo Han, Gang Niu, Lei Fang, Changshui Zhang, and Masashi Sugiyama. Accurate forgetting for heterogeneous federated continual learning. In *ICLR*, 2024.

Chulin Xie, De-An Huang, Wenda Chu, Daguang Xu, Chaowei Xiao, Bo Li, and Anima Anandkumar. Perada: Parameter-efficient federated learning personalization with generalization guarantees. In *CVPR*, 2024.

Ning Xie, Farley Lai, Derek Doran, and Asim Kadav. Visual entailment: A novel task for fine-grained image understanding. *arXiv preprint arXiv:1901.06706*, 2019.

Binqian Xu, Xiangbo Shu, Haiyang Mei, Guosen Xie, Basura Fernando, and Jinhui Tang. Fedmllm: Federated fine-tuning mllm on multimodal heterogeneity data. *arXiv preprint arXiv:2411.14717*, 2024.

Prateek Yadav, Derek Tam, Leshem Choshen, Colin A Raffel, and Mohit Bansal. Ties-merging: Resolving interference when merging models. *NeurIPS*, 2023.

Semih Yagcioglu, Aykut Erdem, Erkut Erdem, and Nazli Ikizler-Cinbis. RecipeQA: A challenge dataset for multimodal comprehension of cooking recipes. In Ellen Riloff, David Chiang, Julia Hockenmaier, and Jun'ichi Tsujii (eds.), *EMNLP*. Association for Computational Linguistics, October-November 2018.

An Yang, Baosong Yang, Beichen Zhang, Binyuan Hui, Bo Zheng, Bowen Yu, Chengyuan Li, Dayiheng Liu, Fei Huang, Haoran Wei, et al. Qwen2. 5 technical report. *arXiv preprint arXiv:2412.15115*, 2024a.

Enneng Yang, Li Shen, Guibing Guo, Xingwei Wang, Xiaochun Cao, Jie Zhang, and Dacheng Tao. Model merging in llms, mllms, and beyond: Methods, theories, applications and opportunities. *arXiv preprint arXiv:2408.07666*, 2024b.

Qiang Yang, Anbu Huang, Lixin Fan, Chee Seng Chan, Jian Han Lim, Kam Woh Ng, Ding Sheng Ong, and Bowen Li. Federated learning with privacy-preserving and model ip-right-protection. *Machine Intelligence Research*, 20(1):19–37, 2023. ISSN 2731-538X. doi: 10.1007/s11633-022-1343-2. URL https://www.mi-research.net/en/article/doi/10.1007/s11633-022-1343-2.

Dixi Yao. Exploring system-heterogeneous federated learning with dynamic model selection. *arXiv preprint arXiv:2409.08858*, 2024.

Rui Ye, Rui Ge, Xinyu Zhu, Jingyi Chai, Du Yaxin, Yang Liu, Yanfeng Wang, and Siheng Chen. Fedllm-bench: Realistic benchmarks for federated learning of large language models. *NeurIPS*, 37:111106–111130, 2024.

Shih-Ying Yeh, Yu-Guan Hsieh, Zhidong Gao, Bernard BW Yang, Giyeong Oh, and Yanmin Gong. Navigating text-to-image customization: From lycoris fine-tuning to model evaluation. In *The Twelfth International Conference on Learning Representations*, 2023.

Liping Yi, Gang Wang, Xiaoguang Liu, Zhuan Shi, and Han Yu. Fedgh: Heterogeneous federated learning with generalized global header. In *ACM Multimedia*, pp. 8686–8696, 2023.

Jaehong Yoon, Wonyong Jeong, Giwoong Lee, Eunho Yang, and Sung Ju Hwang. Federated continual learning with weighted inter-client transfer. In *ICML*, pp. 12073–12086. PMLR, 2021.

Ron Yosef, Yonatan Bitton, and Dafna Shahaf. IRFL: Image recognition of figurative language. In Houda Bouamor, Juan Pino, and Kalika Bali (eds.), *EMNLP*, pp. 1044–1058, Singapore, December 2023. Association for Computational Linguistics. doi: 10.18653/v1/2023.findings-emnlp.74. URL https://aclanthology.org/2023.findings-emnlp.74/.

Jiahui Yu, Zirui Wang, Vijay Vasudevan, Legg Yeung, Mojtaba Seyedhosseini, and Yonghui Wu. Coca: Contrastive captioners are image-text foundation models. *arXiv preprint arXiv:2205.01917*, 2022.

Weihao Yu, Zhengyuan Yang, Linjie Li, Jianfeng Wang, Kevin Lin, Zicheng Liu, Xinchao Wang, and Lijuan Wang. Mm-vet: Evaluating large multimodal models for integrated capabilities. *arXiv preprint arXiv:2308.02490*, 2023.

Betul Yurdem, Murat Kuzlu, Mehmet Kemal Gullu, Ferhat Ozgur Catak, and Maliha Tabassum. Federated learning: Overview, strategies, applications, tools and future directions. *Heliyon*, 2024.

Jianyi Zhang, Saeed Vahidian, Martin Kuo, Chunyuan Li, Ruiyi Zhang, Tong Yu, Guoyin Wang, and Yiran Chen. Towards building the federatedgpt: Federated instruction tuning. In *ICASSP*. IEEE, 2024a.

Jiarui Zhang. Guided profile generation improves personalization with llms. In *ACL*, 2024.

Kai Zhang, Lingbo Mo, Wenhu Chen, Huan Sun, and Yu Su. Magicbrush: A manually annotated dataset for instruction-guided image editing. *Advances in Neural Information Processing Systems*, 36:31428–31449, 2023a.

Yukun Zhang, Guanzhong Chen, Zenglin Xu, Jianyong Wang, Dun Zeng, Junfan Li, Jinghua Wang, Yuan Qi, and Irwin King. Fedcvd: The first real-world federated learning benchmark on cardiovascular disease data. *arXiv preprint arXiv:2411.07050*, 2024b.

Zhehao Zhang, Ryan A Rossi, Branislav Kveton, Yijia Shao, Diyi Yang, Hamed Zamani, Franck Dernoncourt, Joe Barrow, Tong Yu, Sungchul Kim, et al. Personalization of large language models: A survey. *arXiv preprint arXiv:2411.00027*, 2024c.

Zhuo Zhang, Xiangjing Hu, Jingyuan Zhang, Yating Zhang, Hui Wang, Lizhen Qu, and Zenglin Xu. Fedlegal: The first real-world federated learning benchmark for legal nlp. In *ACL*, pp. 3492–3507, 2023b.

Lianmin Zheng, Wei-Lin Chiang, Ying Sheng, Siyuan Zhuang, Zhanghao Wu, Yonghao Zhuang, Zi Lin, Zhuohan Li, Dacheng Li, Eric Xing, et al. Judging llm-as-a-judge with mt-bench and chatbot arena. *Advances in neural information processing systems*, 36:46595–46623, 2023.

Ligeng Zhu, Zhijian Liu, and Song Han. Deep leakage from gradients. *NeurIPS*, 32, 2019.

# A TECHNICAL APPENDICES AND SUPPLEMENTARY MATERIAL

This document provides a comprehensive overview of the technical appendices

**Theoretical Foundations**

- **Section A.1:** Theoretical justification for freezing matrices $A$ and $B$ in PQ-LoRA, proving that this approach achieves zero aggregation error in federated learning.
- **Section A.2:** Proof of Theorem 1 showing that orthogonal initialization of $A$ and $B$ maximizes the representational capacity of PQ-LoRA.

**Implementation Details**

- **Section A.3:** Details on client model selection methodology in heterogeneous PFL scenarios.
- **Section A.4:** Consistency of FedMosaic over diverse random heterogeneous PFL scenarios.
- **Section A.5:** In-depth explanation of PQ-LoRA, including initialization with orthogonal sets, weight alignment, and orthogonality-enforcing post-processing.
- **Section A.6:** Comprehensive description of experimental configurations, including model architecture details, benchmark specifications, evaluation metrics, and hyperparameter settings.
- **Section A.7:** Summary of client model configuration of all heterogeneous PFL experiments.
- **Section A.8:** Comparative analysis of memory and computational costs across various baselines.
- **Section A.9:** Comparative analysis of communication (transmission) cost of FedMosaic.
- **Section A.10:** Empirical analysis supporting block-wise aggregation through CKA similarity measurements across heterogeneous models.
- **Section A.28:** Detailed algorithms for the FedMosaic framework, including initialization, alignment, and training procedures.

**Extended Experimental Results**

- **Section A.11:** Results with more diverse heterogeneous PFL scenarios, including experiments with three different model architectures.
- **Section A.12:** Experimental results in homogeneous PFL setups.
- **Section A.13:** Experimental results ins heterogeneous PFL scenarios using Qwen-based LLaVA models.
- **Section A.14:** Additional experiments on various cross-family heterogeneous PFL setups.
- **Section A.15:** Results on the text-only benchmark, complementing our Fed-LLM-Large experiments.
- **Section A.16:** Detailed client-wise accuracy analysis for both homogeneous and heterogeneous PFL setups.
- **Section A.23:** Extended evaluation of fast adaptation capabilities on additional unseen tasks.

**Ablation Studies**

- **Section A.17:** Analysis of the choice (*i.e.*, type and size) of public data $D_P$ for PQ-LoRA alignment.
- **Section A.18:** Analysis of how the change of various hyperparameters introduced in FedMosaic affects performance.
- **Section A.19:** Ablation study on RELA, comparing different strategies for measuring task similarity.
- **Section A.20:** Analysis on the size of $W_s$ for RELA in terms of computational cost and performance in a PFL setup.

- **Section A.21:** Investigation of the effects of weight alignment in PQ-LoRA.
- **Section A.22:** Discussion of RELA and existing similarity-based model aggregation in federated learning and multi-task learning.

**Limitations/Future Work and Benchmark Details**

- **Section A.24:** Comprehensive description of our proposed DRAKE benchmark, including task categories, dataset sources, client configuration, and comparison with existing FL benchmarks.
- **Section A.25**: Comparison between DRAKE and existing FL benchmarks.
- **Section A.26:** Discussion of limitations and potential directions for future work.
- **Section A.27:** Impact statement addressing the broader implications of our research.

### A.1 Theoretical Justification for Freezing $A$ and $B$ in PQ-LoRA

**Recap of PQ-LoRA.** PQ-LoRA consists of LoRA matrices $A \in \mathbb{R}^{r \times d_I}$, $B \in \mathbb{R}^{d_O \times r}$, along with shareable modules $P \in \mathbb{R}^{r \times r}$, $Q \in \mathbb{R}^r$. PQ-LoRA outputs $h_O$ for the given input $h_I$ as:

$$h_O = W_p h_I + B(PAh_I + Q), \tag{8}$$

where $W_p$ refers to the pre-trained weight.

For simplicity, we assume that $Q = \mathbf{0} \in \mathbb{R}^r$, *i.e.*, $h_O = BPAh_I$, and prove under the homogeneous FL setup, but can easily extend to $Q \neq \mathbf{0}$ and the heterogeneous FL setup.

**Definition (Aggregation Error $\delta$).** We first define the aggregation error $\delta$. In an FL setup with $N$ clients, the server aggregates client updates $\Delta W_i = B_i P_i A_i$ for $i \in [N]$. With FedAvg aggregation, the 'ideal' aggregation $\Delta W^*$ (Sun et al., 2024; Guo et al., 2025) should be:

$$\Delta W^* = \frac{1}{N}(B_1 P_1 A_1 + B_2 P_2 A_2 + \cdots + B_N P_N A_N). \tag{9}$$

However, we cannot perform 'ideal' aggregation in FL, since $W^*$ cannot be decomposed into trainable parameters, *i.e.*, $B$, $P$, and $A$, on client sides (Guo et al., 2025). In other words, although $W^*$ can be computed on the server, it cannot be redistributed as trainable parameters on the client side. As a result, instead of directly averaging $\Delta W_i$ for $i \in [N]$, we average the trainable parameters separately and obtain the practical update $\Delta \tilde{W}^*$ as:

$$\Delta \tilde{W}^* = \left(\frac{1}{N}\sum_{i=1}^{N} B_i\right)\left(\frac{1}{N}\sum_{i=1}^{N} P_i\right)\left(\frac{1}{N}\sum_{i=1}^{N} A_i\right). \tag{10}$$

To this end, we define the aggregation error $\delta = |\Delta W^* - \Delta \tilde{W}^*|$. During local training, we update shareable modules $P$ and $Q$, while freezing $A$ and $B$ to preserve alignment. This way, we minimize the aggregation error $\delta$, following Theorem 2.

**Theorem 2.** *If we freeze $A \in \mathbb{R}^{r \times d_I}$ and $B \in \mathbb{R}^{d_O \times r}$, aggregation error $\delta = 0$.*

**Proof of Theorem 2.**

*Proof.* If $A$ is frozen after alignment, then $A = A_1 = A_2 = \cdots = A_N$. Similarly, freezing $B$ implies $B = B_1 = B_2 = \cdots = B_N$. Under this condition, both the ideal update $\Delta W^*$ (Eq. 9) and the practical update $\Delta \tilde{W}^*$ (Eq. 10) can be simplified to:

$$\Delta W^* = \Delta \tilde{W}^* = B\left(\frac{1}{N}\sum_{i=1}^{N} P_i\right)A. \tag{11}$$

Thus, $\delta = 0$. □

### A.2 Proof of Theorem 1

*Proof.* For simplicity, we assume that $Q = \mathbf{0} \in \mathbb{R}^r$.

The weight update for PQ-LoRA is given by:

$$\Delta W = BPA, \tag{12}$$

where $B \in \mathbb{R}^{d_O \times r}$, $P \in \mathbb{R}^{r \times r}$, $A \in \mathbb{R}^{r \times d_I}$.

We can decompose the matrix $P$ using scalar values and basis vectors as follows:

$$P = \sum_{i=1}^{r} \sum_{j=1}^{r} P_{ij} \cdot e_i e_j^T, \tag{13}$$

where $P_{ij}$ refers to the scalar value of $(i, j)$ position of matrix P, and $e_i$ and $e_j$ refers to the standard basis vector in $\mathbb{R}^r$.

Substituting Eq.13 into Eq.12, we get:

$$\Delta W = BPA = B \left( \sum_{i,j} P_{ij} \cdot e_i e_j^{\mathrm{T}} \right) A = \sum_{i,j} P_{ij} \cdot (Be_i) \cdot \left( e_j^{\mathrm{T}} A \right). \tag{14}$$

Since $Be_i = b_i \in \mathbb{R}^{d_O}$ ($i_{\text{th}}$ column of $B$), $e_j^T A = a_j^{\mathrm{T}} \in \mathbb{R}^{d_I}$ ($j_{\text{th}}$ row of $A$), we can simplify Eq. 14 as:

$$\Delta W = \sum_{i,j} P_{ij} \cdot b_i a_j^{\mathrm{T}}. \tag{15}$$

Therefore, representation space of $\Delta W$, denoted as $S_{PQ}$, is defined as:

$$S_{PQ} = \text{span}\{b_i a_j^{\mathrm{T}} \mid i, j = 1, \ldots, r\}. \tag{16}$$

Since both $\{b_1, b_2, \ldots, b_r\} \subset \mathbb{R}^{d_O}$ and $\{a_1^{\mathrm{T}}, a_2^{\mathrm{T}}, \ldots, a_r^{\mathrm{T}}\} \subset \mathbb{R}^{d_I}$ form orthogonal sets, their outer products $\{b_i a_j^{\mathrm{T}}\}_{i,j=1}^{r}$ are linearly independent.

Therefore, the representation space $S_{PQ}$ has the maximum possible dimension:

$$\dim(S_{PQ}) = r^2. \tag{17}$$

□

To satisfy Eq.17, it is sufficient for the column vectors of $B$ and the row vectors of $A$ to form linearly independent sets, even if they are not strictly orthogonal. However, compared to initialization with linearly independent vectors, orthogonal initialization offers additional advantages, such as faster (Hu et al., 2020) and stable (Nowak et al., 2024) convergence. Therefore, motivated by both the practical advantages and the theoretical justification provided in Theorem 1, we initialize $A$ and $B$ with orthogonal sets.

### A.3 Details of Client Model Selection in the Heterogeneous PFL Scenario

In the heterogeneous PFL scenarios, we assign each client's model based on supervised fine-tuning (SFT) performance on their respective tasks. Specifically, clients are assigned larger models when these models exhibit significantly better SFT performance than smaller ones. Conversely, when the performance difference between model sizes is negligible, we allocate smaller models to maximize computational efficiency, as larger models require substantially more computational resources. We summarize the SFT performance of each LLaVA-Llama3 variant model and the resulting client-wise model allocation in Tab. 8.

| | DRAKE | | | | | | | | | |
|---|---|---|---|---|---|---|---|---|---|---|
| Model | Client 1 | Client 2 | Client 3 | Client 4 | Client 5 | Client 6 | Client 7 | Client 8 | Client 9 | Client 10 |
| LLaVA-Llama3.2-1B | 78.43 | 57.98 | 65.05 | 62.53 | 63.15 | 63.35 | 47.56 | 51.68 | 53.07 | 50.95 |
| LLaVA-Llama3.2-3B | **79.33** | **59.01** | **66.75** | **63.33** | **66.00** | **76.15** | **63.40** | **68.21** | **63.08** | **57.32** |
| Allocated Model | LLaVA-Llama3.2-**1B** | | | | LLaVA-Llama3.2-**3B** | | | | | |

| | HFLB | | | | | | | | |
|---|---|---|---|---|---|---|---|---|---|
| Model | Client 1 | Client 2 | Client 3 | Client 4 | Client 5 | Client 6 | Client 7 | Client 8 | Client 9 |
| LLaVA-Llama3.2-1B | 79.78 | **98.18** | 51,23 | 80.73 | 71.58 | 80.48 | 71.64 | 76.45 | 89.45 |
| LLaVA-Llama3.2-3B | **80.33** | 97.32 | **52.85** | **81.85** | **73.84** | **82.75** | **74.47** | **79.50** | **91.50** |
| Allocated Model | LLaVA-Llama3.2-**1B** | | | LLaVA-Llama3.2-**3B** | | | | | |

Table 8: **Per-client SFT performance of different LLaVA-Llama3 model variants.** We assign the larger model (*i.e.*, LLaVA-Llama-3.2-3B) to clients whose SFT performance shows a substantial gain, while the smaller model (*i.e.*, LLaVA-Llama-3.2-1B) is assigned otherwise.

### A.4 Effect of Client Model Assignment

To validate whether FedMosaic consistently achieves strong performance regardless of the specific model assigned to each client, we conduct experiments with varying ratios of LLaVA-1B and LLaVA-3B models, where model assignments are randomly determined in each run. In Table 9, we summarize the PFL results of supervised fine-tuning (SFT) and FedMosaic across diverse heterogeneous PFL scenarios, each corresponding to a different configuration of client model selections in the DRAKE-dynamic benchmark. We observe that FedMosaic consistently outperforms SFT with minimal performance variance across heterogeneous setups, demonstrating its robustness to the composition of client models.

| | | Self | | Others | |
|---|---|---|---|---|---|
| Scenario | Method | $A_{last}$ ↑ | $A_{\text{AUC}}$ ↑ | $A_{last}$ ↑ | $A_{\text{AUC}}$ ↑ |
| 3×1B Clients / 7×3B Clients | SFT | 65.57±0.83 | 57.46±0.44 | 47.80±0.17 | 46.80±0.10 |
| | FedMosaic | 67.02±0.34 | 58.85±0.15 | 51.55±0.31 | 49.62±0.04 |
| | Δ (FedMosaic- SFT) | +1.45 | +1.39 | +3.75 | +2.82 |
| 4×1B Clients / 6×3B Clients | SFT | 64.08±0.77 | 56.61±0.42 | 46.82±0.44 | 46.24±0.23 |
| | FedMosaic | 66.28±0.23 | 58.47±0.17 | 51.20±0.40 | 49.26±0.29 |
| | Δ (FedMosaic- SFT) | +2.20 | +1.86 | +4.38 | +3.02 |
| 5×1B Clients / 5×3B Clients | SFT | 63.72±0.77 | 56.61±0.16 | 46.70±0.07 | 45.99±0.06 |
| | FedMosaic | 65.34±0.21 | 58.25±0.17 | 51.08±0.23 | 49.07±0.25 |
| | Δ (FedMosaic- SFT) | +1.62 | +1.64 | +4.38 | +3.08 |
| 6×1B Clients / 4×3B Clients | SFT | 63.49±0.93 | 56.02±0.28 | 46.63±0.07 | 45.63±0.02 |
| | FedMosaic | 65.75±0.54 | 57.96±0.18 | 50.57±0.23 | 48.65±0.18 |
| | Δ (FedMosaic- SFT) | +2.26 | +1.94 | +3.94 | +3.02 |
| 7×1B Clients / 3×3B Clients | SFT | 62.72±0.19 | 55.54±0.02 | 45.54±0.22 | 44.83±0.07 |
| | FedMosaic | 65.40±0.53 | 57.56±0.07 | 49.41±0.18 | 47.54±0.08 |
| | Δ (FedMosaic- SFT) | +2.68 | +2.02 | +3.87 | +2.71 |

Table 9: **Effect of heterogeneous PFL scenarios on DRAKE-Dynamic.** We change the number of LLaVA-Llama3.2-1B and LLaVA-Llama3.2-3B models and randomly assign the model size of each client. The '4×1B Clients / 6×3B Clients' scenario here is different with the client model selection in Tab. 8.

### A.5 More Details of PQ-LoRA

As discussed in Sec.4.2.2, we enforce orthogonality on the $A$ and $B$ matrices to maximize the capacity of PQ-LoRA, following Theorem1. This is achieved through (i) initializing $A$ and $B$ with orthogonal sets, (ii) weight alignment, and (iii) orthogonality-enforcing post-processing.

**Initialization with Orthogonal Set.** We initialize row vectors of $A \in \mathbb{R}^{r \times d_I}$ and column vectors of $B \in \mathbb{R}^{d_O \times r}$ with an orthogonal set, as follows:

$$AA^\top = I_r, \quad B^\top B = I_r, \tag{18}$$

where $I_r$ refers to the $r \times r$ identity matrix.

**Weight Alignment.** For $B_i$ and $B_j$, we align them using canonical correlation analysis (CCA), as follows:

$$B_j = (\Pi_i{}^{-1})^T \cdot (\Pi_i)^T \cdot B_i, \tag{19}$$

where $\Pi_i$ and $\Pi_j$ are projection matrices that project $B_i$ and $B_j$ into to the maximally correlated space, respectively. During alignment, $B_j$ remains orthogonal because $B_i$ is initialized with orthogonal vectors, and the projection in Eq. 19 preserves this orthogonality.

However, during the alignment of $A_i$ and $A_j$ in Sec. 4.2.2, orthogonality can be disrupted due to L2 loss training. To prevent significant deviation from orthogonality, we add a regularization term to the objective function of $A$ alignment as follows:

$$\min_{A_j} \frac{1}{|\mathcal{D}_p|} \sum_{(x,y)\in\mathcal{D}_p} \|(A_i(x) - A_j(x)\|_2^2 + \lambda \left\|A_j^\top A_j - I\right\|_F^2, \tag{20}$$

where $\|\cdot\|_F$ denotes the Frobenius norm. Despite the regularization, $A_j$ may not strictly satisfy orthogonality. Therefore, to ensure exact orthogonality, we perform an additional post-processing step.

**Orthogonality-Enforcing Post-processing.** To enforce orthogonality in $A_j$, we apply orthogonal projection. Specifically, we aim to find the closest orthogonal matrix $A_j^*$ from $A_j$ by minimizing the Frobenius norm, as follows:

$$\min_{A_j^{*T} A_j^* = I} \|A_j - A_j^*\|_F. \tag{21}$$

This optimization can be efficiently solved using the Singular Value Decomposition (SVD). We compute the SVD of $A$:

$$A_j = U\Sigma V^T, \tag{22}$$

where $U \in \mathbb{R}^{r\times r}$, $\Sigma \in \mathbb{R}^{r\times d_I}$, and $V \in \mathbb{R}^{d_I \times d_I}$.

The closest orthogonal matrix $A_j^*$ is then given by:

$$A_j^* = UV^T. \tag{23}$$

As a result, we get $A_i$ and $B_i$, initialized with orthogonal sets and kept frozen during alignment, and $A_j^*$ and $B_j$, which are aligned with $A_i$ and $B_i$ while maintaining orthogonality.

### A.6 Details of Experimental Setups

**Models.** To employ LLaVA-Llama3 variant models (*i.e.*, LLaVA-Llama3.2-1B, LLaVA-Llama3.2-3B, LLaVA-Llama3.1-8B) and LLaVA-Qwen2.5 variant models (*i.e.*, LLaVA-Qwen2.5-0.5B, LLaVA-Qwen2.5-1.5B, and LLaVA-Qwen2.5-3B) in heterogeneous PFL scenarios, we instruction-tune them on LLaVA-Instruct-158K (Liu et al., 2023b), following the original LLaVA training setup (Liu et al., 2023b). We summarize the performance of the instruction-tuned variants in Tab. 10 and Tab. 11. We use Llama-3 base models for text-only benchmarks.

**Benchmarks.** We evaluate FedMosaic on Multi-modal FL benchmarks, such as our proposed DRAKE and HFLB, and LLM-FL benchmarks, such as Fed-Scope and Fed-Aya, and Fed-LLM-Large. We summarize the details of benchmarks in Tab. 12. As shown in the table, unlike HFLB, which focuses solely on VQA tasks, DRAKE covers diverse task types and involves more images per sample due to its multi-image inputs. In DRAKE-Dynamic, each client learns four tasks, where all data samples are randomly mixed in PFL-Static, while the samples from each task are introduced incrementally in PFL-Dynamic. We provide more details of DRAKE in Sec. A.24.

| Model | VQAv2 (Goyal et al., 2017) | GQA (Hudson & Manning, 2019) | VizWiz (Gurari et al., 2018) | SciQA (Lu et al., 2022) | TextVQA (Singh et al., 2019) |
|---|---|---|---|---|---|
| LLaVA-1.5-7B | 78.5 | 62.0 | 50.0 | 66.8 | 58.2 |
| LLaVA-Llama3.2-1B | 75.3 | 59.7 | 45.3 | 67.3 | 49.0 |
| LLaVA-Llama3.2-3B | 78.7 | 62.6 | 45.3 | 75.7 | 55.8 |
| LLaVA-Llama3.1-8B | 79.8 | 64.2 | 47.6 | 76.4 | 57.9 |
| LLaVA-Qwen2.5-0.5B | 71.8 | 56.5 | 37.3 | 58.1 | 43.4 |
| LLaVA-Qwen2.5-1.5B | 75.3 | 59.3 | 40.9 | 69.5 | 51.8 |
| LLaVA-Qwen2.5-3B | 77.2 | 61.4 | 50.9 | 74.1 | 54.7 |

Table 10: **Zero-Shot performance of instruction-tuned LLaVA-1.5 variants on academic-task-oriented benchmarks.** We use the CLIP ViT-L/336px model as the vision encoder for all variants.

| Model | POPE (Li et al., 2023c) | MME (Fu et al., 2023a) | MMBench (Liu et al., 2024) | SEED-Bench (Li et al., 2023a) | LLaVA-Wild (Liu et al., 2023b) | MM-Vet (Yu et al., 2023) |
|---|---|---|---|---|---|---|
| LLaVA-1.5-7B | 85.9 | 1510.7 | 64.3 | 58.6 | 65.4 | 31.1 |
| LLaVA-Llama3.2-1B | 85.0 | 1338.1 | 61.3 | 57.8 | 59.6 | 28.7 |
| LLaVA-Llama3.2-3B | 86.1 | 1446.5 | 70.9 | 62.5 | 67.0 | 34.5 |
| LLaVA-Llama3.1-8B | 86.3 | 1486.1 | 72.5 | 64.1 | 73.7 | 32.7 |
| LLaVA-Qwen2.5-0.5B | 86.2 | 1251.9 | 53.6 | 53.1 | 55.0 | 23.1 |
| LLaVA-Qwen2.5-1.5B | 86.4 | 1376.4 | 66.8 | 60.6 | 60.0 | 27.9 |
| LLaVA-Qwen2.5-3B | 87.2 | 1447.6 | 71.4 | 63.2 | 66.7 | 33.1 |

Table 11: **Zero-Shot performance of instruction-tuned LLaVA-1.5 variants on instruction-following benchmarks.** We use the CLIP ViT-L/336px model as the vision encoder for all variants.

HFLB includes 7 VQA datasets, where we assign them into 9 clients by partitioning GQA Hudson & Manning (2019) into three clients based on the QA types (*e.g.*, Yes/No, 2 Multi-choice, and 4 Multi-choice). We further split each assigned dataset into four tasks to allow experiments on the PFL-Dynamic setup. We use keywords in questions or GPT to categorize each sample, where the details are provided in Tab. 13.

To simulate PFL in NLP, we modify existing sets (*i.e.*, Fed-Aya and Fed-Scope) and compose larger mixtures (*i.e.*, Fed-LLM-Large) to increase task variety and heterogeneity across clients. Specifically, Fed-Aya is composed of 12 different languages equally sampled from different language families. We further separate the tasks based on the topic of the QA using GPT-4. Fed-Scope (Kuang et al., 2024) includes coding, mathematics, and general capability datasets, where each client learns either one of the three datasets. Fed-LLM-Large is a large-scale text-only benchmark designed for personalized federated learning. To diversify the personal tasks among clients, we combined tasks from three sources, Fed-ChatbotIT and Fed-aya from Fed-LLM (Ye et al., 2024), and Fed-FLAN Long et al. (2024). This results in 52 clients and 2 tasks per client, where each client fine-tunes on either instruction following tasks from different sources or in different languages (note that all other benchmarks have 4 tasks per client).

| Benchmark | # of Images | # of Questions | # of clients | # of rounds $R$ | # of local steps | Task types |
|---|---|---|---|---|---|---|
| DRAKE | 357K | 274K | 10 | 20 | 100 | Visual Relation, Multi-modal Reasoning, VQA |
| HFLB | 217K | 314K | 9 | 20 | 100 | VQA |
| Fed-Scope | - | 30K | 5 | 20 | 30 | General Capability, Mathematics, Coding |
| Fed-Aya | - | 36K | 8 | 20 | 50 | Question-Answering in 12 Languages |
| Fed-LLM-Large | - | 31K | 52 | 4 | 10 | Instruction Following |

Table 12: **Benchmark details and federated learning configurations.**

**Metrics.** We measured the accuracy metrics, $A_{last}$ and $A_{\text{AUC}}$, based on the correct choice for multi-choice questions and the correct tokens compared to the ground-truth answer for the open-ended questions. For Fed-Aya, we used GPT to rate the generated response compared to the given ground-truth response. We use the same prompt template shown in Fig. 8 from the original paper (Singh et al., 2024). For Fed-Scope, we follow the evaluation process of the original paper (Kuang et al., 2024) and use MMLU (Hendrycks et al., 2020), GSM8K (Cobbe et al., 2021), and HumanEval (Chen et al., 2021) benchmarks to evaluate general capability, math and coding skills, respectively. For Fed-LLM-Large, we use Rouge-L (Lin, 2004) metric as it is commonly used metric to assess LLM generation quality compared to ground-truth (Long et al., 2024; Li et al., 2024c).

| Client 1 | Client 2 | Client 3 |
|---|---|---|
| **GQA** (Hudson & Manning, 2019)<br>: Yes/No<br>• Attribute<br>• Relation<br>• Object<br>• Global | **GQA** (Hudson & Manning, 2019)<br>: Four-choice<br>• Attribute<br>• Relation<br>• Category<br>• Global | **GQA** (Hudson & Manning, 2019)<br>: Two-choice<br>• Attribute<br>• Relation<br>• Category<br>• Global |
| **Client 4** | **Client 5** | **Client 6** |
| **Abstract VQA** (Antol et al., 2015)<br>• Attribute<br>• Number<br>• Yes/No<br>• Others | **SNLI-VE** (Xie et al., 2019)<br>• Action<br>• Scene Context & Obj Relations<br>• Object-Centric<br>• Commonsense | **COCOQA** (Ren et al., 2015)<br>• Object<br>• Number<br>• Color<br>• Location |
| **Client 7** | **Client 8** | **Client 9** |
| **NLVR2** (Suhr et al., 2019)<br>• Presupposition Negation Universal<br>• Spatial Comparative<br>• Cardinality Existential<br>• Coordination Coreference | **VizWiz** (Gurari et al., 2018)<br>• Food, Brand, and Label Identification<br>• Color and Type Identification<br>• Optical Character Recognition<br>• General Object Identification | **AQUA** (Garcia et al., 2020)<br>• "standing" keyword<br>• "sit" keyword<br>• "wear", "hold", "walk", "talk" keywords<br>• Other keywords |

Table 13: **Per-client task configuration of HFLB.** Datasets are partitioned into question-type subsets using keyword rules or GPT judgement.

**[Instruction]**
Please act as an impartial judge and evaluate the quality of the response provided by an AI assistant to the user question displayed below. A good answer should follow these rules:
1. It should be in the same language as the question.
2. It should answer the request in the instruction.
3. It should be factually and semantically comprehensible.
4. It should be grammatically correct and fluent.

Begin your evaluation by providing a short explanation. Be as objective as possible. After providing your explanation, you must rate the response on a scale of 1 to 10 by strictly following this format: "`[[rating]]`", for example: "Rating: `[[5]]`". A human-annotated answer is given for reference.

**[Question]**
`{question}`

**[The Start of Assistant's Answer]**
`{answer}`
**[The End of Assistant's Answer]**

**[Reference]**
`{reference}`

Figure 8: **Prompt template used in GPT-4 judge.**

**Implementation Details and Hyperparameters.** We set the batch size to 4, the learning rate for PQ-LoRA to $5 \times 10^{-5}$, and for other parameters to $2 \times 10^{-5}$. We use the Constant LR scheduler and the AdamW optimizer (Loshchilov & Hutter, 2019) for all datasets. We use the LoRA rank $r$ of 128 attached to all linear layers in the LLM backbone. For LLM experiments, we set the learning rate to $3 \times 10^{-4}$ and the LoRA rank to 16. For federated learning, we set the total number of communication rounds $R$ to 20, with the local training step of 100. For a fair comparison, we adjust the local training step for each baseline and FedMosaic to use the same computational cost as SFT, following (Seo et al., 2025). For the PFL-Dynamic setup, we employ memory-only training, where newly encountered samples are added to episodic memory, and training batches are retrieved solely from memory, following (Koh et al., 2023; Seo et al., 2024; 2025). For episodic memory,

we adopt a memory-infinite setup (Prabhu et al., 2023; Seo et al., 2025), assuming all data can be stored in memory, reflecting that memory cost is not a bottleneck in real-world scenarios. For $\tau$, the softmax temperature parameter used in RELA, we use 0.5 in all experiments. For $\alpha$, the EMA ratio of client-wise gradient in Eq. 2, we use 0.5 in all experiments. For $\lambda$, the loss balancing coefficient between the L2 loss and the regularization term in Eq. 20, we use 0.5. For $N_s$, gradient sampling ratio for sanitized gradient $\tilde{g}_i$, we use 40%. For $\mu$, the noise scale applied to $\epsilon$, we set $\mu = 10^{-4}$. We set $N_B$, the number of layers employing PQ-LoRA, to 4 in all experiments. See Sec. A.18 for detailed hyperparameter analysis.

Federated distillation baselines (*i.e.*, TAKFL, PerAda, and FedMKT) share knowledge between heterogeneous models via logits, while FedMosaic employs PQ-LoRA. For the other baselines, we combine them with Fed-ET (Cho et al., 2022), which aggregates models among homogeneous clients. For $W_s$, a small-scale pre-trained MLLM used for calculating client-wise gradients in RELA, we adopt the smallest model among all client models. For example, in Table 16, where clients have three different types of heterogeneous architectures (*i.e.*, LLaVA-Llama3.2-1B, LLaVA-Llama3.2-3B, and LLaVA-Llama3.1-8B), we employ LLaVA-Llama3.2-1B as $W_s$ for all clients. This choice ensures computational efficiency and maintains gradient dimension consistency for cosine similarity calculation. Note that we can employ a lighter $W_s$ (*e.g.*, reduced size or lower-bit quantization) to further decrease the computation overhead of gradient calculation in RELA, as detailed in Sec. A.20. All experiments are executed in Python 3.10, on four Ubuntu 20.04 machines, with 8 NVIDIA RTX A6000 GPUs each. Each experiment runs on a single RTX A6000 GPU in a day.

### A.7 Client Model Configurations

We summarize the model configurations for each PFL experiment, including model types and their counts, in Tab. 14. For experiments on multi-modal benchmarks, we use LLaVA-Llama3 or LLaVA-Qwen2.5 variants, while for text-only benchmarks, we use Llama-3 variants.

| | | **LLaVA-Llama3** | | | **LLaVA-Qwen2.5** | | | **Llama-3** | | |
|---|---|---|---|---|---|---|---|---|---|---|
| **Benchmark** | **Experiment** | **1B** | **3B** | **8B** | **0.5B** | **1.5B** | **3B** | **1B** | **3B** | **8B** |
| Multi-modal | Tab. 2 DRAKE-Dynamic | 4 | 6 | 0 | 0 | 0 | 0 | – | – | – |
| | Tab. 2 HFLB-Dynamic | 3 | 6 | 0 | 0 | 0 | 0 | – | – | – |
| | Tab. 3 DRAKE-Static | 4 | 6 | 0 | 0 | 0 | 0 | – | – | – |
| | Tab. 4 DRAKE-Dynamic | 0 | 3 | 0 | 0 | 4 | 3 | – | – | – |
| | Tab. 7 DRAKE-Dynamic | 4 | 6 | 0 | 0 | 0 | 0 | – | – | – |
| | Tab. 16 DRAKE | 3 | 5 | 2 | 0 | 0 | 0 | – | – | – |
| | Tab. 17 DRAKE-Homo | 0 | 10 | 0 | 0 | 0 | 0 | – | – | – |
| | Tab. 17 HFLB-Homo | 0 | 9 | 0 | 0 | 0 | 0 | – | – | – |
| | Tab. 18 DRAKE-Homo | 0 | 0 | 0 | 0 | 0 | 10 | – | – | – |
| | Tab. 18 DRAKE-Hetero | 0 | 0 | 0 | 3 | 2 | 5 | – | – | – |
| | Tab. 19 Llama 3B / Qwen 1.5B | 0 | 6 | 0 | 0 | 4 | 0 | – | – | – |
| | Tab. 19 Llama 1B / 3B / Qwen 1.5B | 2 | 5 | 0 | 0 | 3 | 0 | – | – | – |
| | All other analysis / ablation experiments | 4 | 6 | 0 | 0 | 0 | 0 | – | – | – |
| Text-only | Tab. 6 Fed-LLM-Large-Dynamic | – | – | – | – | – | – | 26 | 26 | 0 |
| | Tab. 7 Fed-Scope-Static | – | – | – | – | – | – | 0 | 3 | 2 |
| | Tab. 20 Fed-aya-Dynamic | – | – | – | – | – | – | 4 | 4 | 0 |
| | Tab. 20 Fed-Scope-Static | – | – | – | – | – | – | 0 | 3 | 2 |

Table 14: **Client model configuration details for each experiment.** Counts per model family/size.

### A.8 Comparison of Computational and Memory Costs

We compare the computational cost $\mathcal{C}$ and memory cost $\mathcal{M}$ of various baselines and summarize the results in Tab. 15. Following (Seo et al., 2025), we measure computational cost in FLOPs per iteration and memory cost in Bytes. Specifically, for each baseline, we report the relative FLOPs and relative Bytes in comparison to supervised fine-tuning (SFT), which only requires a single forward and backward pass without any extra computation and memory overhead.

**Comparison of Computational Cost $\mathcal{C}$.** We first compare the computational cost of FL methods. PerAda (Xie et al., 2024) incurs approximately twice the computational cost compared to other

| Methods | Memory Cost $\mathcal{M}$ | | Computational Cost $\mathcal{C}$ | |
|---|---|---|---|---|
| | Overhead Type | Relative $\mathcal{M}$ to SFT | Overhead Type | Relative $\mathcal{C}$ to SFT |
| SFT | - | 1.000 | - | 1.000 |
| DITTO (ICML 2021) | Dual Adapter | 1.052 | Double Forward/Backward | 2.000 |
| FedSim (ICML 2022) | Dual Adapter | 1.052 | Double Forward | 1.487 |
| FedIT (ICASSP 2024) | - | 1.000 | - | 1.000 |
| TAKFL (NeurIPS 2024) | - | 1.000 | Distill Logit Extract | 1.294 |
| PerAda (CVPR 2024) | Dual Adapter | 1.052 | Double Forward/Backward & Logit Extraction | 2.294 |
| FedDAT (AAAI 2024) | Triple Adapter | 1.104 | Double Forward/Backward | 2.564 |
| FedDPA (NeurIPS 2024) | Dual Adapter | 1.052 | Double Forward/Backward | 2.051 |
| FedMKT (COLING 2025) | Public data Logit Share | 1.002 | Logit Extraction | 1.574 |
| FedMosaic (**Ours**) | PQ-LoRA | 1.053 | Last Layer Gradient Compute & Client-wise Similarity Compute | 1.098 |

Table 15: **Comparison of memory and computational costs.** FedMosaic incurs additional computational and memory costs compared to SFT, but only by approximately 5.3% and 9.8%, respectively.

baselines, since it sequentially updates both the personalized adapter and the local adapter. Similarly, FedDAT (Chen et al., 2024) independently optimizes the local adapter and the dual adapter teacher (DAT), which also results in a double computational cost. FedMKT, PerAda, and TAKFL perform knowledge distillation and transfer using logits (*e.g.*, from public data), which introduces additional forward computation for logit extraction.

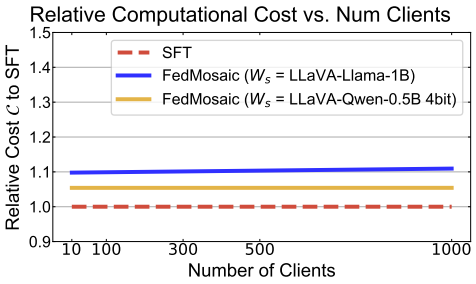


Figure 9: **Relative Computational Cost to SFT *vs.* Number of clients of FedMosaic.**

Our proposed FedMosaic incurs a minor additional computational cost due to (i) gradient computation from the frozen pre-trained model used for measuring task similarity and (ii) dual adapter structure, but this overhead amounts to only approximately 9.8% more FLOPs. The reason for the small increase in computation is that (i) we apply 60% gradient compression for similarity calculation in RELA, (ii) we only use the last layer gradient of the small-scale pre-trained frozen model, and (iii) we perform gradient computation once every 10 batch iterations rather than on all batches for computational efficiency, as mentioned in Sec. 4.1. Note that while FedMosaic also introduces a dual adapter structure, *i.e.*, maintaining the local adapter and the global adapter separately, similar to PerAda, FedDAT, and FedDPA, we optimize the dual-adapter at once using a learnable balancing parameter in PQ-LoRA, which adaptively balances local and global output. In contrast, the baselines separately optimize each adapter, thus incurring a double computational cost. Thanks to these designs, the relative overhead remains approximately at 10% even under large-scale client setups (*e.g.*, 1000 clients), as shown by the blue line in Fig. 9. Finally, the cost can be further reduced by adopting smaller or quantized $W_s$, as discussed in Sec. A.20. For example, using a LLaVA-Qwen-0.5B-4bit model as $W_s$ reduces the overhead to approximately 5% with 1000 clients (yellow line in Fig. 9), while achieving performance comparable to LLaVA-Llama-1B (Sec. A.20).

**Comparison of Memory Cost $\mathcal{M}$.** We then compare the memory cost of FL methods. FedMKT incurs a marginal additional memory overhead, as it requires storing logits from clients for knowledge aggregation. DITTO, FedSim, PerAda, FedDAT, FedDPA, as well as FedMosaic employ a dual adapter structure, which maintains both local and global adapters separately, to preserve global knowledge. It incurs additional memory cost, but since we adopt the LoRA adapter (Hu et al., 2022), which occupies significantly less memory compared to pre-trained weights (Qi et al., 2024), the dual adapter only consumes about 5% additional memory cost compared to using a single LoRA adapter.

### A.9 Details of Communication Costs in FedMosaic

The only additional transmission in FedMosaic compared to Vanilla in Tab. 7 (*i.e.*, FedMosaic w/o RELA and w/o PQ-LoRA) is a single EMA-updated gradient vector per client, adding 8.6% overhead compared to sending only local LoRA parameters. However, as mentioned in Sec. 4.1, we apply gradient compression by randomly selecting only $N_s\%$ of the client-specific gradient vectors, thereby reducing communication costs. With $N_s = 40\%$, the communication overhead drops to 3.4%.

Moreover, while baselines transmit full LoRA modules (*i.e.*, $A \in \mathbb{R}^{r\times d}$ and $B \in \mathbb{R}^{d\times r}$) across all layers, FedMosaic freezes $A$ and $B$ in PQ-LoRA layers and transmits only $P \in \mathbb{R}^{r\times r}$ and $Q \in \mathbb{R}^{r}$, significantly reducing 14.3% communication cost. Combining the marginal overhead from client-specific vectors with the reduction from PQ-LoRA, FedMosaic consequently achieves 10.9% lower communication cost than even the most efficient baseline (*i.e.*, FedAvg), regardless of the number of clients, ensuring scalability and communication efficiency (Blue line in Fig. 10).

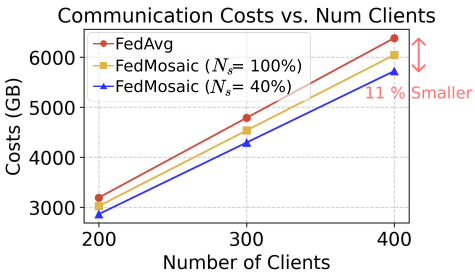


Figure 10: **Communication Cost vws. Number of clients of FedMosaic.**

### A.10 Empirical Analysis of Block-Wise Aggregation

To identify layer-wise correspondences between depth-heterogeneous models, we analyze representation alignment using CKA (Kornblith et al., 2019). Specifically, we measure similarity across layers within the Llama-3 family (1B, 3B, 8B) and the Qwen-2.5 family (0.5B, 1.5B, 3B), as illustrated in Fig. 11. As shown in the figure, layers with the same relative depth exhibit strong alignment, indicating approximately linear alignment within both the Llama-3 and Qwen-2.5 families. Moreover, we observe near-linear alignment even across families, *i.e.*, between Llama-3 and Qwen-2.5, despite weaker linearity than intra-family alignment. This empirical analysis supports our block-wise aggregation of PQ-LoRA. We provide an illustration of the block-wise PQ-LoRA in Fig. 12.

### A.11 Experimental Results in More Diverse Heterogeneous PFL Scenarios

We evaluate FedMosaic in heterogeneous PFL using three different heterogeneous architectures, *i.e.*, LLaVA-Llama3.2-1B, LLaVA-Llama3.2-3B, and LLaVA-Llama3.1-8B, and summarize the results in Tab. 16. Consistent with the previous heterogeneous PFL scenario with two different types of architectures (*i.e.*, LLaVA-Llama3.2-1B and LLaVA-Llama3.2-3B), FedMosaic consistently outperforms the baselines in both PFL-Dynamic and PFL-Static settings. These results demonstrate that PQ-LoRA effectively enables knowledge sharing across various heterogeneous architectures, highlighting its applicability to real-world scenarios where each client possesses individual heterogeneous models.

| | DRAKE-Dynamic | | | | DRAKE-Static | | | |
|---|---|---|---|---|---|---|---|---|
| | Self | | Others | | Self | | Others | |
| Method | $A_{last}$ ↑ | $A_{\text{AUC}}$ ↑ | $A_{last}$ ↑ | $A_{\text{AUC}}$ ↑ | $A_{last}$ ↑ | $A_{\text{AUC}}$ ↑ | $A_{last}$ ↑ | $A_{\text{AUC}}$ ↑ |
| SFT | 66.41±0.84 | 59.17±0.64 | 47.94±0.18 | 47.10±0.19 | 68.86±2.16 | 62.30±3.12 | 47.98±0.27 | 47.44±0.20 |
| DITTO (ICML 2021) | 61.56±0.01 | 56.36±0.20 | 48.19±0.26 | 47.41±0.01 | 65.48±0.97 | 60.34±0.32 | 48.49±0.03 | 48.09±0.01 |
| FedSim (ICML 2022) | 65.00±0.41 | 58.18±0.46 | 47.47±0.10 | 46.61±0.04 | 67.39±0.32 | 62.42±0.25 | 47.08±0.05 | 47.10±0.03 |
| FedIT (ICASSP 2024) | 66.18±0.22 | 58.95±0.02 | 47.54±0.02 | 46.97±0.01 | 68.78±0.22 | 64.07±0.92 | 47.34±0.55 | 47.33±0.29 |
| TAKFL (NeurIPS 2024) | 64.73±0.49 | 58.33±0.53 | 47.85±0.46 | 47.16±0.08 | 68.17±0.75 | 63.19±1.21 | 47.28±0.14 | 46.90±1.00 |
| FedDPA (NeurIPS 2024) | 63.26±0.09 | 57.31±0.02 | 48.04±0.26 | 47.21±0.07 | 67.71±0.95 | 63.03±0.24 | 48.18±0.53 | 48.22±0.13 |
| FedDAT (AAAI 2024) | 60.43±0.54 | 56.82±0.29 | 49.79±0.21 | 48.25±0.25 | 61.97±0.58 | 57.64±0.45 | 49.76±0.46 | 47.99±0.21 |
| PerAda (CVPR 2024) | 58.10±2.74 | 54.84±1.68 | 46.90±0.22 | 46.69±0.21 | 61.57±0.97 | 56.22±0.38 | 45.01±0.37 | 47.06±0.71 |
| FedMKT (COLING 2025) | 63.25±0.05 | 57.23±0.18 | 47.88±0.29 | 47.25±0.15 | 65.50±0.37 | 61.12±0.56 | 48.27±0.04 | 47.70±0.31 |
| FedMosaic (**Ours**) | **68.94±0.68** | **60.96±0.06** | **52.18±0.34** | **50.11±0.03** | **70.41±1.27** | **65.12±1.15** | **52.67±0.20** | **50.91±0.70** |

Table 16: **Quantitative comparison in heterogeneous PFL with three different types of models.** 'Self' denotes evaluation on a client's own data, while 'Others' denotes evaluation on data from other clients. 3 clients use LLaVA-Llama3.2-1B model, 5 clients use LLaVA-Llama3.2-3B model, and 2 clients use LLaVA-Llama3.1-8B model. SFT refers to supervised fine-tuning on each client's data without cross-client knowledge sharing.

### A.12 Experiment Results on Homogeneous PFL Setup

In addition to the heterogeneous PFL scenario (Sec. 6.2), where both data distributions and model architectures vary across clients, we also evaluate FedMosaic in a homogeneous PFL setting, where clients share the same model architecture but have heterogeneous data distributions. We assume all clients use LLaVA-3B models and summarize the results in Tab.17. Consistent with results in the heterogeneous setup, FedMosaic significantly outperforms baselines in generalization ability (*i.e.*, 'Others') and even surpasses SFT in personalization performance (*i.e.*, 'Self').

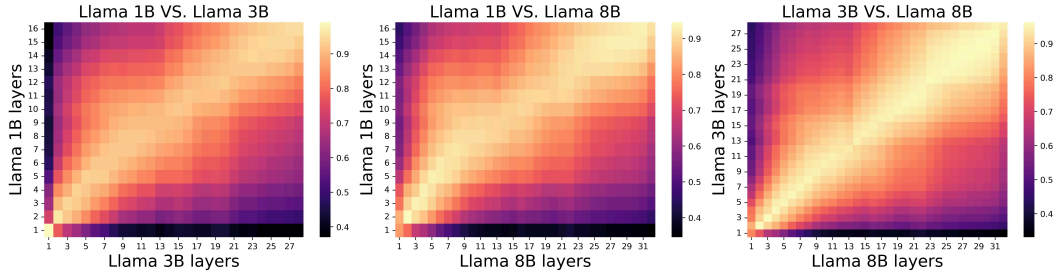


(a) Llama-3 family (1 B, 3 B, 8 B)

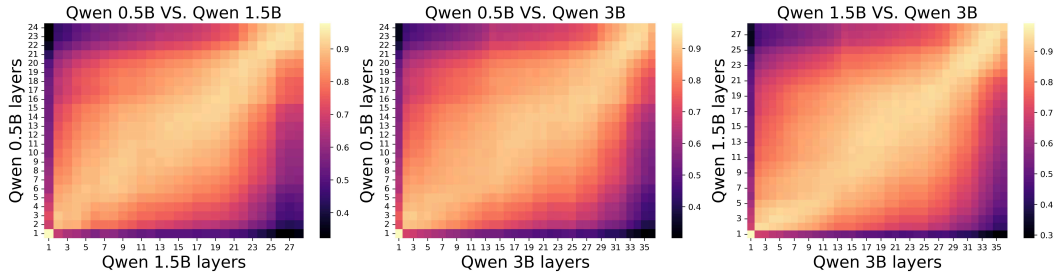


(b) Qwen-2.5 family (0.5 B, 1.5 B, 3 B)

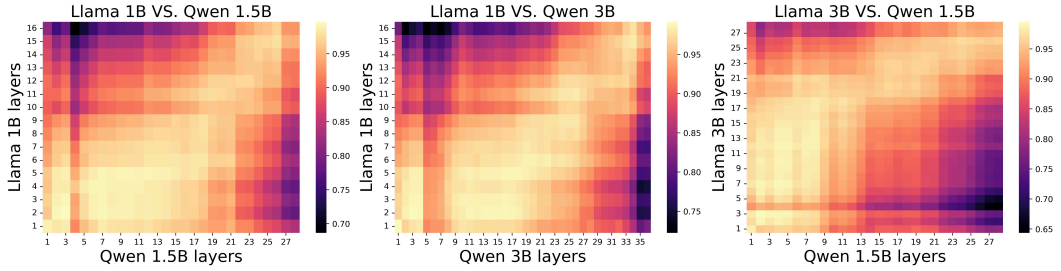


(c) Llama - Qwen mixed

Figure 11: **Layer-wise similarity across model scales measured with CKA.** Each heat-map cell reports the centered-kernel–alignment (CKA) similarity between the hidden representations of heterogeneous multi-modal LLMs at every pair of layers. Here, lighter colors indicate higher similarity. **(a)** For the Llama-3–based heterogeneous models and **(b)** for the Qwen-2.5–based heterogeneous models, the brightest (*i.e.*, the highest similarity) band appears roughly along the main diagonal, indicating that layers with *relative depth* align most strongly. The near-linear trend supports our proposed block-wise aggregation, which transfers knowledge from smaller to larger models that have the same relative depth within the same architectural family.

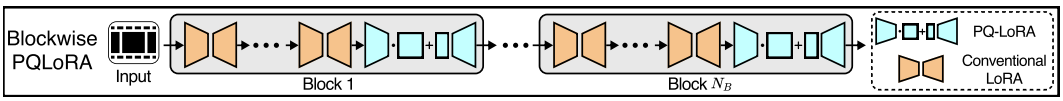


Figure 12: **Illustration of blockwise PQ-LoRA.** When a model has $N_B$ PQ-LoRA modules, each block employs PQ-LoRA at its last layer, while the remaining layers adopt conventional LoRA. Each block contains the same number of layers.

### A.13 Experiment Results on Qwen-based LLaVA

In addition to heterogeneous PFL scenarios with LLaVA-Llama3 variants, we also compare FedMosaic with baselines using Qwen-based LLaVA models. Specifically, we use LLaVA-Qwen2.5-0.5B for the small model and LLaVA-Qwen2.5-3B for the large model. For baselines, we select the top-3 well-performing baselines in heterogeneous PFL scenarios using LLaVA-Llama3 variants, as well as supervised fine-tuning (*i.e.*, SFT). We summarize the results in Tab. 18.

| Method | DRAKE-Dynamic | | | | HFLB-Dynamic | | | |
|---|---|---|---|---|---|---|---|---|
| | Self | | Others | | Self | | Others | |
| | $A_{last}$ ↑ | $A_{\text{AUC}}$ ↑ | $A_{last}$ ↑ | $A_{\text{AUC}}$ ↑ | $A_{last}$ ↑ | $A_{\text{AUC}}$ ↑ | $A_{last}$ ↑ | $A_{\text{AUC}}$ ↑ |
| SFT | 67.57±0.14 | 59.18±1.26 | 49.70±0.02 | 48.04±1.18 | 80.26±1.14 | 77.98±0.49 | 63.24±0.23 | 62.90±0.60 |
| DITTO (ICML 2021) | 64.09±0.55 | 57.22±0.01 | 49.92±0.27 | 49.05±0.07 | 79.34±0.41 | 76.72±0.84 | 64.10±0.40 | 63.57±0.06 |
| FedSim (ICML 2022) | 67.05±0.98 | 60.69±0.84 | 47.94±1.69 | 47.55±1.14 | 79.60±0.77 | 76.93±0.78 | 60.85±1.15 | 60.50±0.82 |
| FedIT (ICASSP 2024) | 67.62±0.49 | 60.35±0.69 | 49.84±0.19 | 48.95±0.13 | 79.34±0.59 | 78.40±1.21 | 62.51±1.30 | 62.38±0.96 |
| TAKFL (NeurIPS 2024) | 67.02±0.04 | 59.86±0.36 | 50.03±0.06 | 48.85±0.09 | 79.45±0.69 | 77.15±0.99 | 63.01±0.66 | 62.70±0.96 |
| FedDPA (NeurIPS 2024) | 66.59±0.86 | 58.68±0.71 | 49.92±0.24 | 48.81±0.13 | 80.57±0.62 | 77.65±0.61 | 63.58±0.30 | 63.02±0.09 |
| FedDAT (AAAI 2024) | 61.95±0.90 | 57.22±0.45 | 51.50±0.13 | 50.28±0.08 | 79.58±0.53 | 76.82±1.13 | 67.33±0.13 | 66.47±0.29 |
| PerAda (CVPR 2024) | 63.78±0.70 | 57.44±0.16 | 49.79±0.25 | 49.10±0.02 | 78.88±0.96 | 76.31±1.24 | 63.35±1.26 | 63.09±0.56 |
| FedMKT (COLING 2025) | 65.20±0.43 | 58.73±0.12 | 49.68±0.29 | 48.84±0.22 | 79.43±0.69 | 77.24±0.61 | 62.66±0.38 | 62.79±0.86 |
| FedMosaic (**Ours**) | **70.80±0.23** | **62.18±0.64** | **53.93±0.36** | **51.72±0.28** | **80.75±0.14** | **78.87±0.20** | **68.30±0.69** | **67.46±0.22** |

| Method | DRAKE-Static | | | | HFLB-Static | | | |
|---|---|---|---|---|---|---|---|---|
| | Self | | Others | | Self | | Others | |
| | $A_{last}$ ↑ | $A_{\text{AUC}}$ ↑ | $A_{last}$ ↑ | $A_{\text{AUC}}$ ↑ | $A_{last}$ ↑ | $A_{\text{AUC}}$ ↑ | $A_{last}$ ↑ | $A_{\text{AUC}}$ ↑ |
| SFT | 70.56±0.27 | 66.31±0.37 | 50.37±0.04 | 49.99±0.16 | 80.89±0.85 | 80.01±0.12 | 63.40±0.41 | 63.09±0.17 |
| DITTO (ICML 2021) | 66.19±0.38 | 62.05±0.69 | 50.59±0.05 | 49.95±0.08 | 80.37±0.37 | 79.05±0.25 | 63.93±0.24 | 63.52±0.10 |
| FedSim (ICML 2022) | 68.65±0.86 | 63.96±0.78 | 49.27±0.22 | 48.85±0.14 | 80.05±0.01 | 79.36±0.79 | 61.22±0.30 | 61.31±0.12 |
| FedIT (ICASSP 2024) | 70.14±0.03 | 66.08±0.59 | 50.09±0.15 | 49.87±0.26 | 80.63±1.23 | 79.97±0.01 | 63.34±0.11 | 63.09±0.04 |
| TAKFL (NeurIPS 2024) | 68.75±0.04 | 64.39±0.07 | 49.70±0.16 | 49.60±0.03 | 79.97±0.11 | 79.41±0.81 | 63.67±0.39 | 63.30±0.25 |
| FedDPA (NeurIPS 2024) | 67.40±2.73 | 63.71±1.24 | 50.45±0.38 | 49.92±0.30 | 79.99±1.23 | 79.02±0.35 | 63.45±0.07 | 63.11±0.02 |
| FedDAT (AAAI 2024) | 64.09±1.16 | 61.10±0.60 | 52.20±0.26 | 51.47±0.04 | 79.80±0.50 | 78.43±0.68 | 68.92±0.44 | 67.66±0.27 |
| PerAda (CVPR 2024) | 65.64±0.48 | 61.93±0.58 | 50.53±0.02 | 49.94±0.05 | 80.25±0.45 | 79.01±0.26 | 64.00±0.13 | 63.58±0.31 |
| FedMKT (COLING 2025) | 67.85±0.92 | 62.93±1.16 | 49.23±1.54 | 48.77±1.69 | 79.85±0.67 | 79.72±0.60 | 63.84±0.20 | 63.39±0.07 |
| FedMosaic (**Ours**) | **72.02±0.37** | **67.18±0.13** | **54.21±0.05** | **52.94±0.05** | **81.69±0.16** | **80.54±0.09** | **68.70±0.26** | **67.75±0.23** |

Table 17: **Quantitative comparison in homogeneous PFL.** 'Self' denotes evaluation on a client's own data, while 'Others' denotes evaluation on data from other clients. All clients use LLaVA-3B models. SFT refers to supervised fine-tuning on each client's data without cross-client knowledge sharing.

As shown in the table, FedMosaic significantly outperforms baselines in both homogeneous and heterogeneous PFL scenarios, consistent with results from LLaVA-Llama3 variants. This demonstrates that our proposed PQ-LoRA consistently facilitates knowledge sharing across heterogeneous models and RELA reduces interference during local model aggregation, regardless of architecture.

| Method | DRAKE-Homonegeous | | | | DRAKE-Heterogeneous | | | |
|---|---|---|---|---|---|---|---|---|
| | Self | | Others | | Self | | Others | |
| | $A_{last}$ ↑ | $A_{\text{AUC}}$ ↑ | $A_{last}$ ↑ | $A_{\text{AUC}}$ ↑ | $A_{last}$ ↑ | $A_{\text{AUC}}$ ↑ | $A_{last}$ ↑ | $A_{\text{AUC}}$ ↑ |
| SFT | 68.79±1.36 | 59.06±0.18 | 47.87±0.40 | 47.10±0.04 | 65.79±0.17 | 58.24±0.14 | 44.40±0.86 | 44.06±0.43 |
| FedIT (ICASSP 2024) | 68.40±0.07 | 60.58±0.41 | 49.70±0.52 | 48.54±0.07 | 66.02±0.72 | 58.26±1.06 | 44.47±0.30 | 44.06±0.43 |
| FedDPA (NeurIPS 2024) | 66.73±0.42 | 60.21±0.47 | 49.39±0.07 | 48.69±0.11 | 65.43±0.64 | 57.79±0.08 | 44.48±0.43 | 44.53±0.26 |
| FedMKT (COLING 2025) | 65.95±0.35 | 58.81±0.64 | 49.73±0.09 | 48.52±0.24 | 62.85±0.99 | 56.71±0.33 | 44.73±1.35 | 44.24±0.75 |
| FedMosaic (**Ours**) | **70.38±0.34** | **62.84±0.23** | **54.25±0.33** | **51.85±0.20** | **67.36±0.21** | **59.95±0.71** | **50.43±0.01** | **48.51±0.29** |

Table 18: **Quantitative comparison in PFL-Dynamic using Qwen-based LLaVA.** 'Self' denotes evaluation on a client's own data, while 'Others' denotes evaluation on data from other clients. In DRAKE-Homogeneous, all clients use LLaVA-Qwen2.5-3B models, while in DRAKE-Heterogeneous, 3 clients use LLaVA-Qwen2.5-0.5B model, 2 clients use LLaVA-Qwen2.5-1.5B model, and 5 client uses LLaVA-Qwen2.5-3B model. SFT refers to supervised fine-tuning on each client's data without cross-client knowledge sharing.

### A.14 Experiment Results in Cross-Family Heterogeneous PFL Scenarios

In addition to Tab. 4, we further evaluate FedMosaic under cross-family heterogeneity using clients with either Qwen- and Llama-based LLaVAs on DRAKE-Dynamic. As shown in Tab. 19, FedMosaic consistently outperforms all baselines, demonstrating its generalizability and transferability beyond the same family heterogeneous models (*e.g.*, LLaVA-Llama-1B, LLaVA-Llama-3B).

### A.15 Experimental Results on Text-Only Benchmarks

In addtion to Fed-LLM-Large (Sec.6.2), we evaluate FedMosaic on other text-only PFL benchmarks, Fed-Aya and Fed-Scope, and summarize the results in Tab. 20. As shown in the table, FedMosaic outperforms baselines in both personalization and generalization, consistent with results from other MLLM PFL benchmarks, such as DRAKE and HFLB.

| Method | Llama 3B / Qwen 1.5B | | | | Llama 1B / Llama 3B / Qwen 1.5B | | | |
|---|---|---|---|---|---|---|---|---|
| | Self | | Others | | Self | | Others | |
| | $A_{last}$ ↑ | $A_{\text{AUC}}$ ↑ | $A_{last}$ ↑ | $A_{\text{AUC}}$ ↑ | $A_{last}$ ↑ | $A_{\text{AUC}}$ ↑ | $A_{last}$ ↑ | $A_{\text{AUC}}$ ↑ |
| SFT | 68.41±0.39 | 61.04±0.33 | 48.48±0.15 | 47.75±0.07 | 67.24±0.07 | 60.42±0.33 | 47.48±0.02 | 46.73±0.10 |
| DITTO (ICML 2021) | 64.34±0.35 | 57.72±0.09 | 48.35±0.38 | 47.63±0.22 | 63.78±0.37 | 57.11±0.78 | 47.88±0.29 | 47.09±0.09 |
| FedSim (ICML 2022) | 66.40±0.94 | 59.08±0.53 | 47.32±0.59 | 46.74±0.33 | 65.24±0.21 | 58.33±0.24 | 46.73±0.64 | 46.07±0.41 |
| FedIT (ICASSP 2024) | 67.81±0.73 | 60.46±0.61 | 48.37±0.24 | 47.41±0.06 | 67.21±0.51 | 60.05±0.07 | 47.25±0.04 | 46.62±0.03 |
| TAKFL (NeurIPS 2024) | 65.41±0.27 | 58.52±0.07 | 47.51±0.62 | 47.34±0.32 | 66.13±1.23 | 58.47±0.44 | 47.70±0.83 | 46.70±0.41 |
| FedDPA (NeurIPS 2024) | 65.92±0.49 | 58.73±0.01 | 48.30±0.20 | 47.41±0.19 | 65.93±0.20 | 58.42±0.07 | 47.67±0.08 | 46.64±0.05 |
| FedDAT (AAAI 2024) | 63.86±1.33 | 58.41±0.63 | 50.08±0.34 | 49.23±0.09 | 63.16±1.65 | 57.74±0.78 | 49.13±0.33 | 48.16±0.15 |
| PerAda (CVPR 2024) | 64.11±0.73 | 57.89±0.54 | 48.52±0.51 | 47.76±0.27 | 62.87±1.89 | 57.07±0.62 | 47.54±0.04 | 46.87±0.01 |
| FedMKT (COLING 2025) | 65.38±0.99 | 58.57±0.16 | 47.60±0.49 | 47.29±0.04 | 64.29±1.34 | 58.31±0.43 | 47.13±0.35 | 46.71±0.37 |
| FedMosaic (**Ours**) | **70.62±0.29** | **63.33±0.26** | **52.56±0.08** | **50.76±0.01** | **69.64±0.77** | **62.09±0.51** | **51.69±0.15** | **49.85±0.13** |

Table 19: **Quantitative comparison in cross-family heterogeneous PFL on DRAKE-dynamic.** 'Self' denotes evaluation on a client's own data, while 'Others' denotes evaluation on data from other clients. 'Llama 3B / Qwen 1.5B' experiment is with 6 clients using LLaVA-Llama3.2-3B model and 4 clients using LLaVA-Qwen2.5-1.5B model, while 'Llama 1B / Llama 3B / Qwen 1.5B' experiment is with 2 clients using LLaVA-Llama3.2-1B model, 5 clients using LLaVA-Llama3.2-3B model, and 3 clients using LLaVA-Qwen2.5-1.5B model. SFT refers to supervised fine-tuning on each client's data without cross-client knowledge sharing.

| Method | Fed-Aya | | | | Fed-Scope | | | |
|---|---|---|---|---|---|---|---|---|
| | Self | | Others | | Self | | Others | |
| | $A_{last}$ ↑ | $A_{\text{AUC}}$ ↑ | $A_{last}$ ↑ | $A_{\text{AUC}}$ ↑ | $A_{last}$ ↑ | $A_{\text{AUC}}$ ↑ | $A_{last}$ ↑ | $A_{\text{AUC}}$ ↑ |
| SFT | 2.34±0.08 | 2.17±0.03 | 2.01±0.02 | 1.99±0.01 | 25.21±1.31 | 29.35±0.61 | 25.83±1.03 | 27.30±0.73 |
| FedSim (ICML 2022) | 1.99±0.03 | 1.98±0.04 | 1.92±0.01 | 1.92±0.03 | 21.13±0.97 | 24.03±0.45 | 15.57±0.87 | 18.59±0.30 |
| FedIT (ICASSP 2024) | 2.27±0.08 | 2.18±0.02 | 2.19±0.11 | 2.10±0.04 | 25.06±1.36 | 28.89±0.66 | 25.86±0.94 | 27.94±0.44 |
| TAKFL (NeurIPS 2024) | 2.34±0.12 | 2.17±0.06 | 2.19±0.10 | 2.08±0.03 | 26.18±1.03 | 27.84±0.57 | 28.53±0.33 | 28.27±0.19 |
| FedDPA (NeurIPS 2024) | 2.39±0.09 | 2.27±0.02 | 2.20±0.05 | 2.13±0.01 | 24.93±1.06 | 27.51±0.55 | 26.72±0.67 | 27.69±0.27 |
| FedDAT (AAAI 2024) | 2.14±0.14 | 2.09±0.04 | 1.98±0.08 | 1.96±0.04 | 24.93±0.55 | 27.51±0.28 | 26.72±0.53 | 27.69±0.33 |
| FedMKT (COLING 2025) | 2.31±0.06 | 2.12±0.05 | 2.06±0.02 | 1.96±0.00 | 24.92±0.96 | 27.51±0.63 | 29.55±0.43 | 30.57±0.19 |
| FedMosaic (**Ours**) | **2.51±0.01** | **2.32±0.03** | **2.25±0.01** | **2.17±0.02** | **30.58±0.84** | **32.68±0.64** | **31.01±1.46** | **32.50±0.62** |

Table 20: **Quantitative comparison of heterogeneous LLM clients on the text-only benchmarks.** In Fed-aya experiment, 4 clients use Llama-3.2-1B and 4 clients use Llama-3.2-3B. In Fed-Scope experiment, 3 clients use Llama-3.2-3B and 2 clients use Llama-3.1-8B.

### A.16 Client-Wise Accuracy

In addition to reporting the average accuracy across all clients in Sec. 6.2, we report client-wise accuracy in both homogeneous and heterogeneous PFL setups.

**Homogeneous PFL Setups.** We first compare client-wise performance in the homogeneous PFL-Dynamic setups on DRAKE and HFLB, and summarize the results in Tab.21 and Tab.22, respectively. As shown in the tables, personalization performance is improved for all clients compared to SFT (*i.e.*, supervised fine-tuning on local data) except Client 8 in Tab. 22. We highlight this result because SFT is a strong baseline for personalization (Ghari & Shen, 2024), as we also show in Tab. 17, where it outperforms all baselines except for FedMosaic. Moreover, supervised fine-tuning may be sufficient for personalization in some tasks (Woźniak et al., 2024; Mosbach et al., 2021), as seen with Client 6 in Tab. 21, where there are only marginal improvements compared to SFT. However, for more challenging tasks, properly leveraging knowledge from other clients significantly improves personalization, *e.g.*, FedMosaic shows a gain of 8.2% in $A_{last}$ for Client 9 and 6.4% for Client 7, as well as a 7.1% improvement in $A_{\text{AUC}}$ for Client 5. In summary, even though there is only a 1–3% gain in the average performance across clients, this is because in clients where SFT is sufficient for personalization, the gain from PFL seems smaller. Consistent with the PFL-Dynamic setup, FedMosaic outperforms SFT in the PFL-Static scenario, as shown in Tab. 23.

**Heterogeneous PFL Setups.** Consistent with the results in the homogeneous PFL setups, FedMosaic enhances personalization ability in most clients, as shown in Tab.24 and Tab.25. As shown in the tables, not only do clients using smaller models (*i.e.*, LLaVA-Llama3.2-1B, LLaVA-Llama3.2-3B) benefit from knowledge sharing through PFL, but clients with larger models (*i.e.*, LLaVA-Llama3.2-8B) also see significant improvements, *e.g.*, a 6.5% improvement in $A_{last}$ and 9.4% improvement

| Method | $A_{last}$ / $A_{\text{AUC}}$ | | | | | | | | | |
|---|---|---|---|---|---|---|---|---|---|---|
| | Client 1 | Client 2 | Client 3 | Client 4 | Client 5 | Client 6 | Client 7 | Client 8 | Client 9 | Client 10 |
| SFT | 81.90 / 62.11 | 65.23 / 59.28 | 67.38 / 60.31 | 70.28 / 60.40 | 63.69 / 62.07 | 76.05 / 67.35 | 63.40 / 54.17 | 66.93 / 59.31 | 62.70 / 52.20 | 58.16 / 54.58 |
| FedMosaic | **82.73 / 66.11** | **67.31 / 63.76** | **68.97 / 62.53** | **72.60 / 67.51** | **68.67 / 63.58** | **76.98 / 68.56** | **69.83 / 58.86** | **70.11 / 60.08** | **70.89 / 54.89** | **59.88 / 55.89** |
| *Difference* | +0.83 / +4.01 | +4.98 / +1.51 | +2.08 / +4.48 | +1.59 / +2.23 | +2.31 / +7.12 | +0.93 / +1.21 | +6.43 / +4.69 | +3.18 / +0.77 | +8.19 / +2.69 | +1.71 / +1.31 |

Table 21: **Per-client performance of FedMosaic vs. SFT in a homogeneous PFL-Dynamic setup on DRAKE.** The *Difference* row shows the performance gain/loss of FedMosaic compared to SFT. All clients use the LLaVA-Llama3.2-3B model.

| Method | $A_{last}$ / $A_{\text{AUC}}$ | | | | | | | | |
|---|---|---|---|---|---|---|---|---|---|
| | Client 1 | Client 2 | Client 3 | Client 4 | Client 5 | Client 6 | Client 7 | Client 8 | Client 9 |
| SFT | 82.28 / 79.13 | 96.26 / 96.59 | 52.73 / 50.22 | **82.16** / 81.52 | 72.79 / 72.93 | 86.65 / 84.74 | 76.04 / 73.79 | 81.13 / 79.83 | **90.58** / 83.02 |
| FedMosaic | **82.77 / 79.79** | **96.60 / 97.08** | **52.99 / 50.88** | 81.89 / **81/98** | **74.31 / 74.95** | **88.20 / 86.55** | **76.78 / 74.74** | **81.94 / 80.33** | 90.00 / **83.25** |
| *Difference* | +0.49 / +0.67 | +0.34 / +0.48 | +0.26 / +0.67 | -0.27 / +0.46 | +1.52 / +2.02 | +1.55 / +1.81 | +0.74 / +0.94 | +0.81 / +0.50 | -0.58 / +0.23 |

Table 22: **Per-client performance of FedMosaic vs. SFT in a Homogeneous PFL-Dynamic setup on HFLB.** The *Difference* row shows the performance gain/loss of FedMosaic compared to SFT. All clients use the LLaVA-Llama3.2-3B model.

| Method | $A_{last}$ / $A_{\text{AUC}}$ | | | | | | | | |
|---|---|---|---|---|---|---|---|---|---|
| | Client 1 | Client 2 | Client 3 | Client 4 | Client 5 | Client 6 | Client 7 | Client 8 | Client 9 |
| SFT | 83.09 / 81.54 | 96.62 / 96.70 | 51.81 / 51.38 | 80.62 / 80.32 | 72.34 / 73.66 | 92.21 / 90.82 | 77.56 / 75.12 | **82.66 / 80.74** | **91.04** / 89.83 |
| FedMosaic | **83.21 / 81.98** | **97.96 / 97.68** | **53.29 / 52.24** | **81.59 / 81.92** | **76.20 / 74.54** | **92.34 / 91.13** | **77.77 / 75.59** | 81.80 / 80.15 | **91.08 / 89.99** |
| *Difference* | +0.12 / +0.44 | +1.33 / +0.98 | +1.48 / +0.86 | +0.97 / +1.60 | +3.86 / +0.87 | +0.13 / +0.31 | +0.21 / +0.46 | -0.86 / -0.59 | +0.05 / +0.16 |

Table 23: **Per-client performance of FedMosaic vs. SFT in a homogeneous PFL-Static setup on HFLB.** The *Difference* row shows the performance gain/loss of FedMosaic compared to SFT. All clients use the LLaVA-Llama3.2-3B model.

in $A_{\text{AUC}}$ for Client 9 in Tab. 24. We believe this is due to PQ-LoRA effectively sharing knowledge between heterogeneous architectures, allowing both smaller and larger models to provide meaningful information to each other.

| | $A_{last}$ / $A_{\text{AUC}}$ | | | | | | | | | |
|---|---|---|---|---|---|---|---|---|---|---|
| | LLaVA-Llama3.2-**1B** | | | LLaVA-Llama3.2-**3B** | | | | | LLaVA-Llama3.1-**8B** | |
| Method | Client 1 | Client 2 | Client 3 | Client 4 | Client 5 | Client 6 | Client 7 | Client 8 | Client 9 | Client 10 |
| SFT | 77.31 / 66.56 | 61.22 / 57.80 | 67.59 / 62.22 | 77.84 / 71.02 | 66.82 / 57.36 | 66.56 / 56.91 | 66.49 / 64.58 | 62.06 / 58.61 | 64.63 / 57.17 | 72.05 / 69.91 |
| FedMosaic | **78.26 / 67.94** | **61.35 / 59.93** | **67.61 / 63.08** | **78.56 / 74.71** | **72.35 / 60.50** | **71.45 / 62.36** | **67.90 / 65.63** | **61.88 / 59.48** | **71.12 / 66.58** | **73.65 / 70.97** |
| *Difference* | +0.95 / +1.37 | +0.13 / +2.13 | +0.02 / +0.85 | +0.73 / +3.70 | +5.53 / +3.14 | +4.89 / +5.45 | +1.41 / +1.05 | -0.19 / +0.87 | +6.49 / +9.41 | +1.60 / +1.05 |

Table 24: **Per-client performance of FedMosaic vs. SFT in a heterogeneous PFL-Static setup on DRAKE.** The *Difference* row shows the performance gain/loss of FedMosaic compared to SFT. Clients 1-3 use LLaVA-Llama3.2-1B, Clients 4-8 use LLaVA-Llama3.2-3B, and Clients 9-10 use LLaVA-Llama3.1-8B.

| | $A_{last}$ / $A_{\text{AUC}}$ | | | | | | | | |
|---|---|---|---|---|---|---|---|---|---|
| | LLaVA-Llama3.2-**1B** | | | | LLaVA-Llama3.2-**3B** | | | | |
| Method | Client 1 | Client 2 | Client 3 | Client 4 | Client 5 | Client 6 | Client 7 | Client 8 | Client 9 |
| SFT | 80.69 / 77.18 | **97.41** / 95.25 | 50.95 / 47.72 | 82.39 / 81.49 | 73.99 / 73.00 | **92.10** / 88.23 | 76.58 / 74.19 | 81.00 / 79.94 | 89.32 / 83.12 |
| FedMosaic | **81.69 / 77.53** | 96.46 / **96.18** | **51.38 / 47.85** | **82.70 / 82.41** | **74.49 / 75.09** | 91.80 / **88.36** | **76.95 / 74.92** | **82.24 / 80.25** | **89.94 / 83.62** |
| *Difference* | +1.00 / +0.36 | -0.96 / +0.93 | +0.43 / +0.13 | +0.32 / +0.92 | +0.49 / +2.08 | -0.30 / +0.13 | +0.36 / +0.73 | +1.24 / +0.31 | +0.62 / +0.50 |

Table 25: **Per-client performance of FedMosaic vs. SFT in a heterogeneous PFL-Dynamic setup on HFLB.** The *Difference* row shows the performance gain/loss of FedMosaic compared to SFT. Clients 1-3 use LLaVA-Llama3.2-1B, while Clients 4-9 use LLaVA-Llama3.2-3B.

### A.17 Details of Public Data $D_p$

For the public data $D_p$, we use a subset of the MLLM's pretraining data, as briefly mentioned in Sec. 4.2.2. Specifically, since our experiments are based on LLaVA, we adopt its instruction tuning dataset, LLaVA-Instruct-158K (Liu et al., 2023b), as $D_p$. For the alignment details, we randomly sample 5,000 examples from $D_p$ and align PQ-LoRA for 1 epoch using a batch size of 4, a learning rate of $5 \times 10^{-5}$, and the Adam optimizer with cosine scheduler. To further assess the effect of $D_p$, we explore the effect of $D_p$'s size and its distributional alignment with the client data.

| Size of $D_p$ | Self | | Others | |
|---|---|---|---|---|
| | $A_{last}$ ↑ | $A_{\text{AUC}}$ ↑ | $A_{last}$ ↑ | $A_{\text{AUC}}$ ↑ |
| 625 | 67.25±0.08 | 59.17±0.05 | 51.02±0.04 | 49.05±0.09 |
| 1250 | 67.97±0.04 | **59.86±0.16** | 51.33±0.03 | **49.58±0.07** |
| 2500 | **68.11±0.06** | 59.76±0.04 | 51.35±0.31 | 49.52±0.13 |
| 5000 | 67.96±0.05 | 59.83±0.15 | **51.46±0.04** | 49.56±0.06 |
| 10000 | 67.44±0.18 | 59.34±0.16 | 51.04±0.16 | 49.37±0.03 |

Table 26: **Effect of public data $D_p$ size.** FedMosaic performs best on moderate-sized datasets (*i.e.*, 1,250-5,000)

| Dataset $D_p$ | Self | | Others | |
|---|---|---|---|---|
| | $A_{last}$ ↑ | $A_{\text{AUC}}$ ↑ | $A_{last}$ ↑ | $A_{\text{AUC}}$ ↑ |
| LLaVA-Instruct-158K (Liu et al., 2023b) | 67.96±0.05 | 59.83±0.15 | **51.46±0.04** | 49.56±0.06 |
| ChatbotIT (Zheng et al., 2023) | **68.42±0.18** | **60.17±0.26** | 51.16±0.22 | **49.78±0.13** |
| Visual Storytelling (Li et al., 2024d) | 67.90±0.09 | 59.86±0.12 | 51.06±0.05 | 49.41±0.07 |

Table 27: **Effect of domain gap between $D_p$ and clients' data.** FedMosaic shows consistent performance across multiple benchmarks, even on text-only NLP benchmarks (*i.e.*, ChatbotIT).

We first assess the effect of public data size in Tab 26. As shown, using too little data results in insufficient alignment of PQ-LoRA, leading to degraded performance. Interestingly, using too much public data also causes slight performance drops, likely due to overfitting to the $D_p$ distribution, which hinders generalizable alignment to clients' distributions. Considering this trade-off, we selected a moderate dataset size (*i.e.*, 5,000 samples).

Next, we assess robustness under domain mismatch between $D_p$ and the clients' distribution. Specifically, we use ChatbotIT (Zheng et al., 2023) (text-only NLP benchmark) and Visual Storytelling (Li et al., 2024d) (multi-sentence outputs) as $D_p$, both differing from the clients' multi-modal, short-answer tasks. To ensure a fair comparison, we fix the size of $D_p$ to 5,000 samples. As shown in Tab. 27, using Visual Storytelling shows comparable performance with LLaVA-Instruct-158K. Similarly, using text-only NLP benchmark shows performance comparable to (and even surpassing) LLaVA-Instruct-158K, demonstrating resilience of FedMosaic to distribution misalignment between $D_p$ and clients' data.

### A.18 Hyperparameter Analysis

Since dataset-specific hyperparameter search is undesirable under distribution shifts (*i.e.*, Dynamic setup), where future data are unknown, we adopt a single set of hyperparameters across all benchmarks and setups, determined from the DRAKE-Dynamic setup.

**Effect of Communication Rounds $R$ and Local Steps.** We analyze the trade-off by varying the number of communication rounds and local steps under a fixed training budget. As shown in Tab. 28, more rounds (*i.e.*, fewer local steps per round) degrade personalization ('Self'). We attribute this to insufficient local adaptation, which weakens the personalized models and reduces the quality of shared knowledge during communication, ultimately limiting improvements in generalizability. Conversely, significantly reducing rounds (*i.e.*, increasing local steps) improves personalization but harms generalization ('Others') due to limited inter-client knowledge sharing, reducing generalizability. To balance this trade-off, we adopt a moderate setting with 20 rounds and 100 local steps per round.

**Effect of Low Rank $r$ in PQ-LoRA** We study how varying the rank $r$ in PQ-LoRA affects performance, and summarize the results in Fig. 13. As shown in the figure, while both excessively high and low values of $r$ lead to degraded performance, a broad range of intermediate values shows stable performance. While a larger $r$ increases shareable capacity ($\mathbb{R}^{r\times r}$), it may cause overfitting (Lin et al., 2024; Cho et al., 2024). In contrast, a smaller $r$ helps mitigate overfitting but may introduce capacity limitations, resulting in suboptimal performance (He et al., 2022). By balancing the trade-off, we select an adequate low rank $r = 128$.

| Total Rounds | Local Steps per Round | Self | | Others | |
|---|---|---|---|---|---|
| | | $A_{last}$ ↑ | $A_{\text{AUC}}$ ↑ | $A_{last}$ ↑ | $A_{\text{AUC}}$ ↑ |
| 5 | 400 | 66.66±0.89 | **60.21±0.61** | 47.36±0.13 | 46.65±0.01 |
| 10 | 200 | 65.66±0.47 | 58.58±0.29 | 47.44±0.03 | 46.63±0.26 |
| 20 | 100 | **67.86±0.51** | 59.83±0.15 | **51.36±0.04** | 49.46±0.06 |
| 40 | 50 | 67.05±0.54 | 59.49±0.11 | 51.10±0.11 | 49.42±0.02 |
| 80 | 25 | 66.83±0.38 | 59.23±0.06 | 51.16±0.04 | **49.47±0.21** |

Table 28: **Effect of communication rounds and local steps on DRAKE under Fixed Total Training Cost (*i.e.*, Total rounds × Local steps per round).**

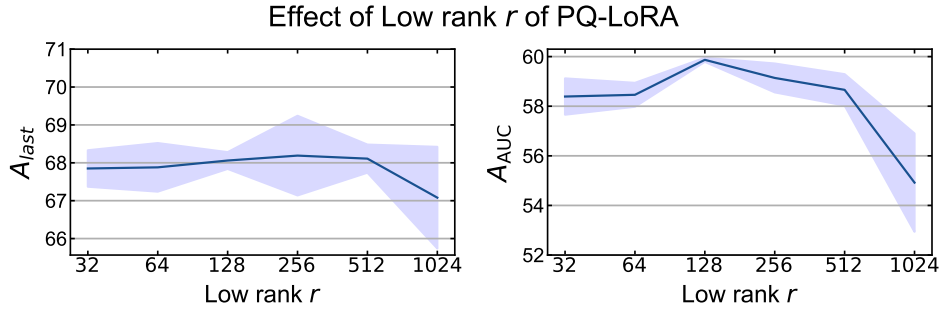


Figure 13: **Accuracy on different low rank $r$ values in PQ-LoRA on DRAKE-Dynamic setup.** Extremely low or high ranks degrade performance, but a wide intermediate range maintains stable accuracy.

**Effect of $N_B$ in PQ-LoRA** We study the effect of $N_B$, the number of layers employing PQ-LoRA, and summarize the results in Tab.29. In a model $W$ with $|W|$ layers, increasing $N_B$ reduces the layers using conventional LoRA to $|W| - N_B$. Since PQ-LoRA has fewer trainable parameters (*i.e.*, $r^2 + r$) than conventional LoRA (*i.e.*, $r \times (d_I + d_O)$), increasing $N_B$ decreases the total number of learnable parameters in $W$, as $A \in \mathbb{R}^{r \times d_I}$ and $B \in \mathbb{R}^{d_O \times r}$ are frozen, with only $P \in \mathbb{R}^{r \times r}$ and $Q \in \mathbb{R}^r$ being trainable. Despite the reduced number of parameters, as shown in the SFT performance in the table, performance remains stable even as $N_B$ increases. We attribute this to orthogonal and frozen $A$ and $B$, which maximize and preserve the expressiveness of PQ-LoRA (Theorem1), despite the lower trainable parameter count.

However, there is a trade-off in $N_B$ in the PFL setup: increasing $N_B$ improves generalizability (*e.g.*, $N_B = 2$ vs. $N_B = 4$ in $A_{\text{AUC}}$ of 'Others' in FedMosaic) but can degrade personalization (*e.g.*, $N_B = 4$ vs. $N_B = 8$ in $A_{\text{last}}$ and $A_{\text{AUC}}$ of 'Self' in FedMosaic). This is because, while increasing $N_B$ enables heterogeneous models to share knowledge across more layers, the number of trainable parameters for local training decreases due to the reduction in the number of conventional LoRA modules. As a result, by balancing this trade-off, we employ a moderate value of $N_B$, *i.e.*, $N_B = 4$.

| Method | Self | | Others | |
|---|---|---|---|---|
| | $A_{last}$ ↑ | $A_{\text{AUC}}$ ↑ | $A_{last}$ ↑ | $A_{\text{AUC}}$ ↑ |
| SFT ($N_B = 2$) | 66.14±0.02 | 57.02±0.09 | 47.75±0.42 | 46.02±0.14 |
| SFT ($N_B = 4$) | 66.24±0.68 | 57.71±0.27 | 47.63±0.15 | 46.62±0.14 |
| SFT ($N_B = 8$) | 66.21±0.62 | 57.87±0.20 | 47.86±0.29 | 46.76±0.20 |
| FedMosaic ($N_B = 2$) | **68.07±0.10** | **59.90±0.68** | 51.07±0.06 | 48.78±0.15 |
| FedMosaic ($N_B = 4$) | 67.86±0.51 | 59.83±0.16 | 51.26±0.04 | **49.36±0.08** |
| FedMosaic ($N_B = 8$) | 67.52±0.77 | 59.39±0.23 | **51.27±0.27** | 49.26±0.14 |

Table 29: **Accuracy on different number of blocks ($N_B$) in PQ-LoRA in heterogeneous PFL-dynamic setup on DRAKE.** Given a model $W$ with $|W|$ layers, using $N_B$ blocks means that $N_B$ layers adopt PQ-LoRA, while the remaining $|W| - N_B$ layers use conventional LoRA.

**Effect of Orthogonality-regularization Scale $\lambda$ in PQ-LoRA** We study how varying the orthogonality-regularization scale $\lambda$ in PQ-LoRA alignment process (Eq. 20) affects performance, and summarize the results in Fig. 14. We observe that the 'Self' performance does not fluctuate on larger $\lambda$,

but reduces for small $\lambda$. This indicates that insufficient weighting of the orthogonality-regularization term weakens the enforced orthogonality among $A$ matrices from heterogeneous models, thereby reducing the representational capacity (*i.e.*, Span) of PQ-LoRA, as mentioned in Theorem 1.

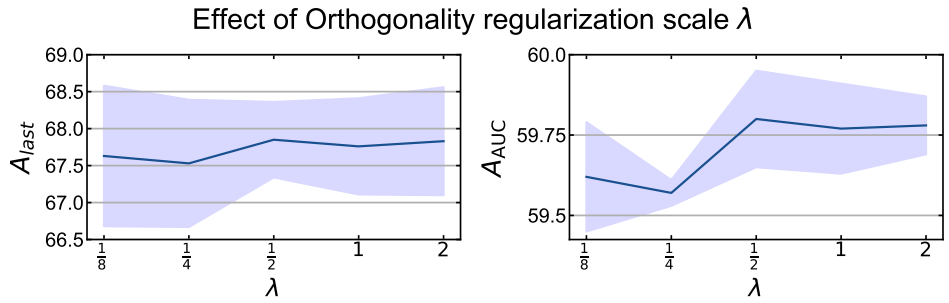


Figure 14: **Accuracy on different L2 regularization scale $\lambda$ values in PQ-LoRA on DRAKE-Dynamic setup.** Extremely low $\lambda$ degrades performance, but a wide intermediate range maintains stable accuracy.

**Effect of Temperature $\tau$ in RELA** We analyze the effect of the softmax temperature $\tau$ in RELA (Eq. 4), which controls the aggregation sharpness, *i.e.*, lower $\tau$ focuses aggregation on similar clients, while higher $\tau$ aggregates weights across more diverse ones. Interestingly, as shown in Fig. 15, neither decreasing nor increasing the temperature $\tau$ consistently improves personalization or generalization. Instead, we observe two trends: (i) Extremely low $\tau$ degrades both personalization and generalization (ii) Increasing $\tau$ too much reduces personalization, while generalization gradually stabilizes.

This is because low $\tau$ limits the diversity of aggregation, restricting knowledge sharing even among moderately relevant clients. In contrast, high $\tau$ encourages sharing across dissimilar tasks, which can reduce personalizability due to the inclusion of unrelated knowledge in the global model. However, increasing $\tau$ does not continuously improve generalization; it converges after a certain point. We believe this is because, although a higher $\tau$ promotes aggregation of more diverse knowledge, it also increases parameter interference (*e.g.*, sign conflicts) when combining models trained on distinct tasks (Yeh et al., 2023; Ding et al., 2024). Consequently, we adopt a moderate temperature of $\tau = 0.5$ for all experiments.

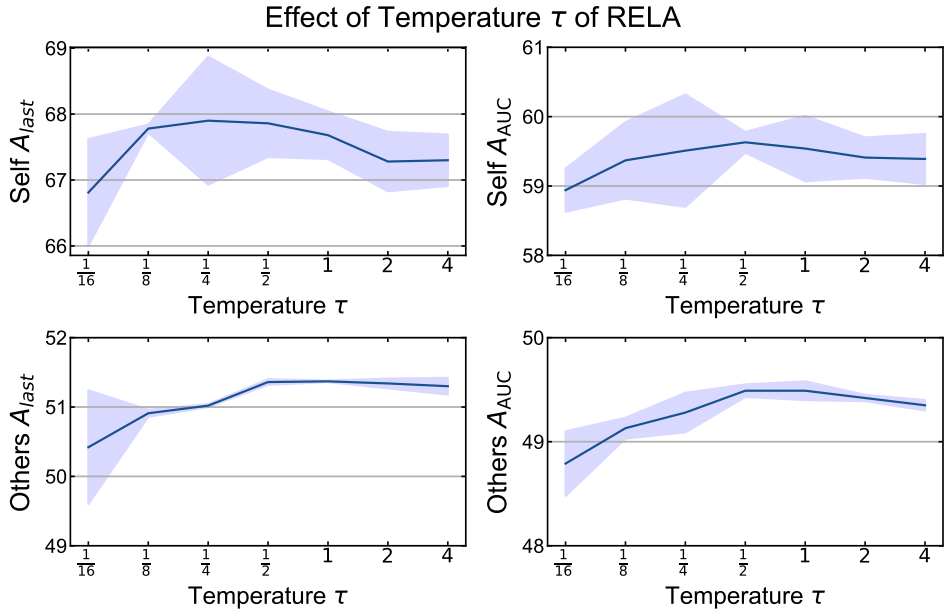


Figure 15: **Accuracy under different temperatures $\tau$ on DRAKE-Dynamic setup.** Extremely low or high temperatures degrade performance, but a wide intermediate range maintains stable accuracy.

**Effect of Gradient sampling ratio $N_s$ in RELA** We analyze the effect of gradient sampling ratio $N_s$ and summarize the results in Fig. 16. As shown, sampling only a very small number of dimensions from the decayed client-wise gradient $\hat{g}_i$ to construct the sanitized gradient $\tilde{g}_i$ significantly degrades performance, as it undermines the representativeness and informativeness of the compressed gradient vector (Li et al., 2024b). However, using up to $N_s = 40\%$ of the gradient dimensions maintains comparable performance while reducing both communication costs and privacy risks from gradient inversion. Accordingly, we consistently set $N_s = 40\%$ for RELA in all experiments.

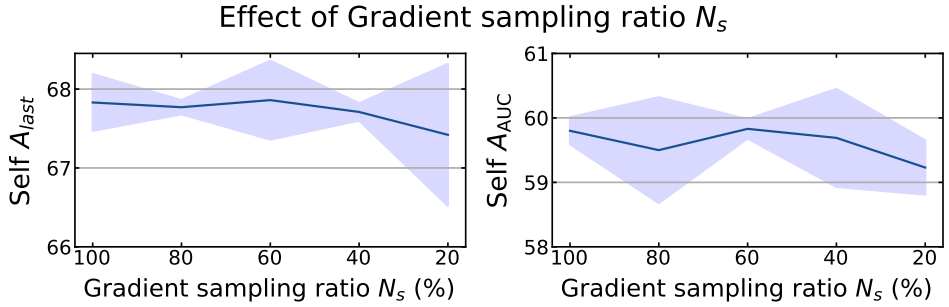


Figure 16: **Accuracy under different gradient sampling ratio $N_s$ on DRAKE-Dynamic setup.** Extremely low gradient sampling ratio degrades performance, but a wide range maintains stable accuracy.

**Effect of decaying EMA ratio $\alpha$ in RELA** We analyze the effect of gradient deacying EMA ratio $\alpha$ and summarize the results in Fig. 17. Too small $\alpha$ ignores current task information, while too large $\alpha$ ignores previously learned tasks. Balancing the trade-off, we consistently set $\alpha = 0.5$ for RELA in all experiments.

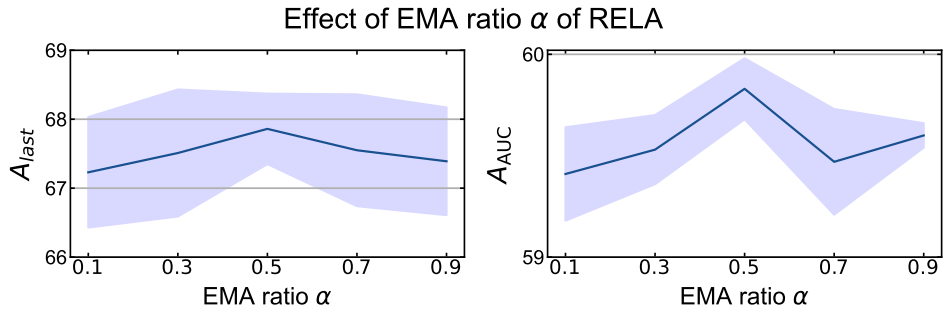


Figure 17: **Accuracy under different gradient decaying EMA ratio $\alpha$ on DRAKE-Dynamic setup.** Balance between current and old ($\alpha = 0.5$) shows the best result.

**Effect of noise scale $\mu$ in RELA sanitized gradient** We also study the noise scale $\mu$ in sanitized gradient $\tilde{g}$ (Eq. 3) in RELA and visualize the results in Fig. 18. We clearly see the decreasing trend in the results when we increase the noise scale. While stronger random noise enhances privacy by better concealing sensitive information, excessive noise severely distorts the gradient signal, undermining the reliable estimation of task relevance based on gradient similarity.

### A.19 Ablation Study of RELA

Our proposed RELA measures task similarity among clients using client-wise gradients to construct a similarity-aware customized global model for each client. Specifically, for the $i$-th client, we maintain a decayed gradient $\hat{g}_i$, updated via exponential moving average (EMA) from the current gradient $g_i$, which is computed using the current batch and a small, frozen pre-trained model. Note that we use the last-layer gradient of the frozen model, not the training model, as mentioned in Sec. 4.1.

We ablate RELA by comparing four aggregation variants: (1) Equal-weight aggregation, which ignores task similarity and aggregates local models uniformly; (2) Training model gradients, using

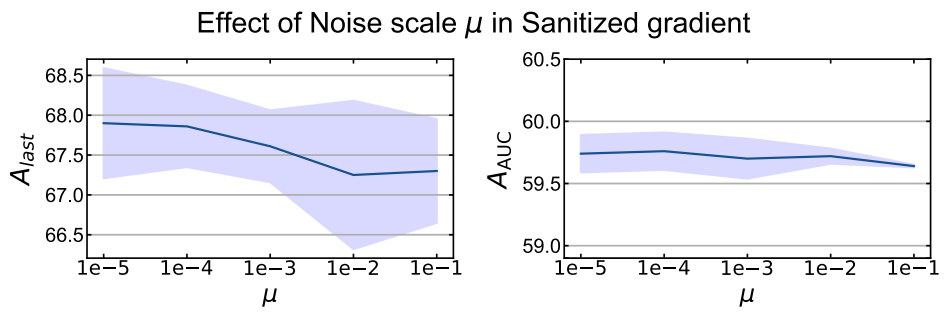


Figure 18: **Accuracy under different noise scale $\mu$ on DRAKE-Dynamic setup.** Strong noise distorts the gradient signal, undermining the reliable estimation of task relevance based on gradient similarity.

current batch gradients from the trainable model; (3) Frozen model gradients, using current batch gradients from the frozen pre-trained model; and (4) Decayed frozen gradient (*i.e.*, RELA), which maintains an EMA of gradients from the frozen pre-trained model to capture model knowledge shifts. We summarize the results in Tab. 30.

As shown in the table, model aggregation considering task similarity measured by client-wise gradients generally improves the 'Self' accuracy. This demonstrates the loss of information in Equal-weight aggregation due to parameter interference. While using gradients from the training model ('Training model gradient') shows improved performance compared to Equal-weight aggregation, it still suffers from data heterogeneity, as gradient similarities from models trained on heterogeneous data may not capture actual similarity (Tang et al., 2020; Evans et al., 2024). Using a frozen model's gradients from the current batch ('Frozen model gradients') can address this limitation, but cannot reflect model knowledge shifts under distribution shifts, as mentioned in Sec. 4.1. In contrast, RELA effectively captures task similarity under data heterogeneity with distribution shifts, thus outperforming other aggregation strategies.

| | Self | |
|---|---|---|
| Method | $A_{last}$ ↑ | $A_{\text{AUC}}$ ↑ |
| Equal-weight aggregation | 66.99±0.77 | 58.39±0.38 |
| Training model gradients | 67.16±0.74 | 59.38±0.53 |
| Frozen model gradients | 67.24±1.27 | 59.45±0.74 |
| Decayed frozen gradients **(RELA)** | **67.86±0.51** | **59.83±0.16** |

Table 30: **Ablation of components in RELA in Heterogeneous PFL-dynamic setup on DRAKE.** 'Equal-weight aggregation' refers to aggregating local models with equal weight, 'Training model gradients' refers to using gradients from the current batch computed with the training model, 'Frozen model gradients' refers to using gradients from the current batch computed with the frozen pre-trained model, and 'Decayed frozen gradients' refer to EMA-estimated gradients from the frozen model (*i.e.*, RELA).

### A.20 RELA WITH LIGHTER $W_s$

To extract per-client gradients for RELA, we employ the smallest MLLM among all clients' models (*e.g.*, LLaVA-1.5-1B). To further reduce the computational overhead of RELA, we can utilize an even smaller model (*e.g.*, LLaVA-Qwen-0.5B) or apply lower-bit quantization (*e.g.*, 4-bit and 8-bit), as shown in Tab. 31. The results show that FedMosaic maintains consistent performance even with smaller models and lower-bit quantization, demonstrating that computational costs can be further reduced without sacrificing performance.

### A.21 DIFFERENT WEIGHT ALIGNMENT METHODS IN PQ-LORA

To ensure shared initialization across heterogeneous architectures, we align $A$ matrices from heterogeneous architectures (*i.e.*, $A_i \in \mathbb{R}^{r\times d_i}$, $A_j \in \mathbb{R}^{r\times d_j}$) using L2 loss, and $B$ matrices (*i.e.*, $B_i \in \mathbb{R}^{d_i'\times r}$,

| $W_s$ | Relative computational costs ↓ | Self | | Others | |
|---|---|---|---|---|---|
| | | $A_{last}$ ↑ | $A_{\text{AUC}}$ ↑ | $A_{last}$ ↑ | $A_{\text{AUC}}$ ↑ |
| LLaVA-Llama3.2-1B (16bit) | 1.0 | **67.86±0.51** | **59.83±0.15** | 51.16±0.04 | 49.36±0.08 |
| LLaVA-Qwen-0.5B (16bit) | 0.52 | 67.84±0.19 | 59.42±0.75 | 51.40±0.12 | 49.37±0.19 |
| LLaVA-Qwen-0.5B (8bit) | 0.26 | 67.36±0.14 | 59.22±0.43 | **51.74±0.06** | **49.56±0.07** |
| LLaVA-Qwen-0.5B (4bit) | 0.13 | 67.23±0.49 | 59.41±0.13 | 51.34±0.42 | 49.43±0.09 |

Table 31: **Effect of $W_s$'s model size and quantization on DRAKE-Dynamic.** Relative computational costs denote the ratio of computation compared to LLaVA-1.5-1B (16-bit). Comparable performance is maintained with both a smaller model (*i.e.*, 0.5B) and quantized models (*i.e.*, 4-bit, 8-bit).

$B_j \in \mathbb{R}^{d'_j \times r}$) using canonical correlation analysis (CCA), as detailed in Sec.4.2.2. We ablate the effects of aligning $A$ and $B$ matrices, and summarize the results in Tab. 32. Note that the results in the table report the average performance across all clients, which can make the overall average improvements appear small, as mentioned in Sec. 6.2.

As shown, alignment improves both personalization ('Self') and generalization ('Others') performance. This occurs because aligning both $A$ and $B$ in PQ-LoRA ensures heterogeneous models share initialization and follow consistent optimization paths, allowing aggregation without weight interference (Wortsman et al., 2022a;b; Yadav et al., 2023). In contrast, misalignment in either matrix introduces initialization discrepancies between models, leading to weight interference during aggregation and degrading performance (Jordan et al., 2023; Neyshabur et al., 2020; Stoica et al., 2025).

| Initialization | | Self | | Others | |
|---|---|---|---|---|---|
| A | B | $A_{last}$ ↑ | $A_{\text{AUC}}$ ↑ | $A_{last}$ ↑ | $A_{\text{AUC}}$ ↑ |
| Random | Random | 67.95±1.71 | 63.50±0.66 | 47.71±0.08 | 47.46±0.05 |
| Random | Aligned (CCA) | 68.22±1.84 | 63.59±0.62 | 47.80±0.06 | 47.56±0.08 |
| Aligned (L2) | Random | 68.29±1.57 | 63.58±0.60 | 47.72±0.14 | 47.41±0.04 |
| Aligned (L2) | Aligned (CCA) | **68.73±1.92** | **63.82±0.59** | **48.04±0.04** | **47.57±0.08** |

Table 32: **Accuracy on different weight alignment in PQ-LoRA under Heterogeneous PFL-Static setup on DRAKE.** 'Random' initializes matrices randomly, while Aligned (L2) and Aligned (CCA) use matrices aligned by L2 loss and canonical correlation analysis (CCA), respectively.

### A.22 Comparison with Similarity-Aware Model Aggregation

**Federated Learning** We are not the first to try to aggregate client models based on task similarity, but most existing approaches are not applicable to large language model (LLM) federated learning scenarios. pFedSim (Tan et al., 2023) measures the classifier similarity among clients and uses it for weighted model aggregation, which is infeasible for LLM fine-tuning where the pre-trained classifier remains frozen. pFedHR (Wang et al., 2023) computes similarity between client models based on the output logits and performs similarity-aware layer stitching. However, its logit extractions relies on public data, which (as acknowledged by the authors) raises public data sensitivity concerns: the discrepancy between private and public data may leads to inaccurate similarity estimate. Flashback (Aljahdali et al., 2024) conducts dynamic knowledge distillation where teacher logits are adaptively weighted by client-wise label count, but this method is limited to single-dataset classification FL tasks. There is also another approach like FEDLAW (Li et al., 2023d) that adaptively aggregates models based on the optimized learnable weights instead of client similarity. However, it incurs high computational costs and remains highly sensitive to the choice of public data.

RELA, on the contrary, measures the task similarity among clients using sanitized last layer gradients. These gradients from each private data effectively capture task characteristics with minimal additional computation and communication cost, while preserving privacy through EMA updates, noise injection, and gradient compression.

**Multi-Task Learning** Federated learning (FL) and personalized federated learning (PFL) are not the only paradigms that learn heterogeneous tasks concurrently. Multi-task learning (MTL)

trains a single model on multiple tasks simultaneously in a single compute node, not in separate private nodes as in FL. MTL methods, such as NBS (Navon et al., 2022) and Rotograd (Javaloy & Valera, 2022), leverage inter-task relationships to dynamically weight gradients, thereby mitigating interference and promoting a balanced update direction across tasks. This is similar to the motivation of our aggregation method, *i.e.*, RELA, which aims to reduce the interference between multiple tasks. However, these techniques are not directly applicable to personalized federated learning due to differing objectives: similarity-aware MTL strategies target *generalizability* by reshaping task-specific gradients to improve a single shared model, whereas RELA focuses on *personalization*. It provides each client with a customized global model by down-weighting contributions from irrelevant tasks, rather than enforcing a single globally shared one, thereby providing knowledge beneficial for personalization, while still enhancing generalizability as a byproduct.

We also empirically compare RELA with MTL methods (Navon et al., 2022). Note that Rotograd(Javaloy & Valera, 2022) is incompatible with PFL because it aligns gradient directions by optimizing rotation heads using samples from multiple tasks, which is not feasible under federated data isolation and privacy constraints. Therefore, we only compare with NBS, which determines task weights via a Nash bargaining objective that maximizes total loss reduction. In PFL setting, we apply NBS weighting to adapter parameters rather than raw gradients for a shared global model, since FL aggregates parameters. As shown in Tab. 33, NBS shows lower 'Self' performance, while maintaining similar generalization ('Others') performance. We believe NBS's weighting mechanism focuses on harmonizing parameters from multiple tasks to minimize the overall loss, but fails to preserve or share task-relevant information necessary for each client's personal tasks, resulting in poor 'Self' performance.

| | Self | | Others | |
|---|---|---|---|---|
| Method | $A_{last}$ ↑ | $A_{\text{AUC}}$ ↑ | $A_{last}$ ↑ | $A_{\text{AUC}}$ ↑ |
| FedMosaic w/ RELA | **67.86±0.51** | **59.83±0.15** | **51.16±0.04** | **49.36±0.08** |
| FedMosaic w/ NBS (Navon et al., 2022) | 66.89±0.43 | 58.98±0.20 | 51.07±0.09 | 49.09±0.06 |

Table 33: **Quantitative comparison with MTL method.**

### A.23 Extended Fast Adaptation Evaluations

In addition to the fast adaptation evaluation in Sec.6.2, we further assess fast adaptation on additional unseen tasks from DRAKE. We summarize the results in Fig.19. As shown in the figure, models initialized with FedMosaic adapt significantly faster than those with random initialization or other PFL baselines, demonstrating that FedMosaic enhances generalizability by effectively sharing knowledge in heterogeneous PFL setups.

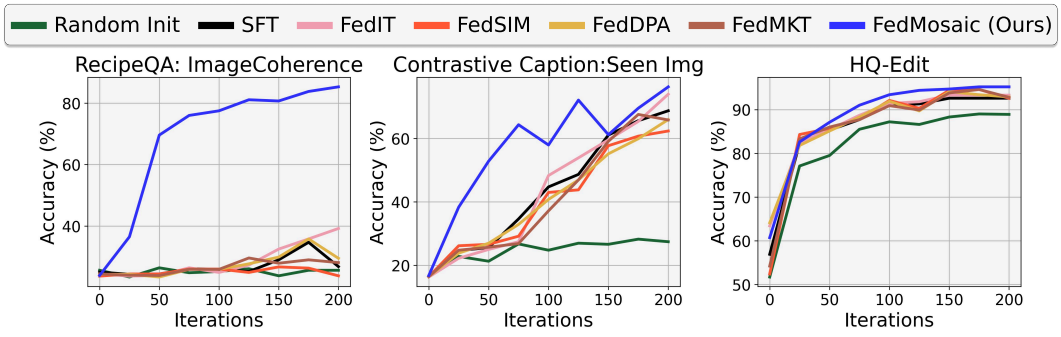


Figure 19: **Comparison of adaptation speed.** We use FedMosaic's unseen tasks as downstream tasks. Random init starts from randomly initialized models, while other baselines are initialized from aggregated local models trained on DRAKE using each respective FL baseline.

### A.24 Additional Details of DRAKE

We curate DRAKE using open-sourced datasets from the Internet. Specifically, we select large-scale multi-modal benchmarks that differ in distribution or properties from LLaVA's pre-training data and provide clear metadata or instructions, enabling task-wise splits for emulating distribution shifts. We refer to diverse multi-modal benchmarks, such as DEMON (Li et al., 2024c), SEED-Bench-2 (Li et al., 2024a), Co-Instruct (Wu et al., 2024b), and HFLB (Chen et al., 2024).

DRAKE consists of 40 distinct tasks, where for each task, we subsample 10,000 training and 1,000 test samples, if the dataset is large; otherwise, we split the data into training and test sets with an 8:2 ratio, totaling 375k images and 274k questions. We illustrate the overall structure of DRAKE as a tree diagram in Fig. 20. As shown in the figure, DRAKE consists of three sub-groups, *i.e.*, visual relation, multi-modal reasoning, and VQA, each comprising multiple fine-grained tasks, with representative examples of each sub-group in Fig. 21. We also provide detailed per-client task configuration of DRAKE in Tab. 34.

**Visual Relation Tasks** Visual relation tasks focus on capturing relationships among visual objects, consist of 12 distinct tasks. We categorize them into three splits: *fashion-relation*, *dual-image relation*, and *spatial/temporal*. The fashion-relation split focuses on fine-grained attribute understanding in clothing images, using the cloth-counting and three-/four-image variants of Fashion200K (Han et al., 2017) as well as the query–reference caption split of FashionIQ (Wu et al., 2021). The dual-image relation split evaluates comparative reasoning across separate images, drawing on NLVR2 (Suhr et al., 2019), CIRR (Liu et al., 2021), the two- and four-image true/false subsets of VISION (Bai et al., 2023), and MagicBrush (Zhang et al., 2023a). The spatial/temporal split targets positional and temporal dependencies, combining single-frame spatial reasoning in VSR (Liu et al., 2023a) with temporal understanding tasks from SEED-Bench-2 (Li et al., 2024a).

**Multi-modal Reasoning Tasks** Multi-modal reasoning tasks require the integration of visual cues with common-sense knowledge, comprising 12 distinct tasks. We include four tasks from IRFL (Yosef et al., 2023) that examine the figurative interpretation of images paired with non-literal language. We also include five additional tasks derived from the positive–negative image groups in Bongard-HOI (Jiang et al., 2022) and Bongard-OpenWorld (Wu et al., 2024d). These tasks require fine-grained discrimination between contrasting sets. We incorporate three reasoning challenges from COMICS (Iyyer et al., 2017), MIT-States (Isola et al., 2015), and VizWiz (Gurari et al., 2018), all sourced from DEMON (Li et al., 2024c).

**VQA Tasks** The *VQA* sub-group includes 16 diverse VQA tasks that differ significantly from LLaVA's pre-training datasets. We include novel question types, such as image-quality queries in Co-Instruct (Wu et al., 2024b), textbook-style diagram interpretation in TQA (Kembhavi et al., 2017), DVQA (Kafle et al., 2018), and knowledge-grounded QA tasks from SEED-Bench-2 (Li et al., 2024a). We also incorporate unfamiliar image domains, including IconQA (Lu et al., 2021) and WCVQA (Winata et al., 2024). We partition Co-Instruct by question type (*e.g.*, Yes/No, How/what questions), IconQA by difficulty and question category (*e.g.*, Multi-choice or Short answering, kindergarten-level or grade 1-level questions), while we divide WCVQA using their original split.

**Unseen Tasks** To assess generalization capability, we add 7 additional tasks that are disjoint from the clients' tasks in DRAKE. We selected challenging benchmarks requiring extensive training, which are far from fast adaptation. The unseen tasks include novel task types (DreamSim (Fu et al., 2023b), ImageCoDe (Krojer et al., 2022)) and novel visual domains with familiar task format (RecipeQA (Yagcioglu et al., 2018) subsets proposed in DEMON (Li et al., 2024c), and HQ-Edit Hui et al. (2025)). In addition, we split the Contrast-Caption subset of Mantis (Jiang et al., 2024; Yu et al., 2022) into two tasks: one with images overlapping LLaVA's pre-training distribution and another with previously unseen images.

### A.25 Comparison with Other FL Benchmarks.

A number of federated learning (FL) benchmarks exist, but most lack critical aspects required for FL of multi-modal foundation models, which DRAKE addresses, with the main differences summarized in Tab. 1.

| Client 1 | Client 2 |
|---|---|
| • Fashion200K (Han et al., 2017): ClothCombination<br>• FashionIQ (Wu et al., 2021)<br>• VISION (Bai et al., 2023): 2_Img<br>• MagicBrush (Zhang et al., 2023a) | • Co-Instruct (Wu et al., 2024b): 2_ImgCompare<br>• SEED–Bench–2 (Li et al., 2024a): KGQA<br>• IconQA (Lu et al., 2021): ShortAnswerEasy<br>• WCVQA (Winata et al., 2024): DishName |
| **Client 3** | **Client 4** |
| • Co-Instruct (Wu et al., 2024b): HowWhat<br>• DVQA (Kafle et al., 2018)<br>• IconQA (Lu et al., 2021): ShortAnswerHard<br>• WCVQA (Winata et al., 2024): ContextDishName | • Co-Instruct (Wu et al., 2024b): 3_ImgCompare<br>• SEED–Bench–2 (Li et al., 2024a): InstanceQA<br>• IconQA (Lu et al., 2021): MultiChoiceEasy<br>• WCVQA (Winata et al., 2024): AdvContextDishName |
| **Client 5** | **Client 6** |
| • Fashion200K (Han et al., 2017): ColorConsistency<br>• NLVR2 (Suhr et al., 2019): Subset1<br>• VISION (Bai et al., 2023): 4_Img<br>• VSR (Liu et al., 2023a) | • Fashion200K (Han et al., 2017): StyleConsistency<br>• NLVR2 (Suhr et al., 2019): Subset2<br>• CIRR (Liu et al., 2021)<br>• SEED–Bench–2 (Li et al., 2024a): TemporalQA |
| **Client 7** | **Client 8** |
| • IRFL (Yosef et al., 2023): MetaphorSimileMatching<br>• Bongard–HOI (Jiang et al., 2022): ActionDetection<br>• VizWiz (Gurari et al., 2018)<br>• MIT–States (Isola et al., 2015) | • IRFL (Yosef et al., 2023): FigurativeVerification<br>• IRFL (Yosef et al., 2023): IdiomMatching<br>• Bongard–OpenWorld (Wu et al., 2024d): ConceptDetection<br>• COMICS (Iyyer et al., 2017): Dialogue |
| **Client 9** | **Client 10** |
| • IRFL (Yosef et al., 2023): PhraseSelection<br>• Bongard–OpenWorld (Wu et al., 2024d): ConceptQuery<br>• Bongard–HOI (Jiang et al., 2022): ConceptQuery<br>• Bongard–HOI (Jiang et al., 2022): ActionIncoherence | • Co-Instruct (Wu et al., 2024b): YesNO<br>• TQA (Kembhavi et al., 2017)<br>• IconQA (Lu et al., 2021): MultiChoiceHard<br>• WCVQA (Winata et al., 2024): Location |

Table 34: **Per-client task configuration of DRAKE.** DRAKE consists of 10 clients, each with 4 distinct tasks. Client 1, 5, 6 tackle visual relation tasks, Client 7, 8, 9 handle multi-modal reasoning tasks, and Client 2, 3, 4, 10 focus on VQA tasks, as illustrated in Fig. 20.

Benchmarks like NonIID-50 (Yoon et al., 2021), LEAF-FCL (Qi et al., 2023), and MNIST-Shuffle (Wuerkaixi et al., 2024) simulate distribution shifts under FL. However, they are single-task and single-modal (*i.e.*, image classification) only, thus cannot reflect real-world task diversity. HC-FMTL (Lu et al., 2024) spans multiple vision tasks, such as depth estimation and semantic segmentation, but still remains unimodal.

On the language side, several text-only FL benchmarks have recently been proposed to target LLM federated learning scenarios. Fed-SNI (Collins et al., 2023) and Fed-FLAN (Long et al., 2024) cover diverse NLP tasks, while Fed-Aya (Ye et al., 2024) focuses on multilingual instruction following. FEDLEGAL (Zhang et al., 2023b) curates a FL benchmark for the privacy-sensitive legal domain where federated learning is necessary. Despite their breadth, they are also limited to a single modality and assume static data distribution, while data distribution often shifts over time in real-world.

For multi-modal PFL, we find only one prior benchmark: HFLB (Chen et al., 2024). Although HFLB includes 7 different datasets, the multi-modal task diversity is limited, and they are mostly single-image settings. Other multi-modal FL benchmarks, *e.g.*, FedMultimodal (Feng et al., 2023), FHBench (Wang et al., 2025), and FedMLLM (Xu et al., 2024), are primarily comprised of only a classification task on different modalities or split one or two VQA datasets, which is insufficient for evaluation personalization under diverse heterogeneous tasks. Importantly, existing benchmarks generally lack an unseen task split to test the generalization ability of the model.

In contrast, DRAKE offers 40 different multi-modal tasks (including multi-image tasks), which is suitable for personalization evaluation and temporal distribution shift. Moreover, DRAKE additionally provides 7 unseen tasks for out-of-distribution generalization evaluation.

### A.26 Limitations and Future Work

While we evaluate FedMosaic across diverse multi-modal FL benchmarks (*e.g.*, HFLB and our proposed DRAKE) and text-only NLP benchmarks (*e.g.*, Fed-Aya, Fed-Scope, and Fed-LLM-Large), it has not yet been tested on other modalities such as speech and time series. Extending evaluations

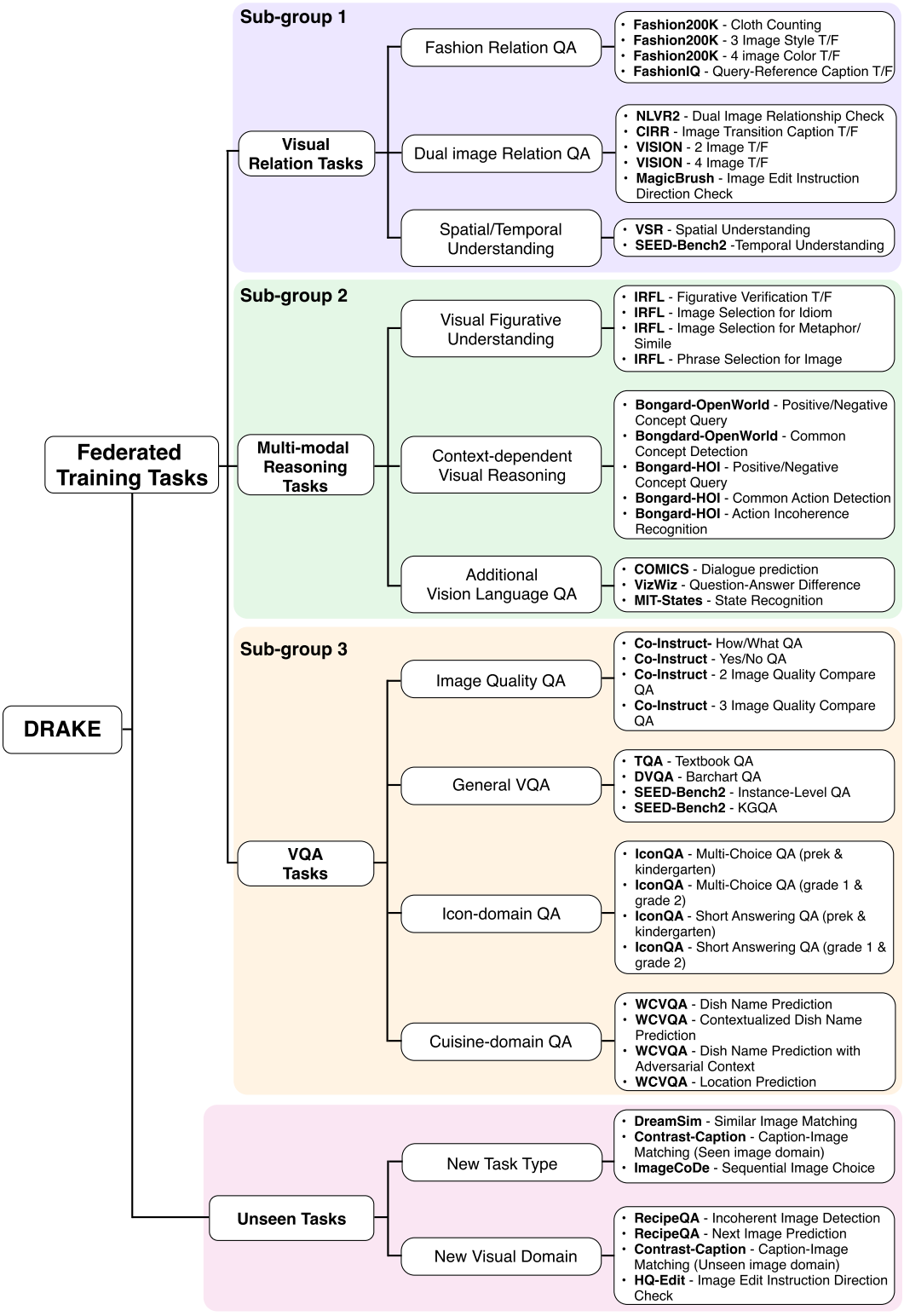


Figure 20: **Detailed configuration of the proposed DRAKE benchmark.**

to these domains would better capture real-world FL scenarios and represent an important direction for future work.

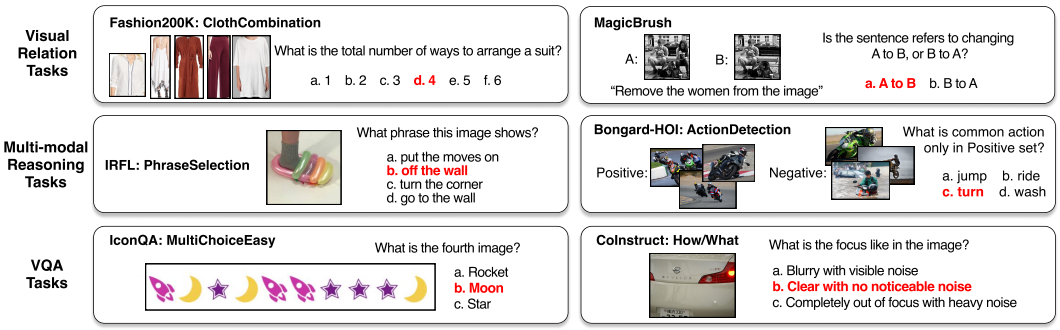


Figure 21: **Data samples from DRAKE.**

Moreover, although LoRA is most commonly used in transformer-based models, it is not restricted to them. Specifically, prior studies (Yeh et al., 2023; Ding et al., 2024) have demonstrated its applicability to convolutional layers, highlighting its architecture-agnostic nature. Therefore, exploring the use of PQ-LoRA beyond transformers to enable knowledge transfer across broader model families represents an important direction for future work.

### A.27 Impact Statements

This work focuses on federated learning, which enables model training in a distributed manner, eliminating the need to share raw data and thereby mitigating data privacy risks. However, since we assume that the model is trained under distribution shifts, there is a potential for the unintended amplification of issues such as model bias and ethical misalignment. We are committed to taking all necessary measures to address these risks, although tackling these concerns is not the primary focus of this work.

### A.28 Detailed Algorithm of FedMosaic

Algorithm 1 provides a pseudocode for the proposed FedMosaic framework. We further provide detailed algorithms for initializing adapters (Algorithm 2) and aligning adapters across heterogeneous clients (Algorithms 3 and 4).

**Algorithm 1:** FedMosaic

```
# Input
#   Number of clients N, Number of client model types K,
#   Set of frozen pre-trained models W = {W_1, ..., W_K},
#   Mapping of client to model V : {1, ..., N} → W, Number of rounds
 R,
#   Batch size B, Learning rate η, Gradient frequency f, EMA
 ratio a, Temperature τ, Gaussian noise std μ, Gradient
 subsample ratio N_s
#   Small-scale pre-trained model W_S, Regularization
 coefficient λ
#   Training data streams of T tasks for N clients
 {D_1, D_2, ..., D_N},
#   where D_i = {D_i^1, D_i^2, ..., D_i^T}, Number of PQ-LoRA blocks N_B,
#   Public dataset D_p, Conventional-LoRA, PQ-LoRA

E = InitializeAdaptersForModels(W, N_B, K) # (Alg. 2)
E = AlignAdapter(W, E, D_p, K, λ) # (Alg. 3, Alg. 4)

# Initialization for each client
for i in range(N) do
    M[i] = [] # Initialize episodic memory
    # Initialize local and global adapters with the aligned
     adapter E
    L[i] = E[i]
    G[i] = E[i]
    # Initialize gradient vector with zeros
    g[i] = torch.zeros(d_[len(V(i))])
    # Initialize gating parameters for each layer in L[i]
    beta[i] = [0.0 for _ in range(len(L[i]))]

# Set Random subsample indices for last layer gradient
subsample_index = random_choice(last_layer_grad size, N_s)

for task t in range(T) do
    for round r in range(R) do
        # Client-side
        for client index i in range(N) do
            W_i = V(i)
            g_t = []
            for j, (x_j, y_j) in D_i^t do
                M[i].append((x_j, y_j))
                x, y = random_choice(M[i], B)
                # Compute loss with mixed local-global adapter
                loss = CrossEntropy(Forward(W_i, L[i], G[i], beta[i],
                 x), y)
                L[i] −= η * Grad(L[i], loss)
                if i % f == 0 then
                    loss = CrossEntropy(Forward(W_S, x), y)
                    g_last = LastLayerGrad(W_S, loss)
                    # Subsample gradient and add gaussian noise
                    eps ∼ N(0, I) # I ∈ R^last_layer_grad size
                    g_sanitized = g_last[subsample_index] + μ *
                     eps[subsample_index]
                    g_t.append(g_sanitized)
            g[i] = (1 − a) * g[i] + a * Average(g_t)
        # Server-side
        # Aggregate global adapters using SIMA
        G = SIMA(L, g)
```

**Algorithm 2:** `InitializeAdaptersForModels`$(\mathcal{W}, N_B, K)$

```
// Initialize the list of adapter lists for each model
E = []
for k in range(1, K) do
    // Initialize adapter list for model W_k
    E_k = []
    // Block size per model (PQ-LoRA assigned)
    B_k = len(W[k]) // N_B
    // Remaining layers not evenly divisible
    B_r = len(W[k]) % N_B
    for l in range(1, len(W[k])) do
        if ∃ n in {1..N_B} s.t.  l == n * B_k + B_r then
            // Append PQ-LoRA
            E_k.append(PQ-LoRA)
        else
            // Append conventional LoRA
            E_k.append(Conventional-LoRA)
    // Add adapter list to full collection
    E.append(E_k)
return E
```

**Algorithm 3:** `AlignAdapter(W, E,` $\mathcal{D}_p$`,` $K$`,` $\lambda$`) - Part 1`

```
# Define hook functions to capture outputs during a forward
 pass
Function hook_fn(module, input, output):
    self.lora_outputs.append(output)

### Combine PQ-LoRA with the pre-trained model
E_indices = []
for i in range(K) do
    E_index = []
    for j in range(len(W[i])) do
        if E[i][j] == PQ-LoRA then
            # Attach PQ-LoRA to pre-trained model layers
            W[i][j] = Attach(E[i][j], W[i][j])
            E_index.append(j)
    E_indices.append(E_index)

### Align PQ-LoRA A matrices
W_p = W[0] # Set pivot model
W_p.freeze() # Freeze pivot model
for i in range(1, K) do
    W_i = W[i]
    ## Step 1.  Attach hooks to LoRA A and perform a forward pass
    # Register hooks to capture the outputs of LoRA A matrix at
     PQ-LoRA attached layers
    for j in E_indices[0] do
        W_p[j].A.register_forward_hook(hook_fn)
    for j in E_indices[i] do
        W_i[j].A.register_forward_hook(hook_fn)

    ## Step 2.  Alignment of A using L2 loss
    total_loss = 0
    for (x, y) in D_p do
        W_p.forward_with_lora_scaled(x, scale=0)
        W_i.forward_with_lora_scaled(x, scale=0)
        total_loss = 0
        # Compute L2 loss for each layer using outputs captured by
         hooks
        for j in range(len(lora_outputs[i])) do
            # Compute L2 between LoRA A outputs of W_i and W_p at
             layer j
            loss_l2 = L2(W_p.lora_outputs[j], W_i.lora_outputs[j])
            # Compute Regularization loss to prevent deviation from
             orthogonality (Eq. 21)
            loss_reg = Reg(W_i[j].A)
            total_loss += loss_l2 + λ * loss_reg
        W_i -= η * Grad(W_i, total_loss)

    ## Step 3.  Post-process A to enforce Orthogonality
    for j in E_indices[i] do
        # Use Singular Value Decomposition to get the closest
         orthogonal matrix
        U, S, Vt = SVD(W_i[j].A)
        W_i[j].A = U*Vt
```

**Algorithm 4:** `AlignAdapter(`$\mathcal{W}$`, `$E$`, `$\mathcal{D}_p$`, `$K$`, `$\lambda$`) - Part 2`

```
### Align PQ-LoRA B matrices
for i in range(1, K) do
    W_i = W[i]

    ## Step 1.  Attach hooks to LoRA B and perform a forward pass
    # Register hooks to capture the outputs of B in PQ-LoRA
     attached layers
    for j in E_indices[0] do
        W_p[j].B.register_forward_hook(hook_fn)
    for j in E_indices[i] do
        W_i[j].B.register_forward_hook(hook_fn)

    # Forward pass to collect outputs of the LoRA B matrices for
     CCA
    for (x, y) in D_p do
        W_p.forward_with_lora_scaled(x, scale=0)
        W_i.forward_with_lora_scaled(x, scale=0)

    ## Step 2.  Apply CCA to align B matrices
    for j in range(len(W_i)) do
        # Extract B matrix outputs from hooks
        X_p = W_p.lora_outputs[j]
        X_i = W_i.lora_outputs[j]

        # Compute CCA projection vectors
        Π_p, Π_i = CCA(X_p, X_i)

        # Initialize B using the CCA transformation
        W_i[j].B = ((Π_i)^-1)^T · (Π_p)^T · W_p[j].B

E_align = []
for i in range(K) do
    for j in range(len(W[i])) do
        if E[i][j] == PQ-LoRA then
            E[i][j] = W[i][j]
    E_align.append(E[i])

return E_align
```